César Fernández Ramírez

Electromagnetic Production of Light Mesons

– Ph.D. Thesis Dissertation –

13th March 2006

Universidad Complutense de Madrid, Spain
Departamento de Física Atómica, Molecular y Nuclear

César Fernández Ramírez

Departamento de Física Nuclear y Física Estadística
Instituto de Estructura de la Materia, CSIC
Serrano 123, E-28006 Madrid, Spain
and
Departamento de Física Atómica, Molecular y Nuclear
Universidad de Sevilla
Apdo. 1065, E-41080 Sevilla, Spain

Electronic address: cesar@nuc2.fis.ucm.es

Physics and Astronomy Classification Scheme (PACS):
13.60.Le (Meson production),
25.20.Lj (Photoproduction reactions),
14.20.Gk (Baryon resonances with $S = 0$),
02.60.Pn (Numerical optimisation)

Key words:
Spin-0 particles photoproduction,
Electromagnetic multipoles,
Nucleon resonances,
Spin-3/2,
E2/M1 ratio,
Genetic algorithms

Ph.D. Thesis Supervisors

Prof. Dr. Elvira Moya Valgañón (E. Moya de Guerra)

Departamento de Física Atómica, Molecular y Nuclear
Facultad de Ciencias Físicas. Universidad Complutense de Madrid
Avenida Complutense s/n, E-28040 Madrid, Spain
and
Departamento de Física Nuclear y Física Estadística
Instituto de Estructura de la Materia, CSIC
Serrano 123, E-28006 Madrid, Spain

Dr. José Manuel Udías Moinelo

Departamento de Física Atómica, Molecular y Nuclear
Facultad de Ciencias Físicas. Universidad Complutense de Madrid
Avenida Complutense s/n, E-28040 Madrid, Spain

Ph.D. Thesis Rapporteurs

Dr. Maria Barbaro

Dipartamento di Fisica Teorica
Universitá di Torino
Via P. Giuria 1, I-10125 Torino, Italy

Dr. Juan Antonio Caballero Carretero

Departamento de Física Atómica, Molecular y Nuclear
Universidad de Sevilla
Apdo. 1065, E-41080 Sevilla, Spain

Dr. Joaquín Retamosa Granado

Departamento de Física Atómica, Molecular y Nuclear
Facultad de Ciencias Físicas. Universidad Complutense de Madrid
Avenida Complutense s/n, E-28040 Madrid, Spain

Dr. Jan Ryckebusch

Vakgroep Subatomaire en stralingsfysica
Universiteit Gent
Proeftuinstraat 86, 9000 Gent, Belgium

Ph.D. Thesis Evaluation Board

Prof. Dr. José María Gómez Gómez (President)

Departamento de Física Atómica, Molecular y Nuclear
Facultad de Ciencias Físicas. Universidad Complutense de Madrid
Avenida Complutense s/n, E-28040 Madrid, Spain

Prof. Dr. Antonio Dobado González (Secretary)

Departamento de Física Teórica I
Facultad de Ciencias Físicas. Universidad Complutense de Madrid
Avenida Complutense s/n, E-28040 Madrid, Spain

Prof. Dr. Dieter Drechsel

Institut für Kernphysik.
Johannes Gutenberg-Universtität Mainz
Johann-Joachim-Becher-Weg 45, D-55099 Mainz, Germany

Prof. Dr. Thomas William Donnelly

Center for Theoretical Physics and Laboratory for Nuclear Science
Department of Physics. Massachusetts Institute of Technology
77 Massachusetts Avenue, Cambridge MA 02139-4307, USA

Prof. Dr. Anton Nikolaiev Antonov

Institute for Nuclear Research and Nuclear Energy
Bulgarian Academy of Sciences
Blvd. Tzarigradsko, chausse 72, BG-1784 Sofia, Bulgaria

Tale potere, che ora dicono maligno ora benigno, ha Anastasia, città ingannatrice: se per otto ore al giorno tu lavori come tagliatore d'agate, onici, crisopazi, la tua fatica che dà forma al desiderio prende dal desiderio la sua forma, e tu credi di godere per tutta Anastasia mentre non ne sei che lo schiavo.

Anastasia, Le Città Invisivili. Italo Calvino.

Preface

ONCE upon a time I was born and bred in Madrid. As time went by, I grew up and became a physicist – just because I earned a degree in Physics, not because I knew much about such topic – and I decided to start a Ph.D. Thesis under the supervision of José Manuel Udías (Universidad Complutense de Madrid) and Elvira Moya (Instituto de Estructura de la Materia, CSIC) instead of being useful (?) to the society working in a private company. A much more profitable task. For more than four years this Ph.D. Thesis has been my commitment and for good or evil several *adventures* happened to me in this period. One of such stories is this Ph.D. Thesis Dissertation, some of them are sketched in this preface, and some will only be told to the mermaids in payment for their singing.

In the begining of my thesis I had to struggle with understanding papers and learning real (not academic) physics in order to improve my knowledge and to overcome the feeling that all was Greek to me (what somehow still remains). Undoubtly I would have preferred to become a knight-errant and fight against dragons, wind-mills, and gorgons, but by that time there were not much of them left, so I had to content myself with pions and nucleon resonances, some of them perhaps much more dangerous. This begining was at Universidad Complutense de Madrid were I spent my time with Armando Relaño, Eduardo Faleiro, Javier Rodríguez, Joaquín Retamosa, José María Gómez, Laura Muñoz, and Rafael Molina, as well as with two exceptional visitors from realms far far away, Anton Antonov and Cristina Martínez. At this time, correspondence with Humberto Garcilazo was helpful to understand pion photoproduction models and to tame the behaviour of the decay width of the resonances.

In this period, I also enjoyed Instituto de Estructura de la Materia (my second castle) with Alberto Escuderos, Diego Escrig, Eduardo Garrido, Jorge Dukelsky, Luis Mario Fraile, María José García, Manuela Turrión, Miguel Madurga, Pedro Sarriguren, and Susana Jiménez. Sometimes sharing time and sometimes sharing viands in the banquet room.

Year 2003 allowed me to gain new experiences travelling overseas to the United States for one week and afterwards to Italy for three months. In the woods of Maine (while I was looking for werewolves and fairy godmothers) I met Vladimir Pascalutsa who showed me how to face and tame one of the most dangerous kinds of nucleon resonances ever known, the spin-3/2 resonances, monsters that I have never seen but which I guess have a slight oblate deformation. For three months I improved my training on the art of physics in the lands of the North of Italy and shared adventures facing the halls of castles and palaces throughout the Italian orography with Ewan Roche, Jorge Sampaio, Sara Pérez, Shufang Ban, and Stefan Fritsch with a base palace at Trento inhabitted by Donatella Rossetti, Luana Slomp, Rachel Weatherhead, and Wolfram Weise, whose comments where very useful.

Until the end of my Ph.D., my time was split between Universidad Complutense de Madrid and Instituto de Estructura de la Materia. At UCM I met Joaquín López and Samuel España. The first one shared time, room, and cables with me at Jefferson Lab. where we stayed a couple of weeks in April 2005. At IEM I met Beatriz Errea, Oscar Moreno, Raúl de Diego, and Sergio Lerma who will inhabit it after my departure. But in this period, I was tired of rolling like a stone so I decided to *lay thy bow of pearl appart, and thy crystal shining quiver*[1] and to retire myself to a monacal life of work and hesitation – only broken by a one week stay in Seville far away the plains of Castile to learn from Juan Antonio Caballero – and tell the stories that happened to me writing this Ph.D. Thesis Dissertation that now the kind reader has on his hands.

Madrid, 13th March 2006, *César Fernández Ramírez*

[1] Benjamin Jonson, The Hymn of Hesperus, *Cynthia's Revel, Act. V, Sc. i.*

Contents

Summary

IN spite of the fact that Quantum Chromodynamics (QCD) is regarded as the theory of the strong interaction, in the energy regime of the mass of the nucleon and its resonances a perturbative approach, is not suitable. Thus, one has to rely on an effective approach if is interested on the properties of nucleon resonances and processes where they are involved – mainly meson production which is the dominant decay channel. This thesis is devoted to pion photoproduction from the nucleon, a classical topic within nuclear and particle physics, which has been proved as one of the best mechanisms to study the nucleon and its resonances as well as to study the role of the pion and resonances in nuclei. I present a pion photoproduction model on the free nucleon based on an Effective Lagrangian Approach (ELA) which includes the nucleon resonances ($\Delta(1232)$, N(1440), N(1520), N(1535), $\Delta(1620)$, N(1650), and $\Delta(1700)$), in addition to Born and vector-meson exchange terms. The model incorporates a new theoretical treatment of spin-3/2 resonances, first introduced by Pascalutsa, avoiding pathologies present in previous models. Other main features of the model are chiral symmetry, gauge invariance, and crossing symmetry. I use the model combined with modern optimization techniques based upon genetic algorithms to assess the parameters of the nucleon resonances on the basis of world data on electromagnetic multipoles. I present results for electromagnetic multipoles, differential cross sections, asymmetries, and total cross sections for all one pion photoproduction processes on free nucleons. I find overall agreement with data from threshold up to 1 GeV in laboratory frame.

1 Introduction

SINCE its advent, the Standard Model [HM 84] has become the usual framework to study particle and intermediate energy physics and it has proved to be a highly succesful theory[1]. This framework deals with three of the interactions present in Nature: the strong, the weak, and the electromagnetic. Under this model, Nature is constituted by twelve spin-1/2 particles. Half of them are quarks (u, d, s, c, b, and t) and the other half are leptons (e, μ, τ, ν_e, ν_μ, and ν_τ). Neutrinos (ν's) only interact weakly; e, μ, and τ leptons interact weakly and electromagnetically; and quarks interact both strongly, weakly, and electromagnetically. Interactions are mediated by gluons (strong interaction), photons (electromagnetic interactions), and W and Z bosons (weak interactions).

Standard Model is a merge of two Quantum Field Theories, Electroweak Model by Glashow, Weinberg and Salam and Quantum Chromodynamics (QCD) [HM 84, TW 01]. The electroweak model takes into account the electromagnetic and the weak interactions, and in its current form it is a theory with remarkably high predictive power. QCD is regarded as the theory of the strong interaction. It is quite succesful in the high energy region, but in the energy regime of the mass of the nucleon and its resonances, a perturbative approach is not suitable. Thus, one has to rely on an effective approach if is interested on the properties of nucleon resonances and processes where they are involved. The best way to study the nucleon and its excitations is through electromagnetic probes, mainly photons and electrons, because the electromagnetic part of the interaction is well known and it is possible to isolate the not so well-known strong interacting vertex and get information about the hadrons.

Three elements play an important role in the study of the nucleon and its excitations (Fig. 1.1):

1. Experiments [Bec 97, Bla 01, Mol 96, Pei 96, Wis 99].
2. Nucleonic models, v.g. quark models [BM 65, BHF 97, CR 00], skyrme models [WW 87], lattice QCD [Ale 05, LDW 93], ...

[1] The existence of a neutrino mass contradicts the Standard Model theory, but its extension to include such effects is straightforward [AW 03].

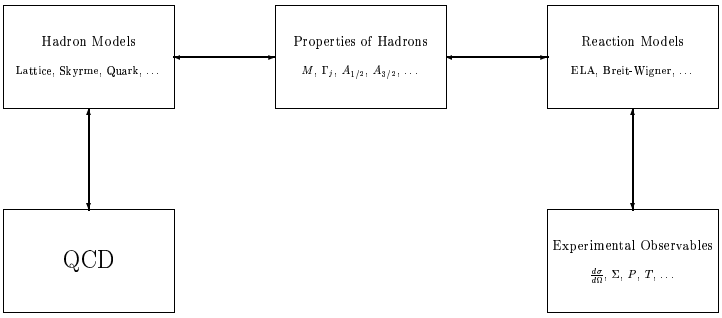

Fig. 1.1. Scheme with the relation of QCD with nucleon models, reaction models, and experimental observables.

3. Reaction models [FMU 03, FMU 06a] which allow to connect the two previous elements.

With regards to experiments, the experimental database [AWLR 90a, ASW 96, ABSW 02, SAID] has been enormously increased thanks to experiments carried out at LEGS (Laser Electron Gamma Source, Brookhaven National Laboratory, USA) [Bla 97, Bla 01, Sha 04] and MAMI (MAinz MIcrotron, Mainz, Germany) [Bec 97, Kru 04, Mol 96, Pei 96, Wis 99] where photons are produced through laser backscattering and bremsstrahlung respectively. Because of this effort, our knowledge of the $\Delta(1232)$ resonance region has been largely increased, though several discrepancies between Mainz and Brookhaven analyses still remain, concerning Compton scattering and unitarity [Bla 01].

Laser backscattering facilities are playing a very important role in the study of photoproduction processes because in such facilities it is possible to achieve a good energy resolution, a high degree of polarisation, and a high photon flux [Fer 04, TL 04] within the same experimental setup. Thus, polarisation observables, differential cross sections, and electromagnetic multipoles have been measured with a precision not possible a few years ago. A full description of the amplitudes in the $\Delta(1232)$ region is now available and the experimentalists intend to improve the knowledge of other kinematical regions and nucleon resonances. The database is expected to grow significantly once data from current experiments have been analysed and when data from new laser backscattering facilities as GRAAL (GRenoble Anneau Accelerateur Laser, Grenoble, France) and LEPS (Laser Electron Photons at SPring-8, Harima, Japan) become available. The last two facilities have started to run recently and operate at higher energies than LEGS. This situation opens a lot of possibilities for research on nucleon resonances.

For further reading, a very good review of the state of the art on experimental meson photoproduction is the paper by Krusche and Schadmand

[KS 03].

Regarding nucleonic models the most important are Constituent Quark Models [BHF 97, Fae 00], Skyrme Models [WW 87], and Lattice QCD [Ale 05, LDW 93]. It is out of the scope of this thesis to go through these models in detail. One of the best references available about the nucleon structure is the book by Thomas and Weise [TW 01], where a broad outlook of the topic is provided. Further reading should include Ref. [Gup 98] which is an excellent but rather technical introduction to lattice QCD and Ref. [CR 00] which is a review on quark models.

In this thesis I am concerned with the third element of this analysis: the reaction model, which allows to connect the nucleonic models with experimental data and to test how reliable the models are [FMU 06a]. I have to keep in mind that in the energy range of nuclear physics ($\lesssim$ GeV) it is not possible to apply QCD straightforwardly due to the strong coupling constant that does not allow to perform a perturbative calculation — this energy region falls in the non-perturbative regime of QCD. One way to overcome this difficulty consists in the development of an Effective Field Theory inspired on QCD using Weinberg's theorem as point of departure. Weinberg's theorem states (quoting Weinberg [Wei 79]):

> "... quantum field theory itself has no content beyond analyticity, unitarity, cluster decomposition, and symmetry. This can be put more precisely in the context of perturbation theory: if one writes down the most general possible Lagrangian, including *all* terms consistent with assumed symmetry principles, and then calculates matrix elements with this Lagrangian to any given order of perturbation theory, the result will simply be the most general possible $\mathcal{S}$-matrix consistent with analyticity, perturbative unitarity, cluster decomposition and the assumed symmetry principles ..."

This theorem has not been proved but it is sensible and no counterexamples are known. Although I cannot apply QCD directly to meson production Weinberg's theorem provides a mechanism to obtain an effective Lagrangian theory because it guarantees that once the effective theory is built, it is the right one, or as good as the right one.

I will only deal with non-strange particles so my starting point will be QCD reduced to quarks u and d. The symmetry group is then $SU_L(2) \times SU_R(2)$ where subindices stand for helicity (L: Left-handed and R: Right-handed). This symmetry is not observed in nuclear physics because the quarks are confined and baryons and mesons are the relevant degrees of freedom. Protons and neutrons constitute the ground state of the theory in the nuclear physics energy range, with the associated isospin symmetry group $SU_I(2)$ where I stands for isospin. Thus, the ground state of QCD does not share

the symmetry group of the Lagrangian but a smaller one. This situation is met quite often in Nature and it is said that the symmetry is spontaneously broken. When this happens, Goldstone theorem applies (quoting Ref. [Bur 00]):

> "... Any system for which a continuous, global symmetry is spontaneously broken, must contain in its spectrum a state, $|G>$ – called a *Goldstone mode*, or *Goldstone boson* since it must be a boson[2] – which has the defining property that it is created from the ground state by performing a spacetime-dependent symmetry transformation. In equations, $|G>$ is defined by the condition that the following matrix element cannot vanish:
>
> $$< G|\rho\left(\vec{r},t\right)|\Omega > \neq 0. \tag{1.1}$$
>
> Here, $|\Omega>$ represents the ground state of the system, and $\rho \equiv j^0$ is the density for the conserved charge – guaranteed by Noether's theorem – for the spontaneously broken symmetry ... "

The Goldstone boson has the following properties (quoting again Ref. [Bur 00]):

> "... The Goldstone boson must be *gapless*, in that its energy must vanish in the limit that its (three-) momentum vanishes. That is:
>
> $$\lim_{p\to 0} E(p) = 0. \tag{1.2}$$
>
> ... In relativistic systems, for which $E(p) = \sqrt{p^2 + m^2}$ where m is the particle mass, the gapless condition, Eq. (1.2), is the massless of the Goldstone particle. ... More generally, the argument just made can be extended to more complicated matrix elements. One finds in this way that the Goldstone boson for any exact symmetry must completely decouple from all of its interactions in the limit that its momentum vanishes ... "

If I apply Goldstone theorem to this case I obtain three goldstone bosons which can be identified with the lightest meson, the pion (π^+, π^0, π^-). In some effective theories, the quarks are substituted by the nucleon as ground state and the gluons are substituted by the pion as strong interaction mediator. Thus, the nucleon, the pion, and the nucleon excitations are of great importance in nuclear physics because they are the relevant degrees of freedom in nuclei [EW 88]. The pion plays a prominent role as the carrier of the strong interaction in the energy range of nuclear physics. An accurate knowledge of the pion, the nucleon, and the nucleon excitations is highly useful in order to acquire further understanding of nuclei.

---

[2] "Supersymmetry is an exception to this statement, since spontaneously broken global symmetry ensures the existence of a Goldstone fermion, the goldstino."

In the last decades, pion photoproduction has been studied through many models and using various approaches to decribe nucleon resonances. Among them there are, Breit-Wigner models [DHKT 99, Wal 69], K matrix [DMW 91, Ols 74, OO 78, Pen 02, PM 02], Effective Lagrangian Approach (ELA) [FM 97, FMU 06a, GM 93, SKPN 96, VHRW 95], dynamical models [FA 03, NBL 90, PT 04, SL 96, SL 01], Breit-Wigner plus a Regge-pole background to take into account the exchange of heavier mesons [Azn 03], as well as quark models with pion treated as an elementary particle [ZALW 02].

– Breit-Wigner models such as MAID model [DHKT 99] have two main contributions, a background which includes the vector-meson exchange and Born terms, and the resonances which are parametrized using Breit-wigner amplitudes. Born terms and meson exchange are built using effective Lagrangians like the ones I use in this thesis. They present problems in the treatment of the background and its effect in the determination of the parameters of the resonances as was shown by Aznauryan [Azn 03]. The inclusion of Regge-poles in order to take into account heavy meson exchange modifies the tail of the $\Delta(1232)$ resonance and changes the values of its constants.
– The K-matrix approach is based upon the use of the reaction matrix K instead of the scattering matrix $\mathcal{S}$. Both matrices are related through the Cayley transform [DM 70, Lan 68]:

$$\mathrm{K} = -i\frac{\mathcal{S}-1}{\mathcal{S}+1}. \tag{1.3}$$

K is an hermitian matrix (real matrix), therefore, the $\mathcal{S}$ matrix obtained from it is unitary by construction. The problem arises on how to calculate te reaction matrix K which requires approximations. In Ref. [DMW 91] the authors use Lagrangians to build the interactions and Watson's theorem [Ros 54, TW 01, Wat 54] (see below) and Olsson's unitarization procedure [Ols 74] to relate the elements of the reaction matrix with the elements of the transition matrix T

$$T = \frac{\mathrm{K}}{1-i\mathrm{K}}, \tag{1.4}$$

up to order e^2 in perturbation theory, which is related to the scattering matrix through:

$$\mathcal{S} = 1 + 2iT. \tag{1.5}$$

The Olsson unitarization procedure relies entirely on Watson's theorem which is valid only up the two pion production threshold. Therefore it is restricted to the $\Delta(1232)$ region and higher energy extensions are not reliable.
A more complete analysis of meson production under the K-matrix approach is provided by Refs. [PM 02, Pen 02] where the K matrix is calculated using the Bethe-Salpeter framework.

I have just mentioned Watson's theorem. It is convenient to provide more information about it. Below two pion production threshold there are only three open channels: $\gamma N \to \gamma N$, $\pi N \to \pi N$, and $\gamma N \leftrightarrow \pi N$. The scattering matrix $\mathcal{S}$ can be expanded in partial waves. Let α stand for a given pion-nucleon partial wave. The unitarity condition $\mathcal{S}\mathcal{S}^\dagger = 1$ determines completely the coupled channel $\mathcal{S}$-matrix (e stands for exponential)

$$\mathcal{S}_\alpha = \begin{bmatrix} \eta_\alpha & i\sqrt{1-\eta_\alpha^2}\,\mathrm{e}^{i\delta_\alpha} \\ i\sqrt{1-\eta_\alpha^2}\,\mathrm{e}^{i\delta_\alpha} & \eta_\alpha \mathrm{e}^{2i\delta_\alpha} \end{bmatrix} \tag{1.6}$$

where δ_α is the real phase shift, and $\eta_\alpha < 1$. Both are real functions of energy. This result is known as Watson's theorem [Ros 54, TW 01, Wat 54].

- In dynamical models, a Hamiltonian is built to act in the restricted Hilbert space $H = \mathrm{N} \oplus \Delta \oplus \pi\mathrm{N} \oplus \gamma\mathrm{N}$. These models are essentially coupled-channel potential models which satisfy unitarity exactly and therefore fulfill Watson's theorem. The models in Ref. [PT 04] and Refs. [SL 96, SL 01] use two different reductions of the Bethe-Salpeter equation and different spin-3/2 treatments. Actually, the model presented in this thesis and the one in Ref. [PT 04] apply the same spin-3/2 Lagrangians. The model by Fuda and Alharbi [FA 03] incorporates also nucleon resonances N(1440), N(1520), and N(1535) and provides results up to 600 MeV. These models have difficulties maintaining electromagnetic gauge invariance and crossing symmetry. For example, model [FA 03] includes only direct contributions from nucleon resonances and the model in Ref. [NBL 90] recovers gauge invariance relaxing four momentum conservation at the πNN vertex.
- The pion photoproduction model of Ref. [ZALW 02] is based upon the model of Ref. [LYL 97] for pseudoscalar meson production. The model of Ref. [ZALW 02] covers only the $\Delta(1232)$ region and applies quark-meson coupling to calculate adequate form factors. The $\Delta(1232)$ resonance is included phenomenologically.

Although in one way or another all models are phenomenological, in this thesis I adopt the ELA method because I consider it appealing in many respects and it is the most suitable approach in the energy range from threshold up to 1 GeV in laboratory frame, where the main low-lying resonances are present. This approach has proved to be a quite succesful tool to study pion photoproduction at low/threshold energy [BKM 92, BKM 95, TW 01] and provides the most natural framework to extend the model to pion electroproduction [GM 93], electromagnetic pion production in composite nuclei [GM 94, GM 95] and halo nuclei [KB 98] (see Fig. 1.2), two pion photoproduction [GO 94, GO 96], meson exchange currents [ABCDM 02a, ABCDM 02b, DBT 94, DKD 76, OD 81], and exclusive X(γ,$N\pi$)Y processes.

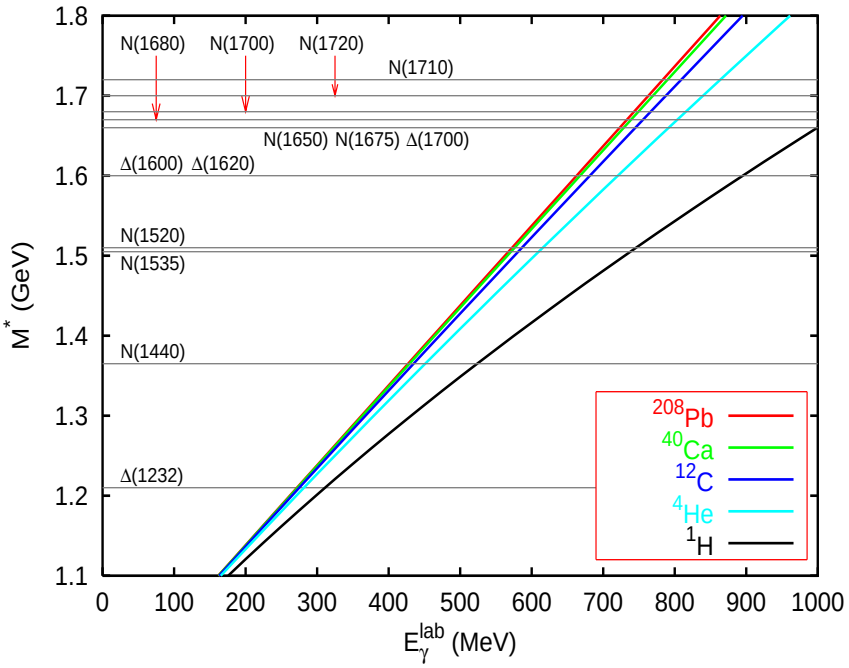

Fig. 1.2. Available energy for resonance excitations with different targets depending on the incident photon energy in the laboratory frame. Pole masses of the nucleon resonances are marked in the figure as horizontal lines (figure provided by J.R. Vignote, Ref. [Fer 04]).

In the last years, the Lagrangian description of spin-3/2 resonances has been greatly improved and many pathologies related to the pion-nucleon-resonance and γ-nucleon-resonance interactions have been overcome [Pas 98]. This fact, combined with the substantial enlargement of the pion photoproduction database, demands to revisit the topic and to make the most of these advances in order to improve our knowledge on nucleon resonances and γ-nucleon-resonance vertices as well as on the pion photoproduction process itself.

I focus on the analysis of pion photoproduction on free nucleons with the aim of establishing a reliable set of coupling constants and achieving an accurate knowledge on nucleon resonances. The latter are needed for further studies of resonances in nuclear medium as well as to study the structure of the nucleon through its excitations. This requires to develop a pion photoproduction model and to study the parameters of the nucleon resonances within the model for further implementation in the calculations previously mentioned. In this regard, I consider this thesis as a first step towards a deeper understanding of the role of the pion and the resonances in more compli-

cated processes. My model is an improvement of the one in Ref. [GM 93] where I have improved the spin-3/2 Lagrangians and explored other variations which allow me to achieve crossing symmetry and a better description of the resonance widths.

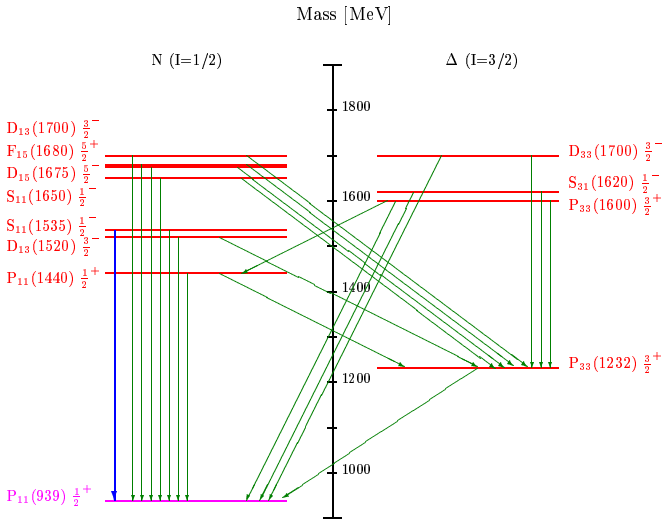

Fig. 1.3. Decays of low-lying nucleon excitations into ground state (nucleon, $P_{11}(939)$) through meson emission. I show the resonances rated with three or four stars by the Particle Data Group (PDG) up to 1.7 GeV [PDG 04]. Masses are the Breit-Wigner ones. The green lines stand for pion decays and the blue line for η decay.

In Fig. 1.3 I show the decay scheme of all the nucleon resonances up to 1.7 GeV of mass with three and four stars in Particle Data Group (PDG in what follows). Notation for nucleon resonances is as follows: The capital letter stands for the angular momentum L of the final πN state (S, $L = 0$; P, $L = 1$; D, $L = 2$; ...), the first subindex is twice the isospin and the second twice the spin. Nucleon resonances are named after their Breit-Wigner mass which is provided between brackets. I note how important is the $\Delta(1232)$ as intermediate state in the two pion decay channel.

The elements included in this model are nucleons, pions, photons, ρ and ω mesons, as well as all four star spin 1/2 and 3/2 nucleon resonances up to 1.7 GeV in PDG [PDG 04]. Spin-5/2 resonances are not expected to play an important role in the data analysis carried out in this thesis and are left for further work.

This thesis is organised in three parts:

Part I Theoretical Framework: This part provides a full description of the theory concerning the pion photoproduction model. I provide the basic features such as conventions and normalisations for cross sections and amplitudes which will be used throughout this thesis. I describe the full model and its features in detail, stressing crossing symmetry and the spin-3/2 treatment which avoids well-known pathologies of previous models.

Part II Study of the Parameters of the Model: In this part I provide all the parameters of the model and a broad explanation on the techniques applied to assess them.

Part III Results: In this part I show results for multipoles, differential cross sections and remaining physical observables. I also provide the final remarks and conclusions of the Ph.D. Thesis.

Part I

Theoretical Framework

2 Conventions and Kinematics

NOTATION for kinematics (using natural units $\hbar = c = 1$) is set to (see Fig. 2.1) $k = (E_\pi, \vec{k})$ for the outgoing pion, $q = (E_\gamma, \vec{q})$ for the incoming photon, $p = (E, \vec{p})$ for the incoming nucleon, and $p' = (E', \vec{p'})$ for the outgoing nucleon. Mandelstam variables are defined as usual [HM 84]:

$$s = (p+q)^2 = (p'+k)^2\,, \tag{2.1}$$

$$u = (p'-q)^2 = (p-k)^2\,, \tag{2.2}$$

$$t = (k-q)^2 = (p-p')^2\,. \tag{2.3}$$

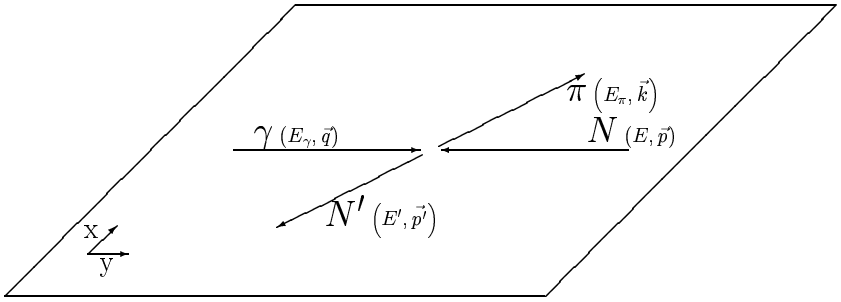

Fig. 2.1. Kinematics of the pion photoproduction process.

The metric tensor:

$$g^{\mu\nu} \equiv diag(1, -1, -1, -1), \tag{2.4}$$

thus, the scalar product is given by

$$p^2 = p^\mu p_\mu = g_{\mu\nu} p^\mu p^\nu = \left(p^0\right)^2 - \vec{p}^{\,2}. \tag{2.5}$$

I define the electromagnetic field

$$F^{\mu\nu} = \partial^\mu \hat{A}^\nu - \partial^\nu \hat{A}^\mu, \tag{2.6}$$

$$\tilde{F}^{\mu\nu} = \frac{1}{2}\epsilon^{\mu\nu\alpha\beta}F_{\alpha\beta}, \tag{2.7}$$

where $\hat{A}^\mu$ is the photon field and $\epsilon^{\mu\nu\alpha\beta}$ is the Levi-Civitá tensor.

In this thesis I use the following conventions for the Levi-Civitá tensor

$$\epsilon_{0123} = 1, \tag{2.8}$$

$$\epsilon_{123} = 1. \tag{2.9}$$

The photon polarisation vectors in spherical basis are

$$A^\mu_{\lambda_\gamma=\pm1} = \mp\frac{1}{\sqrt{2}}\left(0, 1, \pm i, 0\right). \tag{2.10}$$

Under Ref. [HM 84] conventions and normalisation, the differential cross section of 2 to n particles is

$$d\sigma = \delta^{(4)}(p_1 + p_2 - \sum_{j=1}^{n} k_j)\frac{(2\pi)^4}{|\vec{v}_1 - \vec{v}_2|}\frac{\mathcal{S}}{2E_{p_1}E_{p_2}}\overline{|\mathcal{M}|^2}\frac{d^3\vec{k}_1}{2k_1^0(2\pi)^3}\cdots\frac{d^3\vec{k}_n}{2k_n^0(2\pi)^3}, \tag{2.11}$$

where $\mathcal{S} = \prod_j \frac{1}{h_j!}$ if h_j particles are in the final state and $\overline{|\mathcal{M}|^2}$ is the invariant amplitude squared and averaged.

Then, the pion photoproduction differential cross section can be written in the center of mass (c.m.) reference system as

$$\sigma\left(\theta\right) \equiv \frac{d\sigma}{d\Omega^*_\pi} = \frac{1}{64\pi^2}\frac{1}{s^*}\frac{k^*}{E^*_\gamma}\overline{|\mathcal{M}|^2}. \tag{2.12}$$

Whenever a kinematical quantity appears starred it is defined in the c.m. reference frame. In particular the c.m. absolute values of the photon and the pion momenta are denoted by q^* and k^*, which stand for $|\vec{q^*}|$ and $|\vec{k^*}|$ respectively. The transition probability is

$$\overline{|\mathcal{M}|^2} = \frac{1}{4}\sum_{\lambda_1\lambda_2\lambda_\gamma}|\mathcal{A}_{\lambda_1\lambda_2\lambda_\gamma}|^2, \tag{2.13}$$

where $\mathcal{A}_{\lambda_1\lambda_2\lambda_\gamma}$ is the invariant amplitude, with photon polarisation λ_γ, initial nucleon helicity λ_1, and final nucleon helicity λ_2.

The total space where nucleons are represented is build up by means of the direct product of isospin, spin, and Minkowski spaces

$$Total\ \ Space = Isospin \times Spin \times Minkowski. \tag{2.14}$$

Thus, the nucleon wave function $N(p)$ factorizes as the product of an isospin function χ and a spin-1/2 wave function $u(p)$

$$N(p) = u(p)\chi, \tag{2.15}$$

with the spinors normalisation

$$\bar{u}_r\,(p)\,u_s\,(p) = 2M\delta_{rs}, \tag{2.16}$$

where M is the mass, p the four-momentum, and s and r the spins.

I can perform the following isospin decomposition

$$\mathcal{A} = \chi_2^\dagger \left(A^0\tau_j + A^- \frac{1}{2}[\tau_j, \tau_3] + A^+\delta_{j3} \right) \pi_j \chi_1, \tag{2.17}$$

where for simplicity I have dropped helicity subindices. Another two isospin decompositions are used and are introduced when necessary.

Isospin is an internal symmetry of particles which allows to study under the same formalism several similar processes. In this way it is possible to study at the same time $\gamma p \to \pi^+ n$, $\gamma n \to \pi^- p$, $\gamma p \to \pi^0 p$, and $\gamma n \to \pi^0 n$ processes if I put together as an isospin-1/2 particle (nucleon) the proton and the neutron and as an isospin-1 particle (pion) the π^0, π^+, and π^- states. In this thesis I consider isospin 0, 1, 1/2, and 3/2 particles (ω, nucleon, pion, and $\Delta(1232)$). The isospin and the physical basis coincide for the nucleon, but they are different for the pion. Both representations are related by means of the equations

$$\pi_1 = \frac{\sqrt{2}}{2}\left(\pi^+ + \pi^-\right), \tag{2.18}$$

$$\pi_2 = \frac{\sqrt{2}}{2i}\left(\pi^+ - \pi^-\right), \tag{2.19}$$

$$\pi_3 = \pi^0. \tag{2.20}$$

Isospin-3/2 is presented in chapter 3.3.

The isospin decomposition of Eq. (2.17) can be related to the physical amplitudes

$$\mathcal{A}\left(\gamma p \to p\pi^0\right) = A^+ + A^0, \tag{2.21}$$

$$\mathcal{A}\left(\gamma n \to n\pi^0\right) = A^+ - A^0, \tag{2.22}$$

$$\mathcal{A}\left(\gamma n \to p\pi^-\right) = \sqrt{2}\left(A^0 - A^-\right), \tag{2.23}$$

$$\mathcal{A}\left(\gamma p \to n\pi^+\right) = \sqrt{2}\left(A^0 + A^-\right). \tag{2.24}$$

In Eq. (2.17) the τ_j stands for the Pauli matrices

$$\tau_1 = \begin{bmatrix} 0 & 1 \\ 1 & 0 \end{bmatrix}, \tau_2 = \begin{bmatrix} 0 & -i \\ i & 0 \end{bmatrix}, \tau_3 = \begin{bmatrix} 1 & 0 \\ 0 & -1 \end{bmatrix}; \tag{2.25}$$

which define a Lie algebra $\mathfrak{su}(2)$ and hold the commutation relations

$$[\tau_j, \tau_k] = 2\epsilon_{jkl}\tau_l. \tag{2.26}$$

Another algebra that will be needed in this thesis is the Dirac-Pauli algebra, defined by

$$\{\gamma^\mu, \gamma^\nu\} = 2g^{\mu\nu}. \tag{2.27}$$

A representation of this algebra using 4×4 matrices is

$$\gamma^0 = \begin{bmatrix} 1 & 0 \\ 0 & -1 \end{bmatrix} \ , \ \vec{\gamma} = \begin{bmatrix} 0 & \vec{\tau} \\ -\vec{\tau} & 0 \end{bmatrix}. \tag{2.28}$$

Additional matrices based upon Dirac-Pauli algebra that will be used are

$$\gamma^{\mu\nu} = \frac{1}{2}\left[\gamma^\mu, \gamma^\nu\right], \tag{2.29}$$

$$\gamma^{\mu\nu\alpha} = \frac{1}{2}\left(\gamma^\mu\gamma^\nu\gamma^\alpha - \gamma^\alpha\gamma^\nu\gamma^\mu\right), \tag{2.30}$$

$$\gamma^5 \equiv \gamma_5 = -i\gamma_0\gamma_1\gamma_2\gamma_3 = \begin{bmatrix} 0 & 1 \\ 1 & 0 \end{bmatrix}. \tag{2.31}$$

3 The Model

IN this chapter I present a complete description of the model and its features. Using as starting point Weinberg's theorem [Wei 79], I construct a fully relativistic, chiral symmetric, gauge invariant, and crossing symmetric model based on suitable effective Lagrangians for particle couplings. From these Lagrangians I obtain the invariant amplitudes and physical observables. This procedure has been adopted in many papers (see, in particular, Refs. [FM 97, GM 93, SKPN 96, VHRW 95]) and has been proved to be a succesful way to treat the pion photoproduction process. However, previous works had pathologies in the description of the spin-3/2 particles which are not present in my model. The basic idea is to build consistently the most general Lagrangians for vertices, taking into account all possible symmetries (crossing symmetry, gauge invariance, chiral symmetry), and to use Feynman rules to obtain invariant amplitudes which can be related to physical observables. The model can be split into three different types of contributions: Born terms (Fig. 3.1), vector-mesons exchange (Fig. 3.2, diagram (e)), and spin-1/2 and spin-3/2 nucleon resonance excitations (Fig. 3.2, diagrams (f) and (g)). There is no contribution from σ meson exchange because of charge conjugation violation of the $\sigma\pi\gamma$ coupling [DMW 91]. I consider that all the relevant degrees of freedom are taken into account except perhaps spin-5/2 resonances. My choice of Lagrangians is explained and justified in the forthcoming sections. All the invariant amplitudes can be found in chapter 4.

3.1 Born Terms

Born terms are the Feynman diagrams shown in Fig. 3.1 in which only pions, photons, and nucleons are involved. I start with the free Lagrangians for pions (Klein-Gordon) and nucleons (Dirac) and a phenomenological pion-nucleon interaction. This last interaction is chosen as a pseudovector (PV) coupling to the pion because it is the lowest order in derivatives compatible with the low energy behaviour of the pion and with chiral symmetry [BKM 95, Bur 00, Leu 94]:

$$\mathcal{L}_{\pi NN} = \frac{f_{\pi N}}{m_\pi} \bar{N} \gamma_\mu \gamma_5 \tau_j \left(\partial^\mu \pi_j\right) N, \tag{3.1}$$

where m_π is the mass of the pion, $f_{\pi N}$ is the pseudovector coupling constant, and the sign is fixed by phenomenology. According to [ALR 90, Ber 90] $f_{\pi N}$ is set to $f_{\pi N}^2/4\pi = 0.0749$. The use of the PV coupling for the pion in my effective Lagrangian grants that low energy theorems of current algebra and partially conserved axial-vector current (PCAC) hypothesis are incorporated in the model.

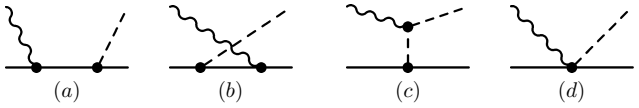

Fig. 3.1. Feynman diagrams for Born terms: (a) direct or s-channel, (b) crossed or u-channel, (c) pion in flight or t-channel, and (d) Kroll-Rudermann (contact).

The nucleon free field is the well-known Dirac Lagrangian:

$$\mathcal{L}_{Dirac}^{Nucleon} = \bar{N}\left(i\partial\!\!\!/ - M\right)N \tag{3.2}$$

where N is defined in equation (2.15), and the pion free field is the Klein-Gordon Lagrangian:

$$\mathcal{L}_{Klein-Gordon}^{Pion} = \frac{1}{2}\partial_\mu\vec{\pi}\partial^\mu\vec{\pi} - \frac{1}{2}m_\pi\vec{\pi}\cdot\vec{\pi} \tag{3.3}$$

The electromagnetic field is included in the usual way by minimal coupling to the photon field ($\partial^\alpha \to \partial^\alpha + ie\hat{Q}\hat{A}^\mu$; where $\hat{Q}$ is the charge operator) and taking phenomenologically into account the anomalous magnetic moment of the nucleon:

$$\mathcal{L} = -\frac{ie}{4M}F_2^V\bar{N}\frac{1}{2}\left(F_2^{S/V} + \tau_3\right)\gamma_{\alpha\beta}NF^{\alpha\beta}. \tag{3.4}$$

$F_2^{S/V}$ is defined as the ratio between isoscalar and isovector form factors ($F_2^{S/V} \equiv F_2^S/F_2^V$).

The interacting Lagrangian for Born terms is:

$$\begin{aligned}\mathcal{L}_{Born} = &- ieF_\pi\hat{A}^\alpha\epsilon_{jk3}\pi_j\left(\partial_\alpha\pi_k\right) - e\hat{A}^\alpha F_1^V\bar{N}\gamma_\alpha\frac{1}{2}\left(F_1^{S/V} + \tau_3\right)N \\ &- ieF_1^V\frac{f_{\pi N}}{m_\pi}\hat{A}^\alpha\bar{N}\gamma_\alpha\gamma_5\frac{1}{2}[\tau_j,\tau_3]\pi_j N \\ &- \frac{ie}{4M}F_2^V\bar{N}\frac{1}{2}\left(F_2^{S/V} + \tau_3\right)\gamma_{\alpha\beta}NF^{\alpha\beta} \\ &+ \frac{f_{\pi N}}{m_\pi}\bar{N}\gamma_\alpha\gamma_5\tau_j N\left(\partial^\alpha\pi_j\right),\end{aligned} \tag{3.5}$$

where e is the absolute value of the electron charge, F_π is the pion form factor and $F_j^V = F_j^p - F_j^n$, $F_j^S = F_j^p + F_j^n$ are the isovector and isoscalar nucleon form factors which at the photon point ($q^2 = 0$) take the values $F_1^S = F_1^V = 1$, $F_2^S = \kappa^p + \kappa^n = -0.12$, $F_2^V = \kappa^p - \kappa^n = 3.70$. I set $F_\pi = F_1^V$ in order to ensure gauge invariance. The $F_\pi = F_1^V$ relation is inferred from the $U(1)$ gauge transformation of the coupling and the fields

$$\partial^\mu \to D^\mu(\theta) = \partial^\mu + ie\hat{Q}\hat{A}^\mu + ie\hat{Q}\partial^\mu\theta, \tag{3.6}$$

$$N \to N(\theta) = \mathrm{e}^{-ie\hat{Q}_N\theta}N, \tag{3.7}$$

$$\vec{\pi} \to \vec{\pi}(\theta) = \mathrm{e}^{-ie\hat{Q}_\pi\theta}\vec{\pi} = \begin{bmatrix} \cos(eF_\pi\theta)\,\pi_1 - \sin(eF_\pi\theta)\,\pi_2 \\ \sin(eF_\pi\theta)\,\pi_1 + \cos(eF_\pi\theta)\,\pi_2 \\ \pi_3 \end{bmatrix}, \tag{3.8}$$

where θ is a continuous parameter and $\hat{Q}$ is the charge operator defined by

$$\hat{Q} = \hat{Q}_N + \hat{Q}_\pi, \tag{3.9}$$

where

$$\hat{Q}_N = \frac{1}{2}F_1^V\left(F_1^{S/V} + \tau_3\right), \tag{3.10}$$

is the charge operator of the nucleon and

$$\hat{Q}_\pi = F_\pi t_3, \tag{3.11}$$

$$t_3 = \begin{bmatrix} 0 & -i & 0 \\ i & 0 & 0 \\ 0 & 0 & 0 \end{bmatrix}, \tag{3.12}$$

is the charge operator of the pion in isospin basis with t_3 a matrix from the Lie algebra $\mathfrak{su}(3)$.

The PV coupling is (I omit global constants):

$$\mathcal{L} = \bar{N}\gamma_\alpha\gamma_5\vec{\tau}\partial^\alpha\vec{\pi}N, \tag{3.13}$$

which after the gauge transformation reads:

$$\begin{aligned} \mathcal{L}(\theta) &= \bar{N}(\theta)\gamma_\alpha\gamma_5\vec{\tau}D^\alpha(\theta)\vec{\pi}(\theta)N(\theta) \\ &= \bar{N}\mathrm{e}^{ie\hat{Q}_N\theta}\gamma_\alpha\gamma_5\vec{\tau}\mathrm{e}^{-ie\hat{Q}_\pi\theta}\mathrm{e}^{-ie\hat{Q}_N\theta}\left(\partial^\alpha + ie\hat{Q}\hat{A}^\alpha\right)\vec{\pi}N \end{aligned} \tag{3.14}$$

where I have used the independence between the nucleon and the pion spaces.

The gauge invariance condition reduces to:

$$\vec{\tau}(\theta)\cdot\vec{\pi}(\theta) = \vec{\tau}\cdot\vec{\pi}, \tag{3.15}$$

where

$$\begin{aligned}\vec{\tau}(\theta) &= \mathrm{e}^{ie\hat{Q}_N\theta}\vec{\tau}\mathrm{e}^{-ie\hat{Q}_N\theta} \\ &= \mathrm{e}^{ieF_1^V\tau_3\theta/2}\vec{\tau}\mathrm{e}^{-ieF_1^V\tau_3\theta/2}. \end{aligned} \tag{3.16}$$

The F_1^S part cancels trivially. Expanding (3.16) in detail

$$\mathrm{e}^{ieF_1^V 2\tau_3\theta/2}\tau_1\mathrm{e}^{-ieF_1^V\tau_3\theta/2} = \cos\left(eF_1^V\theta\right)\tau_1 - \sin\left(eF_1^V\theta\right)\tau_2, \tag{3.17}$$

$$\mathrm{e}^{ieF_1^V\tau_3\theta/2}\tau_2\mathrm{e}^{-ieF_1^V\tau_3\theta/2} = \sin\left(eF_1^V\theta\right)\tau_1 + \cos\left(eF_1^V\theta\right)\tau_2, \tag{3.18}$$

$$\mathrm{e}^{ieF_1^V\tau_3\theta/2}\tau_3\mathrm{e}^{-ieF_1^V\tau_3\theta/2} = \tau_3. \tag{3.19}$$

Thus

$$\vec{\tau}(\theta)\cdot\vec{\pi}(\theta) = \tau_1(\theta)\pi_1(\theta) + \tau_2(\theta)\pi_2(\theta) + \tau_3(\theta)\pi_3(\theta) \tag{3.20}$$

$$\begin{aligned} &= \cos\left[e\left(F_1^V - F_\pi\right)\theta\right](\tau_1\pi_1 + \tau_2\pi_2) + \tau_3\pi_3 \\ &+ \sin\left[e\left(F_1^V - F_\pi\right)\theta\right](\tau_1\pi_2 - \tau_2\pi_1). \end{aligned} \tag{3.21}$$

The gauge invariance condition reduces to

$$\sin\left[e\left(F_1^V - F_\pi\right)\theta\right] = 0 \quad \forall\theta, \tag{3.22}$$

$$\cos\left[e\left(F_1^V - F_\pi\right)\theta\right] = 1 \quad \forall\theta; \tag{3.23}$$

thus

$$F_\pi = F_1^V. \tag{3.24}$$

It is straightforward to check gauge invariance of the amplitudes in chapter 4 performing the replacement $A^\mu \to q^\mu$.

3.2 Vector Mesons

The main contribution of mesons to pion photoproduction is given by ρ (isospin-1 spin-1) and ω (isospin-0 spin-1) exchange. The phenomenological Lagrangians which describe vector mesons are [GM 93, DHKT 99]

$$\mathcal{L}_\omega = -F_{\omega NN}\bar{N}\left[\gamma_\alpha - \frac{iK_\omega}{2M}\gamma_{\alpha\beta}\partial^\beta\right]\omega^\alpha N + \frac{eG_{\omega\pi\gamma}}{m_\pi}\tilde{F}_{\mu\nu}\left(\partial^\mu\pi_j\right)\delta_{j3}\omega^\nu, \tag{3.25}$$

$$\mathcal{L}_\rho = -F_{\rho NN}\bar{N}\left[\gamma_\alpha - \frac{iK_\rho}{2M}\gamma_{\alpha\beta}\partial^\beta\right]\tau_j\rho_j^\alpha N + \frac{eG_{\rho\pi\gamma}}{m_\pi}\tilde{F}_{\mu\nu}\left(\partial^\mu\pi_j\right)\tau_j\rho_j^\nu. \tag{3.26}$$

Often the $\pi\gamma V$ coupling is written as $\mathcal{L} = \frac{eG_{V\pi\gamma}}{2m_\pi}\tilde{F}_{\mu\nu}V^{\mu\nu}\pi$ where $V^{\mu\nu} \equiv \partial^\mu V^\nu - \partial^\nu V^\mu$ and $V^\mu \equiv \rho^\mu, \omega^\mu$ [DHKT 99]. Both couplings yield the same amplitude.

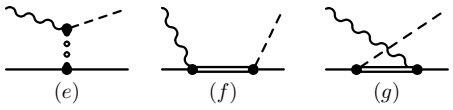

Fig. 3.2. Feynman diagrams for vector-meson exchange (e) and resonance excitations: (f) direct or s-channel and (g) crossed or u-channel.

3.3 Spin-1/2 Nucleon Resonances

In the model I deal with three different kinds of resonances with spin-1/2: S_{11}, S_{31}, and P_{11}. I need Lagrangians and amplitudes to describe their behaviour. The most simple isobar is isospin-1/2 spin-1/2 (S_{11}) which can be described by the following Lagrangian:

$$\mathcal{L}_{S_{11}} = -\frac{h}{f_\pi}\bar{N}\gamma_\alpha\tau_j N^*\partial^\alpha\pi_j - \frac{ie}{4M}\bar{N}\gamma_{\alpha\beta}\gamma_5\left(g_S + g_V\tau_3\right)N^*F^{\alpha\beta} + \text{HC}, \tag{3.27}$$

where HC stands for hermitian conjugate, h is the strong coupling constant which can be related to the width of the resonance decay into a nucleon and a pion, and $f_\pi = 92.3$ MeV is the leptonic decay constant of the pion. g_V and g_S stand for the isovector and isoscalar form factors of the resonance respectively. They are defined as $g_V = g_p - g_n$ and $g_S = g_p + g_n$, where subscripts p and n stand for the resonances originating from the proton and the neutron, and can be related to experimental helicity amplitudes at the photon point as it will be seen in the next sections. The pion coupling has been chosen pseudovector in order to obtain the right low energy behaviour and consistency with Born terms. The coupling to the photon employed preserves gauge invariance.

The next isobar is isospin-3/2 spin-1/2 (S_{31}). To incorporate this isospin-3/2 case I need to define isospinors as in Ref. [Pec 68]:

$$N_1^* = \sqrt{\frac{1}{2}}\begin{pmatrix} N^{*++} - \sqrt{\frac{1}{3}}N^{*0} \\ \sqrt{\frac{1}{3}}N^{*+} - N^{*-} \end{pmatrix}, \tag{3.28}$$

$$N_2^* = i\sqrt{\frac{1}{2}}\begin{pmatrix} N^{*++} + \sqrt{\frac{1}{3}} \\ \sqrt{\frac{1}{3}}N^{*+} + N^{*-} \end{pmatrix}, \tag{3.29}$$

$$N_3^* = -\sqrt{\frac{2}{3}}\begin{pmatrix} N^{*+} \\ N^{*0} \end{pmatrix}. \tag{3.30}$$

Under this basis, the isospin component of the propagator changes for both the s-channel (direct) and the u-channel (crossed):

s-channel

$$\pi_j N_j^* \bar{N}_3^* = iG(v)\left(\frac{2}{3}\delta_{j3}\pi_j - \frac{1}{6}\left[\tau_j,\tau_3\right]\pi_j\right). \tag{3.31}$$

u-channel

$$\pi_j N_3^* \bar{N}_j^* = iG(v)\left(\frac{2}{3}\delta_{j3}\pi_j + \frac{1}{6}\left[\tau_j,\tau_3\right]\pi_j\right). \tag{3.32}$$

where $G(v)$ is the spin-1/2 propagator that will be introduced in section 3.5. For the spin-3/2 propagator, the isospin structure is the same. In this basis and under the same conditions as those for the previous isobar, the S_{31} Lagrangian is

$$\mathcal{L}_{S_{31}} = -\frac{h}{f_\pi}\bar{N}\gamma_\alpha N_j^*\partial^\alpha\pi_j - \frac{ieg}{2M}\bar{N}\gamma_{\alpha\beta}\gamma_5 N_3^* F^{\alpha\beta} + \text{HC}. \tag{3.33}$$

Just one electromagnetic coupling constant is needed here because only the isovector part of the photon couples to the nucleon to produce an isospin-3/2 field.

The P_{11} Lagrangian is closely related to S_{11} being parity the main change. This change is due to the angular momentum of the resonance, which implies a different parity for the coupling:

$$\mathcal{L}_{P_{11}} = -\frac{h}{f_\pi}\bar{N}\gamma_\alpha\gamma_5\tau_j N^*\partial^\alpha\pi_j + \frac{ie}{4M}\bar{N}\gamma_{\alpha\beta}\left(g_S + g_V\tau_3\right)N^* F^{\alpha\beta} + \text{HC}. \tag{3.34}$$

3.4 Spin-3/2 Nucleon Resonances

The treatment of spin-3/2 nucleon-resonance couplings is one of the main improvements of the present model compared to former ones. The choice that I use here is motivated by previous studies that identified pathologies in former spin-3/2 couplings. In what follows I provide a detailed comparison of both traditional (off-shell extension) and gauge invariant (GI) couplings, which exhibits the virtues of the prescription adopted here. With regards to the traditional coupling, I restrict the discussion to the P_{33} (Δ) resonance and its coupling to the pion and the nucleon, although a similar analysis can be made for the other spin-3/2 resonances.

3.4.1 Traditional Δ-Nucleon-Pion Coupling

The basis of the traditional point of view is the seminal paper by Nath, Etemadi, and Kimel [NEK 71], based on the articles by Peccei [Pec 68, Pec 69] in the late sixties which dealt with this coupling. Peccei worked out a chiral Lagrangian with a pseudovector coupling to the pion, to ensure the low energy behaviour, based upon the invariance of the Δ free field under the point transformation $\Delta_\mu \to \Delta_\mu - \frac{1}{4}\gamma_\mu\gamma_\beta\Delta^\beta$ and the ansatz $\gamma^\mu O_{\mu\nu} = 0$. Given the most general Lagrangian $\mathcal{L} = h\bar{\Delta}^\mu_j O_{\mu\nu} N \partial^\nu \pi_j$ I obtain the well known Peccei Lagrangian [Pec 68, Pec 69]:

$$\mathcal{L}_{Peccei} = ih\bar{\Delta}^\alpha_j \left(4g_{\alpha\beta} - \gamma_\alpha\gamma_\beta\right) N\partial^\beta \pi_j + \text{HC}. \tag{3.35}$$

Restrictions such as Peccei's ansatz are needed in order to reduce the number of degrees of freedom (DOF) of the spin-3/2 field. When a massive spin-3/2 particle is described within the Bargmann and Wigner equations [Gre 97], a problem of extra DOF arises because a vector-spinor has sixteen componentes whilst only four are needed. These constraints naturally emerge in the free theory within the the Euler-Lagrange [NEK 71] or the Hamiltonian formalism [Pas 98], but for interacting particles the picture is not so straightforward and additional restrictions have to be imposed.

Nath *et al.* [NEK 71] proved that Peccei's ansatz was too restrictive, developing a generalisation which – despite of its many pathologies [BDM 89, NEK 71, Pas 98, Pas 01] – has become the traditional and most popular approach to interacting spin-3/2 particles for the last thirty years.

The starting point of Nath *et al.* is the massive spin-3/2 free theory, which can be found in Refs. [BDM 89, NEK 71, Pec 68]. The following Lagrangian is defined

$$\begin{aligned}\mathcal{L}_\Delta =& \bar{\Delta}^\alpha \Big[\left(i\partial_\mu\gamma^\mu - M^*\right) g_{\alpha\beta} + i\omega \left(\gamma_\alpha\partial_\beta + \gamma_\beta\partial_\alpha\right) \\ &+ \frac{i}{2}\left(3\omega^2 + 2\omega + 1\right)\gamma_\alpha\partial^\mu\gamma_\mu\gamma_\beta + M^*\left(3\omega^2 + 3\omega + 1\right)\gamma_\alpha\gamma_\beta \Big] \Delta^\beta,\end{aligned} \tag{3.36}$$

where $\omega \neq -\frac{1}{2}$ and the Lagrangian is invariant under the point transformation

$$\Delta^\mu \to \Delta^\mu + a\gamma^\mu\gamma^\nu\Delta_\nu, \tag{3.37}$$

$$\omega \to \frac{\omega - 2a}{1 + 4a}; \tag{3.38}$$

with $a \neq -\frac{1}{4}$. Subsidiary constraints $\gamma_\mu\Delta^\mu = 0$ and $\partial_\mu\Delta^\mu = 0$ appear in order to reduce the number of DOF to four, as expected for a spin-3/2 particle. A detailed description of the DOF counting technique is given in reference [PT 99]. The parameter ω does not affect physical quantities, so that one is free to set it to the most convenient value, usually $\omega = -1$, which recovers the Rarita-Schwinger theory [RS 41].

The point transformation of Eq. (3.37) does not affect the spin-3/2 content of the free field because of the constraint $\gamma_\mu \Delta^\mu = 0$, but for interacting Δ particles this constraint does not apply, and the excess of DOF shows up as a contribution to the spin-1/2 sector.

The best available example of this behaviour is the propagator. Given a spin-λ propagator, it has components with the following spins: λ, $\lambda - 1$, $\lambda - 2$,... For example, for a free, massive, M^* spin-3/2 field, the Rarita-Schwinger spinor ($\omega = -1$) is

$$\Delta^\mu_{r=\pm 3/2,\pm 1/2}(p) = \sum_{l,s} \langle 1, l, \frac{1}{2}, s \mid \frac{3}{2}, r \rangle \varepsilon^\mu_l(p)\, u^s(p)\,, \tag{3.39}$$

where $\langle 1, l, \frac{1}{2}, s \mid \frac{3}{2}, r \rangle$ is a Clebsch-Gordan coefficient [Edm 74] and the spin-1 four vector ε^μ_l is defined by:

$$\varepsilon^\mu_l = \left(\varepsilon^0_l(p), \vec{\varepsilon}_l(p)\right), \tag{3.40}$$

with

$$\varepsilon^0_l = \frac{\vec{p}\cdot\vec{\varepsilon}_l}{M^*}, \tag{3.41}$$

$$\vec{\varepsilon}_l(p) = \vec{\varepsilon}_l + \frac{\vec{p}\cdot\vec{\varepsilon}_l}{M^*}\frac{\vec{p}}{E^*+M^*} \quad , \qquad l = \pm 1, 0; \tag{3.42}$$

and

$$\vec{\varepsilon}_{\pm 1} = \mp\frac{1}{\sqrt{2}}(1, \pm i, 0) \quad , \quad \vec{\varepsilon}_0 = (0, 0, 1)\,; \tag{3.43}$$

The propagator in the Rarita-Schwinger spin-3/2 field theory is

$$G^{3/2}_{\alpha\beta}(v) = \frac{\not{v} + M}{v^2 - M^2}\left[-g_{\alpha\beta} + \frac{1}{3}\gamma_\alpha\gamma_\beta + \frac{2}{3M^2}v_\alpha v_\beta - \frac{1}{3M}\left(v_\alpha\gamma_\beta - \gamma_\alpha v_\beta\right)\right], \tag{3.44}$$

which has spin-3/2 and spin-1/2 components, made apparent if I rewrite the propagator as

$$\begin{aligned} G^{3/2}_{\alpha\beta}(v) = &-\frac{1}{\not{v} - M}P^{3/2}_{\alpha\beta} + \frac{2}{3M^2}(\not{v} + M)\,P^{1/2}_{22,\alpha\beta} \\ &- \frac{1}{\sqrt{3}M}\left(P^{1/2}_{12,\alpha\beta} + P^{1/2}_{21,\alpha\beta}\right), \end{aligned} \tag{3.45}$$

in terms of the spin projectors

$$P^{3/2}_{\alpha\beta} = g_{\alpha\beta} - \frac{1}{3}\gamma_\alpha\gamma_\beta - \frac{1}{3v^2}\left(\not{v}\gamma_\alpha v_\beta + v_\alpha\gamma_\beta\not{v}\right), \tag{3.46}$$

$$P^{1/2}_{11,\alpha\beta} = \frac{1}{3}\gamma_\alpha\gamma_\beta - \frac{v_\alpha v_\beta}{3v^2} + \frac{1}{3v^2}\left(\not{v}\gamma_\alpha v_\beta + v_\alpha\gamma_\beta\not{v}\right), \tag{3.47}$$

$$P^{1/2}_{22,\alpha\beta} = \frac{v_\alpha v_\beta}{v^2}, \tag{3.48}$$

$$P^{1/2}_{12,\alpha\beta} = \frac{1}{\sqrt{3}v^2}v^\mu v_\beta\gamma_{\alpha\mu}, \tag{3.49}$$

$$P^{1/2}_{21,\alpha\beta} = \frac{1}{\sqrt{3}v^2}v_\alpha v^\mu\gamma_{\mu\beta}. \tag{3.50}$$

The most general interacting Lagrangian containing only first-order derivatives of the pion field and consistent with (3.36), (3.37), and (3.38) is given by

$$\mathcal{L}_{int} = \varkappa\bar{\Delta}^\alpha\left(g_{\alpha\beta} + a\gamma_\alpha\gamma_\beta\right)N\partial^\beta\pi + \text{HC}, \tag{3.51}$$

where $\varkappa$ is a coupling constant and a is called the off-shell parameter, which can be set to different values. This is named off-shell extension framework. If $a = -\frac{1}{4}$ I recover Peccei theory. This family of Lagrangians has been widely used in pion-nucleon scattering [FM 98, SKPN 96], pion photoproduction [FM 97, GM 93, NBL 90, SL 96, SL 01, SKPN 96, Pec 68, VHRW 95] and compton scattering [SKPN 96, PS 95] in the Δ-region, as well as for the description of meson exchange currents [ABCDM 02a, ABCDM 02b, DBT 94, DKD 76, OD 81]. The off-shell parameter can be set to a fixed value, $a = -1$ [NEK 71], $a = -\frac{1}{4}$ [GM 93, Pec 68] or just let it run freely [FM 97, PS 95] in order to get the best possible fit.

However, it is not possible to remove the spin-1/2 sector from the amplitude for any value of a [BDM 89]. The physical meaning of the off-shell parameter is unclear and could be considered just as a free parameter with a fuzzy physical meaning employed only for fitting improvement. An important disadvantage is that there is a strong dependence of the coupling constants on the off-shell parameter, as was proved by Feuster and Mosel [FM 97]. Other pathologies related to the coupling shown in Eq. (3.51) are: quantization anomalies (except for $a = -1$), so that the naive Feynman rules I *read* from the Lagrangian are no longer valid [NEK 71, Pas 98]; Johnson-Sudarshan (JS) problem (non-positive definite commutators) [Hag 71, JS 61, Sin 73] and Velo-Zwanziger (VZ) problem (acausal propagations) [Hag 71, Sin 73, VZ 69a, VZ 69b].

A consistent theory for interacting spin-3/2 particles is expected to be free of such problems. Such a theory has been developed in recent years and will be presented in the next paragraphs.

3.4.2 Gauge Invariant Couplings

A different approach to massless fields of arbitrary spin λ was developed in the seventies. It was proved that the massless theory has a simple structure for

both integer [Fro 78] and half-integer [FF 78] spin fields, even if the massive theory is rather complicated. The free massless Lagrangians for half-integer spin fields can be obtained just from first principles requiring the action to be invariant under the gauge transformation $\psi \to \psi + \delta\psi$, where $\delta\psi = \partial\eta$ [Cur 79, Wei 95, WF 80], ψ is a tensor-spinor with rank ℓ which stands for the particle and η a complex tensor-spinor field with rank $\ell-1$. For a spin-3/2 field, $\delta\psi_\mu = \partial_\mu\eta$, with ψ_μ a vector spinor and η a spinor field. This gauge condition reduces the number of DOF of the spin-λ field to two (helicity states $-\lambda$ and $+\lambda$) as it is required for a massless particle. In this framework, it is quite simple to build consistent interactions for half-integer spin fields as suggested by Weinberg and Witten [WW 80] just enforcing them to fulfill this gauge invariance condition. For example, the spin-3/2 ψ_μ field should appear in the interaction as $\partial_\mu\psi_\nu - \partial_\nu\psi_\mu$, the spin-5/2 $\psi_{\mu\nu}$ as $\partial_\mu\partial_\nu\psi_{\rho\sigma} - \partial_\mu\partial_\sigma\psi_{\rho\sigma} - \partial_\rho\partial_\nu\psi_{\mu\sigma} + \partial_\rho\partial_\sigma\psi_{\mu\nu}$, and, more generally, an arbitrary spin-λ tensor-spinor field as the antisymetrization of $\partial_{\alpha_1}\partial_{\alpha_2}\cdots\partial_{\alpha_{(\lambda-1/2)}}\psi_{\beta_1\beta_2\cdots\beta_{(\lambda-1/2)}}$. Thus the vertices $\mathcal{O}^{\mu\cdots}$ of the Feynman diagrams for massless spin-3/2 particles will fulfill the condition $p_\mu\mathcal{O}^{\mu\cdots} = 0$, where p is the four-momentum of the spin-3/2 particle, μ the vertex index which couples to the spin-3/2 field, and the dots stand for other possible indices. This is what is called GI coupling scheme.

I apply this procedure to the Δ case. Starting from Lagrangian (3.36) for a free massless spin-3/2 particle, for $\omega = -1$ it can be written as:

$$\mathcal{L}_{3/2,massless} = \bar{\psi}_\mu\gamma^{\mu\nu\alpha}\partial_\alpha\psi_\nu. \tag{3.52}$$

The inclusion of the mass term:

$$\mathcal{L}_{3/2,massive} = \mathcal{L}_{3/2,massless} - M^*\bar{\psi}_\mu\gamma^{\mu\nu}\psi_\nu, \tag{3.53}$$

breaks gauge symmetry, raising the number of DOF from 2 to 4 as it should be.

Now I consider the interaction. For an interacting massless spin-3/2 particle I write the Lagrangian:

$$\mathcal{L} = \mathcal{L}_{3/2,massles} + \mathcal{L}_{int}. \tag{3.54}$$

The interaction has been built within the GI coupling scheme and can be written as [Pas 98]:

$$\mathcal{L}_{int} = \psi^\dagger_\mu J^\mu + \mathrm{HC}, \tag{3.55}$$

where J^μ has no dependence on ψ^μ and gauge invariance imposes $\partial_\mu J^\mu = 0$. The inclusion of the mass term – if it is properly done as in (3.53) – breaks gauge symmetry increasing the number of DOF of the spin-3/2 field from 2 to 4 and does not affect $\mathcal{L}_{int}$ [Pas 98, Wei 95]. Hence the number of DOF in the interacting massive field is the right one and no unphysical components are present. Focusing on my photoproduction model, I am interested in two

couplings: the Δ to the pion and the nucleon, and the Δ to the photon and the nucleon. The simplest consistent $\Delta N\pi$-coupling is [Pas 98]:

$$\mathcal{L}_{int} = -\frac{h}{f_\pi M^*}\bar{N}\epsilon_{\mu\nu\lambda\beta}\gamma^\beta\gamma^5\left(\partial^\mu N_j^{*\nu}\right)\left(\partial^\lambda\pi_j\right) + \text{HC}. \tag{3.56}$$

I have to clarify that the vector coupling to the pion is a consequence of the GI prescription. Whithin this prescription, the scalar coupling to the pion gives no contribution to the amplitude [Pas 98].

Concerning the ΔNγ coupling, Jones and Scadron [JS 81] suggestion has been widely used in the (G_1, G_2) decomposition with [DMW 91, FM 97, GM 93, VHRW 95, PS 95] or without [NBL 90, SL 96, SL 01] off-shell extension. Another decomposition (G_E, G_M), based upon the same idea as the Sachs form factors for the nucleon [ESW 60], is also possible. This decomposition is directly connected to physical quantities, as electric and magnetic multipoles, in particular to the E2/M1 ratio which is of great interest from both experimental and theoretical points of view [Bla 01, PT 04, TW 01]. This second decomposition is consistent with the GI approach and can be written as [PP 03]:

$$\mathcal{L} = \frac{3e}{2M\left(M+M^*\right)}\bar{N}\left[ig_1\tilde{F}_{\mu\nu} + g_2\gamma^5 F_{\mu\nu}\right]\left(\partial^\mu N_3^{*\nu}\right) + \text{HC}, \tag{3.57}$$

where g_1 and g_2 can be easily related to G_E and G_M [PT 99] by:

$$G_E = -\frac{1}{2}\frac{M^*-M}{M^*+M}g_2, \tag{3.58}$$

$$G_M = g_1 + \frac{1}{2}\frac{M^*-M}{M^*+M}g_2. \tag{3.59}$$

Other possible consistent choices can be found in Refs. [PT 99, KS 01].

GI couplings have been proved to be free of the pathologies which are inherent to the traditional scheme. No anomalies are found in the quantization; neither JS nor VZ problems appear; and no spin-1/2 sector arises when the invariant amplitudes are calculated [Pas 98]. Moreover, Pascalutsa and Timmermans [PT 99] claim that DOF counting is the reason why GI couplings are consistent, while the off-shell extension couplings of Nath *et al.* are not. They blame the unphysical extra components for the appearance of pathologies. Both, GI (3.56) and traditional (3.51) couplings, provide the same result on-shell (if I set properly the coupling constants). However, their off-shell behaviour is completely different.

Based on the previous discussion, the P_{33} Lagrangian that will be used in this work is:

$$\begin{aligned}\mathcal{L}_{\mathrm{P}_{33}} =& -\frac{h}{f_\pi M^*}\bar{N}\epsilon_{\mu\nu\lambda\beta}\gamma^\beta\gamma^5\left(\partial^\mu N_j^{*\nu}\right)\left(\partial^\lambda\pi_j\right)\\ &+\frac{3e}{2M\left(M+M^*\right)}\bar{N}\left[ig_1\tilde{F}_{\mu\nu}+g_2\gamma^5F_{\mu\nu}\right]\left(\partial^\mu N_3^{*\nu}\right)\\ &+\mathrm{HC}.\end{aligned} \tag{3.60}$$

From this expression it is straightforward to obtain phenomenological Lagrangians for other spin-3/2 resonances. To obtain the P_{13} resonance Lagrangian from (3.60) only an isospin change is needed:

$$N_j^{*\alpha}\to\tau_j N^{*\alpha},\quad j=1,2,3; \tag{3.61}$$

for the strong vertex, and

$$N_3^{*\alpha}\to N^{*\alpha},\quad g_j\to\frac{1}{2}\left[g_j^S+g_j^V\tau_3\right],\quad j=1,2; \tag{3.62}$$

for the photon vertex.

Thus the Lagrangian is

$$\begin{aligned}\mathcal{L}_{\mathrm{P}_{13}} =& -\frac{h}{f_\pi M^*}\bar{N}\epsilon_{\mu\nu\lambda\beta}\gamma^\beta\gamma^5\tau_j\left(\partial^\mu N^{*\nu}\right)\left(\partial^\lambda\pi_j\right)\\ &+\frac{3e}{4M\left(M+M^*\right)}\bar{N}\Big[i\left(g_1^S+g_1^V\tau_3\right)\tilde{F}_{\mu\nu}\\ &+\left(g_2^S+g_2^V\tau_3\right)\gamma^5F_{\mu\nu}\Big]\left(\partial^\mu N^{*\nu}\right)+\mathrm{HC}.\end{aligned} \tag{3.63}$$

Lagrangians for D_{33} and D_{13} resonances are obtained easily from P_{33} and P_{13}. I only need to change the parity of the coupling placing an overall γ_5:

$$\begin{aligned}\mathcal{L}_{\mathrm{D}_{33}} =& -\frac{h}{f_\pi M^*}\bar{N}\epsilon_{\mu\nu\lambda\beta}\gamma^\beta\left(\partial^\mu N_j^{*\nu}\right)\left(\partial^\lambda\pi_j\right)\\ &+\frac{3e}{2M\left(M+M^*\right)}\bar{N}\left[ig_1\tilde{F}_{\mu\nu}\gamma_5+g_2F_{\mu\nu}\right]\left(\partial^\mu N_3^{*\nu}\right)\\ &+\mathrm{HC},\end{aligned} \tag{3.64}$$

$$\begin{aligned}\mathcal{L}_{\mathrm{D}_{13}} =& -\frac{h}{f_\pi M^*}\bar{N}\epsilon_{\mu\nu\lambda\beta}\gamma^\beta\tau_j\left(\partial^\mu N^{*\nu}\right)\left(\partial^\lambda\pi_j\right)\\ &+\frac{3e}{4M\left(M+M^*\right)}\bar{N}\Big[i\left(g_1^S+g_1^V\tau_3\right)\tilde{F}_{\mu\nu}\gamma_5\\ &+\left(g_2^S+g_2^V\tau_3\right)F_{\mu\nu}\Big]\left(\partial^\mu N^{*\nu}\right)+\mathrm{HC}.\end{aligned} \tag{3.65}$$

Although I restrict myself to spin-3/2, it is clear that higher spin interactions can be built within the same theoretical framework. This is left to future work.

3.5 Propagators and Widths

To calculate the invariant amplitudes I need five different types of propagators:

1. Spin-0 propagator for the t-channel of the Born terms (pion exchange)

$$iG^0(v) = i\frac{\delta_{jl}}{v^2 - m_\pi^2}. \tag{3.66}$$

2. Spin-1/2 propagator for the s- and u- channels of the Born terms

$$iG_N^{1/2}(v) = i\frac{\not{v} + M}{v^2 - M^2}. \tag{3.67}$$

3. Spin-1 propagator for the vector-meson exchange diagrams

$$iG^1_{\mu\nu}(v) = -\frac{i}{v^2 - m_V^2}\left(g_{\mu\nu} - \frac{v_\mu v_\nu}{m_V^2}\right). \tag{3.68}$$

4. Spin-1/2 propagator with a phenomenological width for spin-1/2 nucleon resonances.
5. Spin-3/2 propagator with a phenomenological width for spin-3/2 nucleon resonances.

With regards to the propagators of the resonances, for a spin-1/2 resonance I use

$$iG(v) = i\frac{\not{v} + M^*}{v^2 - M^{*2} + iM^*\Gamma(s,u)}, \tag{3.69}$$

and for the spin-3/2 propagator I use the Rarita-Schwinger propagator:

$$\begin{aligned} iG_{\alpha\beta}(v) =& i\frac{\not{v} + M^*}{v^2 - M^{*2} + iM^*\Gamma(s,u)} \\ &\times\left[-g_{\alpha\beta} + \frac{1}{3}\gamma_\alpha\gamma_\beta + \frac{2}{3M^{*2}}v_\alpha v_\beta - \frac{1}{3M^*}\left(v_\alpha\gamma_\beta - \gamma_\alpha v_\beta\right)\right], \end{aligned} \tag{3.70}$$

where v is the resonance four-momentum. A phenomenological width $\Gamma(s,u)$ is included in the propagator denominator consistently with what is obtained if I dress it with pions [KS 00, PP 03].

The energy dependence of the width is chosen phenomenologically as

$$\Gamma(s,u) = \sum_j \Gamma_j X_j(s,u), \tag{3.71}$$

where $j = \pi, \pi\pi, \eta$ stands for the different decay channels and

$$X_j(s,u) \equiv X_j(s) + X_j(u) - X_j(s)\,X_j(u), \tag{3.72}$$

with $X_j\,(l)$ given by

$$X_j\,(l) = 2\frac{\left(\frac{|\vec{k}_j|}{|\vec{k}_{j0}|}\right)^{2L+1}}{1+\left(\frac{|\vec{k}_j|}{|\vec{k}_{j0}|}\right)^{2L+3}}\,\Theta\left(l-(M+m_j)^2\right), \tag{3.73}$$

where L is the angular momentum of the resonance, Θ is the Heaviside step function, and

$$|\vec{k}_j| = \sqrt{\left(l-M^2-m_j^2\right)^2-4m_j^2M^2}/\left(2\sqrt{l}\right), \tag{3.74}$$

with $m_{\pi\pi}\equiv 2m_\pi$ and $|\vec{k}_{j0}| = |\vec{k}_j|$ when $l = M^{*2}$.

This parametrization has been built in order to fulfill the following conditions:

(i) $\Gamma = \Gamma_0$ at $\sqrt{s} = M^*$,
(ii) $\Gamma \to 0$ when $|\vec{k}_j| \to 0$,
(iii) a correct angular momentum barrier at threshold $|\vec{k}_j|^{2L+1}$,
(iv) crossing symmetry.

This parametrization of the width is an improvement over the one used in Ref. [GM 93] and includes decays to η and 2π which take into account inelastic channels [DHKT 99] and condition (iv). The width contributes to both s- and u-channels, so that crossing symmetry is preserved due to Eq. (3.72). In [FM 97] the authors made an analysis of the energy dependence of the width. It was concluded that, as long as it provides a decrease of the width beyond the resonance position, the specific way in which X_j is parametrized is not so important.

3.6 Form Factors

For the numerical calculations I include form factors for Born terms and vector mesons, in order to regularize the high energy behaviour of these terms. I choose form factors as suggested by Davidson and Workman [DW 01a, DW 01b] that allow to fulfill gauge invariance and crossing symmetry. Actually, $X_j(s,u)$ in Eq. (3.72) also follows this choice. Thus for Born terms:

$$\begin{aligned}\hat{F}_B(s,u,t) =& F_1(s)+F_2(u)+F_3(t)-F_1(s)F_2(u)\\ &-F_1(s)F_3(t)-F_2(u)F_3(t)+F_1(s)F_2(u)F_3(t),\end{aligned} \tag{3.75}$$

where,

$$F_1(s) = \left[1+\left(s-M^2\right)^2/\Lambda_B^4\right]^{-1}, \tag{3.76}$$

$$F_2(u) = \left[1+\left(u-M^2\right)^2/\Lambda_B^4\right]^{-1}, \tag{3.77}$$

$$F_3(t) = \left[1+\left(t-m_\pi^2\right)^2/\Lambda_B^4\right]^{-1}. \tag{3.78}$$

For vector mesons I adopt $\hat{F}_V(t) = F_3(t)$ with the changes $m_\pi \to m_V$ and $\Lambda_B \to \Lambda_V$. In order to have as few free parameters as possible in the numerical calculations I use the same $\Lambda \equiv \Lambda_B = \Lambda_V$ for both vector mesons and Born terms. For the resonance-pion-nucleon vertex, the form factor $\sqrt{X_\pi\,(s,u)}$ has to be used for consistency with the width employed in the propagator discussed previously.

Models like the ones by Garcilazo and Moya de Guerra [GM 93] and Feuster and Mosel [FM 97] needed a cutoff in the u-channels of spin-3/2 resonances in order to obtain a good description of observables. This cutoff was needed because the high-energy contributions of these diagrams are not reduced by the denominator of the propagator. In Ref. [GM 93] it was argued that the need of this cutoff could be justified by the two possible interpretations of the resonance excitation. From the point of view of an effective field theory, u-channels should be introduced with their full strength. On the other hand if I consider resonances as pure πN rescattering states (Chew-Low description), the contribution from the u-channels should be dropped. Hence, the cutoff was interpreted in Ref. [GM 93] as a way to have an interplay between both descriptions. However, in such approach crossing symmetry was broken. My present model relies entirely on effective field theory, I preserve crossing symmetry, and there is no need for that cutoff in the u-channel amplitudes. Ought to the vector coupling to the resonances, the u-channel amplitudes are suppresed by themselves which is a strong point in favor of the GI coupling.

4 Invariant Amplitudes

IN this chapter I provide all the invariant amplitudes needed for the calculations in the isospin decomposition and the notation for kinematics of chapter 2. I note by v the four momentum of the exchanged particle in each diagram.

4.1 Born Term Amplitudes

s-channel (Diagram (a) in Fig. 3.1)

$$A_s^0 = -F_B(s,u,t)\frac{ef_{\pi N}}{2m_\pi}\bar{u}(p')\not{k}\gamma_5\frac{\not{p}+M}{s-M^2}\left[\not{A}F_1^S - \frac{F_2^S}{2M}A^\alpha\gamma_{\alpha\beta}q^\beta\right]u(p) \quad (4.1)$$

$$A_s^- = A_s^+ = A_s^0\left(F_1^S \to F_1^V, F_2^S \to F_2^V\right) \quad (4.2)$$

u-channel (Diagram (b) in Fig. 3.1)

$$A_u^0 = -F_B(s,u,t)\frac{ef_{\pi N}}{2m_\pi}\bar{u}(p')\left[\not{A}F_1^S - \frac{F_2^S}{2M}A^\alpha\gamma_{\alpha\beta}q^\beta\right]\frac{\not{p}+M}{u-M^2}\not{k}\gamma_5 u(p) \quad (4.3)$$

$$A_u^+ = -A_u^- = A_u^0\left(F_1^S \to F_1^V, F_2^S \to F_2^V\right) \quad (4.4)$$

t-channel (Diagram (c) in Fig. 3.1)

$$A_t^- = -eF_B(s,u,t)F_1^V\frac{f_{\pi N}}{m_\pi}\bar{u}(p')\frac{A\cdot(v+k)}{t-m_\pi^2}\not{p}\gamma_5 u(p) \quad (4.5)$$

Kroll-Rudermann (Contact) Term (Diagram (d) in Fig. 3.1)

$$A_{KR}^- = eF_B(s,u,t)F_1^V\frac{f_{\pi N}}{m_\pi}\bar{u}(p')\not{A}\gamma_5 u(p) \quad (4.6)$$

4.2 Vector-Meson Amplitudes

ρ Meson (Diagram (f) in Fig. 3.2)

$$A^0_\rho = -ieF_\rho(t)\frac{G_{\rho\pi\gamma}F_{\rho NN}}{m_\pi}\bar{u}(p')\frac{\epsilon_{\sigma\lambda\nu\mu}q^\sigma k^\nu A^\lambda g^{\alpha\mu}}{t-m_\rho^2}\left[\gamma_\alpha + \frac{K_\rho}{2M}\gamma_{\alpha\beta}v^\beta\right]u(p) \tag{4.7}$$

ω Meson (Diagram (f) in Fig. 3.2)

$$A^+_\omega = -ieF_\omega(t)\frac{G_{\omega\pi\gamma}F_{\omega NN}}{m_\pi}\bar{u}(p')\frac{\epsilon_{\sigma\lambda\nu\mu}q^\sigma k^\nu A^\lambda g^{\alpha\mu}}{t-m_\omega^2}\left[\gamma_\alpha + \frac{K_\omega}{2M}\gamma_{\alpha\beta}v^\beta\right]u(p) \tag{4.8}$$

4.3 Nucleon Resonance Amplitudes

4.3.1 S_{11} Resonance Amplitudes

s-channel

$$A^0_{s,\mathrm{S}_{11}} = \sqrt{X_\pi(s,u)}\frac{eg_S h}{2Mf_\pi}\bar{u}(p')\not{k}G(v)A^\mu\gamma_{\mu\nu}q^\nu\gamma_5 u(p) \tag{4.9}$$

$$A^+_{s,\mathrm{S}_{11}} = A^-_{s,\mathrm{S}_{11}} = A^0_{s,\mathrm{S}_{11}}(g_S \to g_V) \tag{4.10}$$

u-channel

$$A^0_{u,\mathrm{S}_{11}} = -\sqrt{X_\pi(s,u)}\frac{eg_S h}{2Mf_\pi}\bar{u}(p')A^\mu\gamma_{\mu\nu}q^\nu\gamma_5 G(v)\not{k}u(p) \tag{4.11}$$

$$A^+_{u,\mathrm{S}_{11}} = -A^-_{u,\mathrm{S}_{11}} = A^0_{u,\mathrm{S}_{11}}(g_S \to g_V) \tag{4.12}$$

4.3.2 S_{31} Resonance Amplitudes

s-channel

$$A^+_{s,\mathrm{S}_{31}} = -2A^-_{s,\mathrm{S}_{31}} = \sqrt{X_\pi(s,u)}\frac{2}{3}\frac{egh}{Mf_\pi}\bar{u}(p')\not{k}G(v)A^\mu\gamma_{\mu\nu}q^\nu\gamma_5 u(p) \tag{4.13}$$

u-channel

$$A^+_{u,\mathrm{S}_{31}} = 2A^-_{u,\mathrm{S}_{31}} = -\sqrt{X_\pi(s,u)}\frac{2}{3}\frac{egh}{Mf_\pi}\bar{u}(p')A^\mu\gamma_{\mu\nu}q^\nu\gamma_5 G(v)\not{k}u(p) \tag{4.14}$$

4.3.3 P_{11} Resonance Amplitudes

s-channel

$$A^0_{s,\mathrm{P}_{11}} = \sqrt{X_\pi(s,u)}\frac{eg_S h}{2Mf_\pi}\bar{u}(p')\not{k}\gamma_5 G(v) A^\mu \gamma_{\mu\nu} q^\nu u(p) \tag{4.15}$$

$$A^+_{s,\mathrm{P}_{11}} = A^-_{s,\mathrm{P}_{11}} = A^0_{s,\mathrm{P}_{11}}(g_S \to g_V) \tag{4.16}$$

u-channel

$$A^0_{u,\mathrm{P}_{11}} = \sqrt{X_\pi(s,u)}\frac{eg_S h}{2Mf_\pi}\bar{u}(p') A^\mu \gamma_{\mu\nu} q^\nu G(v)\not{k}\gamma_5 u(p) \tag{4.17}$$

$$A^+_{u,\mathrm{P}_{11}} = -A^-_{u,\mathrm{P}_{11}} = A^0_{u,\mathrm{P}_{11}}(g_S \to g_V) \tag{4.18}$$

4.3.4 P_{33} Resonance Amplitudes

s-channel

$$\begin{aligned} A^+_{s,\mathrm{P}_{33}} = -2A^-_{s,\mathrm{P}_{33}} &= \sqrt{X_\pi(s,u)}\frac{-ihe}{f_\pi M^* M\left(M^*+M\right)} \\ &\times \bar{u}\left(p'\right)\epsilon_{\mu\nu\lambda\beta} v^\mu k^\lambda \gamma^\beta \gamma^5 G^{\nu\alpha}\left(v\right) \\ &\times \left[ig_1 \epsilon_{\omega\alpha\rho\phi} v^\omega q^\rho A^\phi + g_2\gamma^5\left(v\cdot qA_\alpha - v\cdot Aq_\alpha\right)\right] u\left(p\right) \end{aligned} \tag{4.19}$$

u-channel

$$\begin{aligned} A^+_{u,\mathrm{P}_{33}} = 2A^-_{u,\mathrm{P}_{33}} &= \sqrt{X_\pi(s,u)}\frac{ihe}{f_\pi M^* M\left(M^*+M\right)} \\ &\times \bar{u}\left(p'\right)\left[ig_1 \epsilon_{\mu\nu\alpha\beta} v^\mu q^\alpha A^\beta + g_2\gamma^5\left(v\cdot qA_\nu - v\cdot Aq_\nu\right)\right] \\ &\times G^{\nu\phi}\left(v\right)\epsilon_{\omega\phi\lambda\rho} v^\omega k^\lambda \gamma^\rho \gamma^5 u\left(p\right) \end{aligned} \tag{4.20}$$

4.3.5 D_{33} Resonance Amplitudes

s-channel

$$\begin{aligned} A^+_{s,\mathrm{D}_{33}} = -2A^-_{s,\mathrm{D}_{33}} &= \sqrt{X_\pi(s,u)}\frac{ihe}{f_\pi M M^*\left(M+M^*\right)} \\ &\times \bar{u}\left(p'\right)\epsilon_{\mu\nu\lambda\beta} v^\mu k^\lambda \gamma^\beta G^{\lambda\alpha}\left(v\right) \\ &\times \left[ig_1 \epsilon_{\omega\alpha\rho\phi} v^\omega q^\rho A^\phi \gamma^5 + g_2\left(v\cdot qA_\alpha - v\cdot Aq_\alpha\right)\right] u\left(p\right) \end{aligned} \tag{4.21}$$

u-channel

$$\begin{aligned} A^{+}_{u,\mathrm{D}_{33}} &= 2A^{-}_{u,\mathrm{D}_{33}} = \sqrt{X_\pi(s,u)}\frac{ieh}{f_\pi M M^* \left(M+M^*\right)} \\ &\times \bar{u}\left(p'\right)\left[ig_1\epsilon_{\mu\nu\alpha\beta}q^\alpha v^\mu A^\beta\gamma^5 + g_2\left(v\cdot qA_\nu - v\cdot Aq_\nu\right)\right] \\ &\times G^{\nu\lambda}\left(v\right)\epsilon_{\omega\lambda\rho\phi}v^\omega k^\rho\gamma^\phi u\left(p\right) \end{aligned} \tag{4.22}$$

4.3.6 $\mathbf{D_{13}}$ Resonance Amplitudes

s-channel

$$\begin{aligned} A^{0}_{s,\mathrm{D}_{13}} &= \sqrt{X_\pi(s,u)}\frac{3ihe}{4f_\pi M M^* \left(M+M^*\right)} \\ &\times \bar{u}\left(p'\right)\epsilon_{\mu\nu\lambda\beta}v^\mu k^\lambda\gamma^\beta G^{\lambda\alpha}\left(v\right) \\ &\times \left[ig_1^S\epsilon_{\omega\alpha\rho\phi}v^\omega q^\rho A^\phi\gamma^5 + g_2^S\left(v\cdot qA_\alpha - v\cdot Aq_\alpha\right)\right]u\left(p\right) \end{aligned} \tag{4.23}$$

$$A^{+}_{s,\mathrm{D}_{13}} = A^{-}_{s,\mathrm{D}_{13}} = A^{0}_{s,\mathrm{D}_{13}}\left(g^S_{1,2}\to g^V_{1,2}\right) \tag{4.24}$$

u-channel

$$\begin{aligned} A^{0}_{u,\mathrm{D}_{13}} &= \sqrt{X_\pi(s,u)}\frac{3ieh}{4f_\pi M M^* \left(M+M^*\right)} \\ &\times \bar{u}\left(p'\right)\left[ig_1\epsilon_{\mu\nu\alpha\beta}q^\alpha v^\mu A^\beta\gamma^5 + g_2\left(v\cdot qA_\nu - v\cdot Aq_\nu\right)\right] \\ &\times G^{\nu\lambda}\left(v\right)\epsilon_{\omega\lambda\rho\phi}v^\omega k^\rho\gamma^\phi u\left(p\right) \end{aligned} \tag{4.25}$$

$$A^{+}_{u,\mathrm{D}_{13}} = -A^{-}_{u,\mathrm{D}_{13}} = A^{0}_{u,\mathrm{D}_{13}}\left(g^S_{1,2}\to g^V_{1,2}\right) \tag{4.26}$$

5 Vertices and Propagators

THIS chapter provides a summary of all the vertices and propagators used in this thesis.

5.1 Vertices

Vertex $N\gamma N$

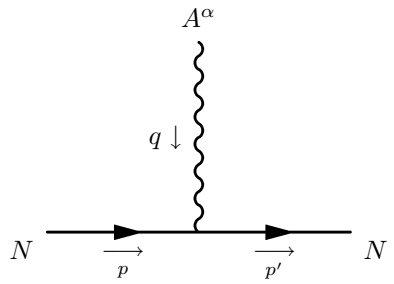

$$\begin{aligned}\Gamma_\alpha = &- ie\left[\frac{1}{2}F_1^V(Q^2)\left(F_1^{S/V}(Q^2)+\tau_3\right)\gamma_\alpha\right.\\ &\left.-\frac{1}{4M}F_2^V(Q^2)\left(F_2^{S/V}(Q^2)+\tau_3\right)\gamma_{\alpha\beta}q^\beta\right]\end{aligned} \tag{5.1}$$

Vertex $\pi\gamma\pi$

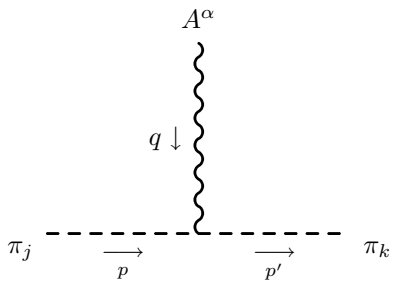

$$\Gamma_\alpha^{jk} = eF_1^V(Q^2)\,(p+p')_\alpha\,\varepsilon_{jk3} \tag{5.2}$$

Vertex $N\gamma\pi N$ (Kroll-Ruderman)

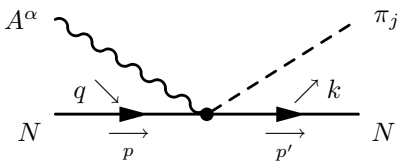

$$\Gamma^j_\alpha = \frac{e f_{\pi N}}{2m_\pi} F_1^V(Q^2)\gamma_\alpha\gamma_5[\tau_j, \tau_3] \tag{5.3}$$

Vertex $N\pi N$

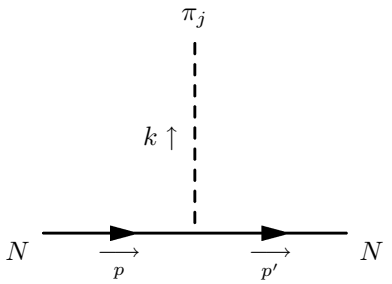

$$\Gamma^j = -\frac{f_{\pi N}}{m_\pi}\gamma_\alpha\gamma_5\tau_j k^\alpha \tag{5.4}$$

Vertex $N\omega N$

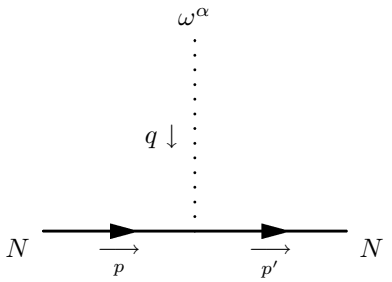

$$\Gamma_\alpha = -iF_{\omega NN}\left[\gamma_\alpha - \frac{K_\omega}{2M}\gamma_{\alpha\beta}q^\beta\right] \tag{5.5}$$

Vertex $\omega\gamma\pi$

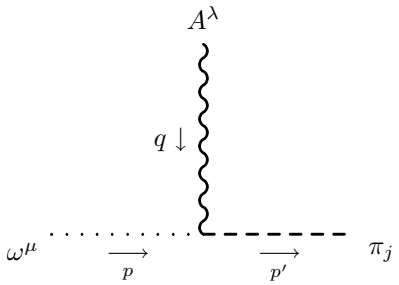

$$\Gamma^j_{\lambda\mu} = \frac{ieG_{\omega\pi\gamma}}{m}\varepsilon_{\sigma\lambda\nu\mu}q^\sigma p'^\nu\delta_{j3} \tag{5.6}$$

Vértice $N\rho N$

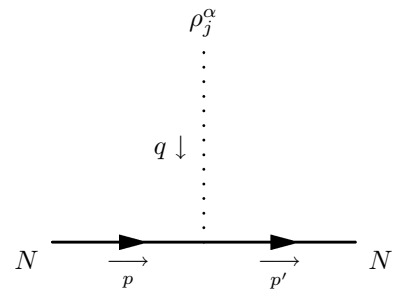

$$\Gamma^j_\alpha = -iF_{\rho NN}\left[\gamma_\alpha - \frac{K_\rho}{2M}\gamma_{\alpha\beta}q^\beta\right]\tau_j \tag{5.7}$$

Vertex $\rho\gamma\pi$.

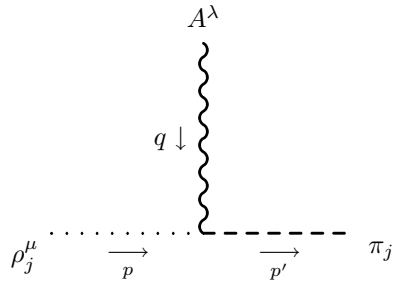

$$\Gamma^j_{\lambda\mu} = \frac{ieG_{\rho\pi\gamma}}{m}\varepsilon_{\sigma\lambda\nu\mu}q^\sigma p'^\nu\tau_j \tag{5.8}$$

Vertex $\mathbf{S_{11}\pi N}$

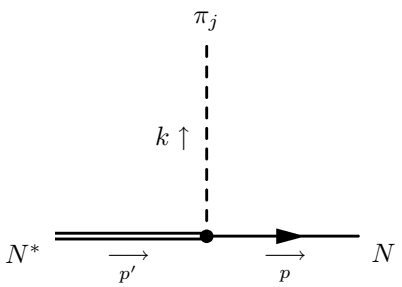

$$\Gamma^j = \frac{h}{f_\pi}\gamma_\alpha k^\alpha \tau_j \tag{5.9}$$

Vertex $\boldsymbol{N\pi S_{11}}$

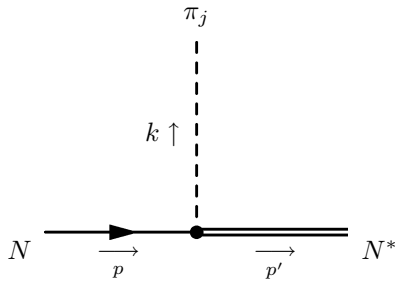

$$\Gamma^j = \frac{h}{f_\pi}\gamma_\alpha k^\alpha \tau_j \tag{5.10}$$

Vertex $\mathbf{S_{11}\gamma N}$

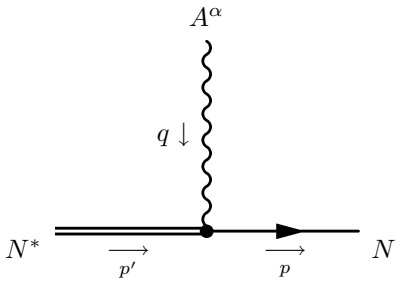

$$\Gamma_\alpha = i\frac{e}{2M}\gamma_{\alpha\beta}\gamma_5 \left(G_S + G_V\tau_3\right) q^\beta \tag{5.11}$$

Vertex $N\gamma S_{11}$

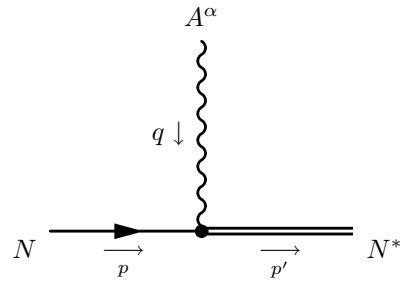

$$\Gamma_\alpha = -i\frac{e}{2M}\gamma_{\alpha\beta}\gamma_5\left(G_S + G_V\tau_3\right)q^\beta \tag{5.12}$$

Vertex $P_{11}\pi N$

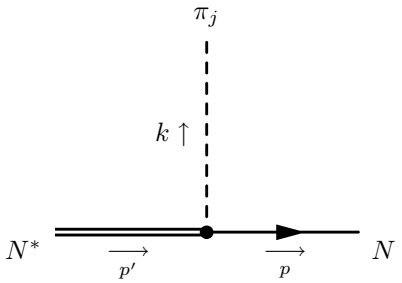

$$\Gamma^j = \frac{h}{f_\pi}\gamma_\alpha\gamma_5 k^\alpha \tau_j \tag{5.13}$$

Vertex $N\pi P_{11}$

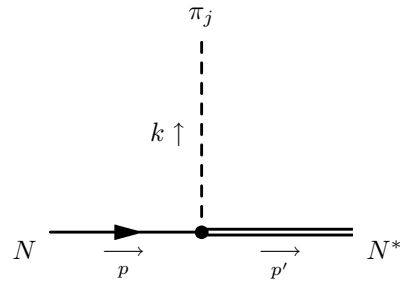

$$\Gamma^j = \frac{h}{f_\pi}\gamma_\alpha\gamma_5 k^\alpha \tau_j \tag{5.14}$$

Vertex $\mathbf{P_{11}\gamma N}$

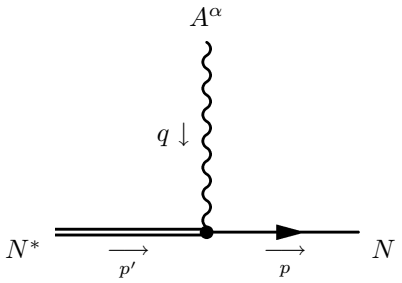

$$\Gamma_\alpha = -i\frac{e}{2M}\gamma_{\alpha\beta}\left(G_S + G_V\tau_3\right)q^\beta \tag{5.15}$$

Vertex $\boldsymbol{N\gamma P_{11}}$

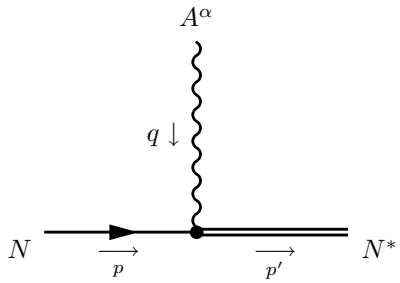

$$\Gamma_\alpha = -i\frac{e}{2M}\gamma_{\alpha\beta}\left(G_S + G_V\tau_3\right)q^\beta \tag{5.16}$$

Vertex $\mathbf{S_{31}\pi N}$

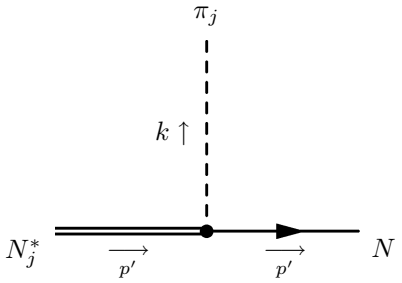

$$\Gamma = \frac{h}{f_\pi}\gamma_\alpha k^\alpha \tag{5.17}$$

Vertex $N\pi S_{31}$

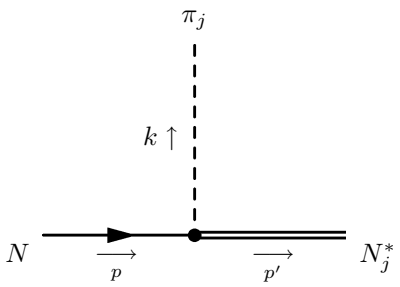

$$\Gamma = \frac{h}{f_\pi}\gamma_\alpha k^\alpha \tag{5.18}$$

Vertex $S_{31}\gamma N$

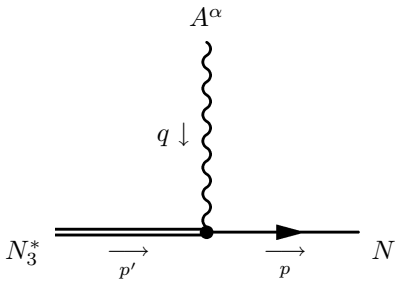

$$\Gamma_\alpha = i\frac{eG}{M}\gamma_{\alpha\beta}\gamma_5 q^\beta \tag{5.19}$$

Vertex $N\gamma S_{31}$

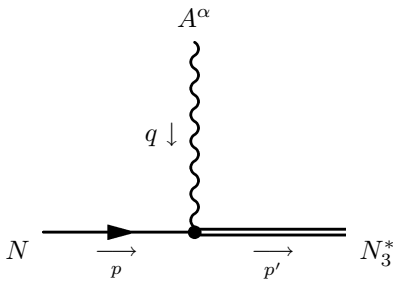

$$\Gamma_\alpha = -i\frac{eG}{M}\gamma_{\alpha\beta}\gamma_5 q^\beta \tag{5.20}$$

Vertex $\mathbf{P_{33}\pi N}$

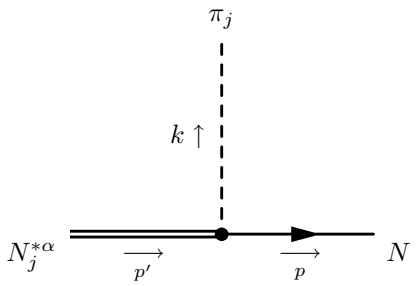

$$\Gamma_\nu = -i\frac{h}{M^* f_\pi}\epsilon_{\mu\nu\lambda\beta}\gamma^\beta p'^\mu k^\lambda \gamma^5 \tag{5.21}$$

Vertex $\boldsymbol{N\pi P_{33}}$

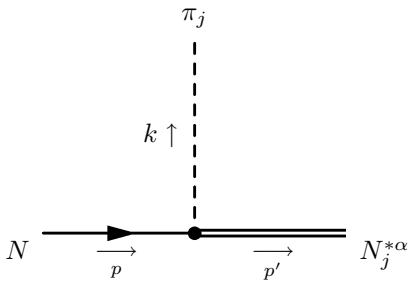

$$\Gamma_\nu = i\frac{h}{M^* f_\pi}\epsilon_{\mu\nu\lambda\beta}\gamma^\beta p'^\mu k^\lambda \gamma^5 \tag{5.22}$$

Vertex $\mathbf{P_{33}\gamma N}$

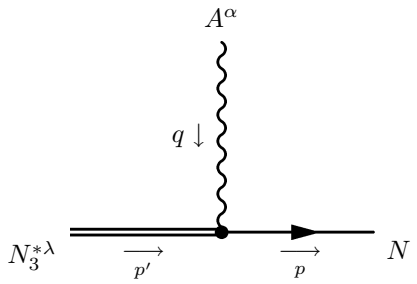

$$\Gamma_{\nu\beta} = -i\frac{3}{2}\frac{e}{M\left(M+M^*\right)}\left[ig_1\epsilon_{\mu\nu\alpha\beta}p'^\mu q^\alpha + g_2\gamma^5\left(p'\cdot q g_{\nu\beta} - p'_\beta q_\nu\right)\right] \tag{5.23}$$

Vertex $N\gamma P_{33}$

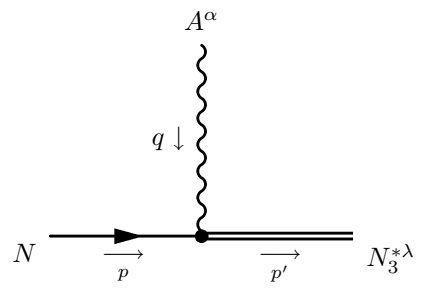

$$\Gamma_{\nu\beta} = -i\frac{3}{2}\frac{e}{M\left(M+M^*\right)}\left[ig_1\epsilon_{\mu\nu\alpha\beta}p'^{\mu}q^{\alpha} + g_2\gamma^5\left(p'\cdot q g_{\nu\beta} - p'_{\beta}q_{\nu}\right)\right] \tag{5.24}$$

Vertex $P_{13}\pi N$

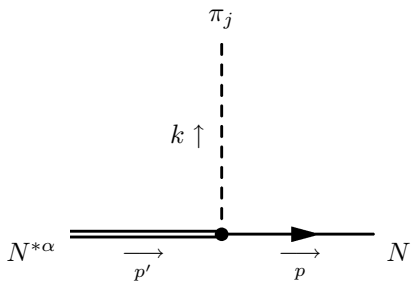

$$\Gamma_{\nu} = -i\frac{h}{M^* f_\pi}\epsilon_{\mu\nu\lambda\beta}\gamma^{\beta}p'^{\mu}k^{\lambda}\gamma^5\tau_j \tag{5.25}$$

Vertex $N\pi P_{13}$

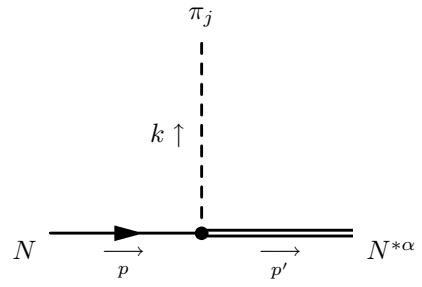

$$\Gamma^j_{\nu} = i\frac{h}{M^* f_\pi}\epsilon_{\mu\nu\lambda\beta}\gamma^{\beta}p'^{\mu}k^{\lambda}\gamma^5\tau_j \tag{5.26}$$

Vertex $\mathbf{P_{13}\gamma N}$

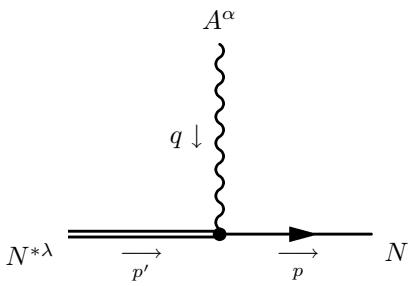

$$\begin{aligned}\Gamma_{\nu\beta} = &-i\frac{3}{4}\frac{e}{M\left(M+M^*\right)}\left[i\left(g_1^S+g_1^V\tau_3\right)\epsilon_{\mu\nu\alpha\beta}p'^{\mu}q^{\alpha}\right.\\ &\left.+\left(g_2^S+g_2^V\tau_3\right)\gamma^5\left(p'\cdot q g_{\nu\beta}-p'_{\beta}q_{\nu}\right)\right]\end{aligned} \tag{5.27}$$

Vertex $\boldsymbol{N\gamma P_{13}}$

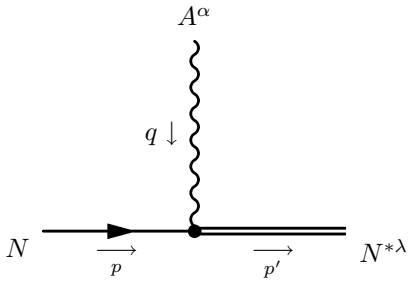

$$\begin{aligned}\Gamma_{\nu\beta} = &-i\frac{3}{4}\frac{e}{M\left(M+M^*\right)}\left[i\left(g_1^S+g_1^V\tau_3\right)\epsilon_{\mu\nu\alpha\beta}p'^{\mu}q^{\alpha}\right.\\ &\left.+\left(g_2^S+g_2^V\tau_3\right)\gamma^5\left(p'\cdot q g_{\nu\beta}-p'_{\beta}q_{\nu}\right)\right]\end{aligned} \tag{5.28}$$

Vertex $\mathbf{D_{33}\pi N}$

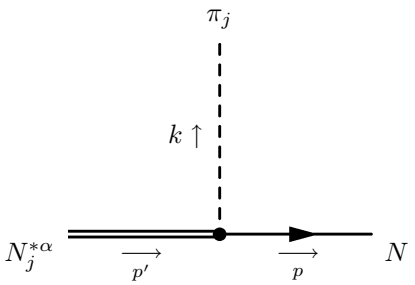

$$\Gamma_{\nu} = -i\frac{h}{M^* f_\pi}\epsilon_{\mu\nu\lambda\beta}\gamma^{\beta}p'^{\mu}k^{\lambda} \tag{5.29}$$

Vertex $N\pi D_{33}$

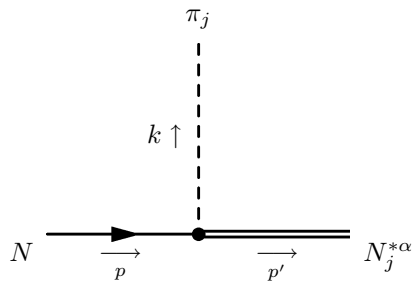

$$\Gamma_\nu = i\frac{h}{M^* f_\pi}\epsilon_{\mu\nu\lambda\beta}\gamma^\beta p'^\mu k^\lambda \tag{5.30}$$

Vertex $D_{33}\gamma N$

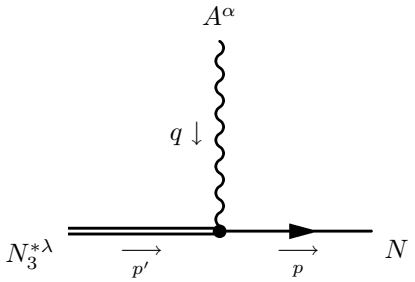

$$\Gamma_{\nu\beta} = i\frac{3}{2}\frac{e}{M\left(M+M^*\right)}\left[ig_1\epsilon_{\mu\nu\alpha\beta}p'^\mu q^\alpha\gamma_5 + g_2\left(p'\cdot q g_{\nu\beta} - p'_\beta q_\nu\right)\right] \tag{5.31}$$

Vertex $N\gamma D_{33}$

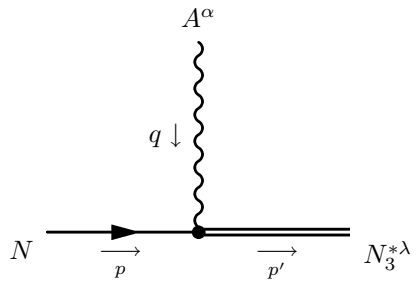

$$\Gamma_{\nu\beta} = -i\frac{3}{2}\frac{e}{M\left(M+M^*\right)}\left[ig_1\epsilon_{\mu\nu\alpha\beta}p'^\mu q^\alpha\gamma_5 + g_2\left(p'\cdot q g_{\nu\beta} - p'_\beta q_\nu\right)\right] \tag{5.32}$$

Vertex $\mathbf{D_{13}\pi N}$

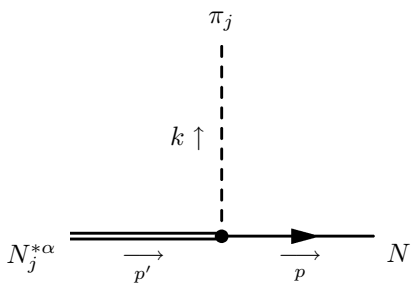

$$\Gamma_\nu^j = -i\frac{h}{M^* f_\pi}\epsilon_{\mu\nu\lambda\beta}\gamma^\beta p'^\mu k^\lambda \tau_j \tag{5.33}$$

Vertex $\mathbf{N\pi D_{13}}$

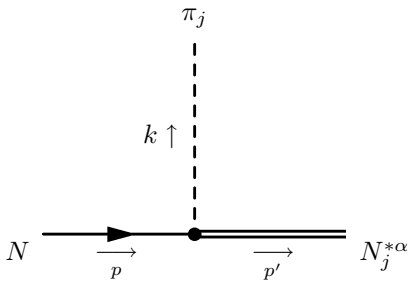

$$\Gamma_\nu^j = i\frac{h}{M^* f_\pi}\epsilon_{\mu\nu\lambda\beta}\gamma^\beta p'^\mu k^\lambda \tau_j \tag{5.34}$$

Vertex $\mathbf{D_{13}\gamma N}$

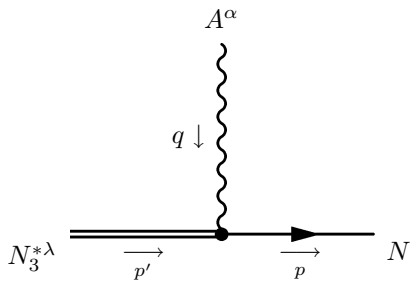

$$\begin{aligned}\Gamma_{\nu\beta} =& i\frac{3}{4}\frac{e}{M\left(M+M^*\right)}\left[i\left(g_1^S+g_1^V\tau_3\right)\epsilon_{\mu\nu\alpha\beta}p'^\mu q^\alpha\gamma_5\right.\\ &\left.+\left(g_2^S+g_2^V\tau_3\right)\left(p'\cdot q g_{\nu\beta}-p'_\beta q_\nu\right)\right]\end{aligned} \tag{5.35}$$

Vertex $N\gamma D_{13}$

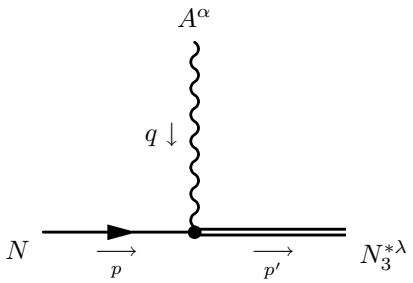

$$\begin{aligned}\Gamma_{\nu\beta} = &-i\frac{3}{4}\frac{e}{M\left(M+M^*\right)}\left[i\left(g_1^S+g_1^V\tau_3\right)\epsilon_{\mu\nu\alpha\beta}p'^{\mu}q^{\alpha}\gamma_5\right.\\ &\left.+\left(g_2^S+g_2^V\tau_3\right)\left(p'\cdot q g_{\nu\beta}-p'_{\beta}q_{\nu}\right)\right]\end{aligned} \tag{5.36}$$

5.2 Propagators

Spin-0 Propagator

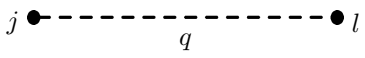

$$iG^0\left(q\right) = i\frac{\delta_{jl}}{q^2-m_\pi^2} \tag{5.37}$$

Spin-1/2 Propagator (Nucleon)

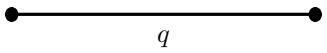

$$iG_N^{1/2}\left(q\right) = i\frac{\not{q}+M}{q^2-M^2} \tag{5.38}$$

Spin-1/2 Propagator (Spin-1/2 Resonances)

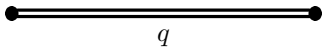

$$iG_R^{1/2}(q) = i\frac{\not{q} + M}{q^2 - M^2 + iM\Gamma(s,u)(q^2)} \tag{5.39}$$

Spin-1 Propagator (Vector Mesons)

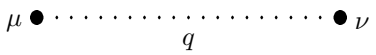

$$iG_{\mu\nu}^{1}(q) = -\frac{i}{q^2 - m_V^2}\left(g_{\mu\nu} - \frac{q_\mu q_\nu}{m_V^2}\right) \tag{5.40}$$

Spin-3/2 Propagator (Spin-3/2 Resonances)

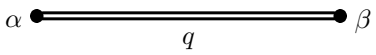

$$\begin{aligned} iG_{\alpha\beta}^{3/2}(q) = i\frac{\not{q} + M}{q^2 - M^2 + iM\Gamma(s,u)(q^2)}\Big[-g_{\alpha\beta} \\ +\frac{1}{3}\gamma_\alpha\gamma_\beta + \frac{2}{3M^2}q_\alpha q_\beta - \frac{1}{3M}(q_\alpha\gamma_\beta - \gamma_\alpha q_\beta)\Big] \end{aligned} \tag{5.41}$$

Part II

Study of the Parameters of the Model

6 Mesonic and Hadronic Coupling Constants

THE first choice that has to be made is the nucleon resonances to be taken into account. I have included seven resonances: $\Delta(1232)$, N(1440), N(1520), N(1535), $\Delta(1620)$, N(1650), and $\Delta(1700)$ which are all the four star nucleon resonances in PDG up to 1.7 GeV and up to spin-3/2. Among four star resonances only spin-5/2 N(1675) and N(1680) resonances are left aside for future work. In table 6.1 I show all the nucleon resonances and their status as they are presented in PDG.

In a Lagrangian model, the determination of the parameters of a single resonance is affected by the determination of the parameters of the other resonances. Thus, I have decided not to include three star resonances because their contribution would be very small and would introduce a sort of noise in the determination of the parameters.

There are quite a number of parameters to be set in the model. Some of them are well known and are established independently of the photoproduction data, such as nucleon and pion masses ($M = 938.9175$ MeV, $m_{\pi^0} = 134.9766$ MeV, $m_{\pi^\pm} = 139.5673$ MeV), but some others have to be established from fits to the pion photoproduction data, namely electromagnetic coupling constants. In the forthcoming paragraphs I give the values of every parameter of the model as well as the procedures employed to establish them.

6.1 Vector-Meson Coupling Constants

Vector-meson contributions are characterized by eleven parameters: m_ω, $F_{\omega NN}$, K_ω, $G_{\omega\pi\gamma}$, m_{ρ^0}, $m_{\rho^\pm}$, $F_{\rho NN}$, K_ρ, $G_{\rho^0\pi\gamma}$, $G_{\rho^\pm\pi\gamma}$, and cutoff Λ. Masses are given by PDG and the $\pi\gamma V$ couplings are related to the decay widths $\Gamma_{\pi\gamma V}$ of PDG [PDG 04] through the equation:

$$\Gamma_{V\to\pi\gamma} = \frac{e^2 G_{V\pi\gamma}^2}{96\pi}\frac{m_V^3}{m_\pi^2}\left(1-\frac{m_\pi^2}{m_V^2}\right)^3, \tag{6.1}$$

which is obtained from the equation for the decay of one particle into two [HM 84]:

Table 6.1. Nucleonic resonances in PDG. Resonances are catalogued by the PDG depending on a certain status Nucleon resonances are clasified according to a status which depends on the available experimental data. The nucleon resonances status is clasified as follows: **** Existence is certain, and properties are at least fairly well explored; *** Existence ranges from very likely to certain, but further confirmation is desirable and/or quantum numbers, branching fractions, etc, are not well determined; ** Evidence of existence is only fair; * Evidence of existence is poor.

Nucleon Resonance		Overall Status	Nucleon Resonance		Overall Status
$N(1440)$	P_{11}	****	$\Delta(1232)$	P_{33}	****
$N(1520)$	D_{13}	****	$\Delta(1600)$	P_{33}	***
$N(1535)$	S_{11}	****	$\Delta(1620)$	S_{31}	****
$N(1650)$	S_{11}	****	$\Delta(1700)$	D_{33}	****
$N(1675)$	D_{15}	****	$\Delta(1750)$	P_{31}	*
$N(1680)$	F_{15}	****	$\Delta(1900)$	S_{31}	**
$N(1700)$	D_{13}	***	$\Delta(1905)$	F_{35}	****
$N(1710)$	P_{11}	***	$\Delta(1910)$	P_{31}	****
$N(1720)$	P_{13}	****	$\Delta(1920)$	P_{33}	***
$N(1900)$	P_{13}	**	$\Delta(1930)$	D_{35}	***
$N(1990)$	F_{17}	**	$\Delta(1940)$	D_{33}	*
$N(2000)$	F_{15}	**	$\Delta(1950)$	F_{37}	****
$N(2080)$	D_{13}	**	$\Delta(2000)$	F_{35}	**
$N(2090)$	S_{11}	*	$\Delta(2150)$	S_{31}	*
$N(2100)$	P_{11}	*	$\Delta(2200)$	G_{37}	*
$N(2190)$	G_{17}	****	$\Delta(2300)$	H_{39}	**
$N(2200)$	D_{15}	**	$\Delta(2350)$	D_{35}	*
$N(2220)$	H_{19}	****	$\Delta(2390)$	F_{37}	*
$N(2250)$	G_{19}	****	$\Delta(2400)$	G_{39}	**
$N(2600)$	$I_{1\,11}$	***	$\Delta(2420)$	$H_{3\,11}$	****
$N(2700)$	$K_{1\,13}$	**	$\Delta(2750)$	$I_{3\,13}$	**
			$\Delta(2950)$	$K_{3\,15}$	**

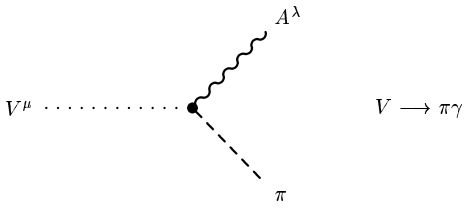

Fig. 6.1. Feynman diagram of the decay of a vector meson into a pion and a photon.

$$\Gamma\left(A \to 1+2\right) = \frac{|\vec{k}_1|}{32\pi^2 M_A^2} \int d\Omega \overline{|\mathcal{M}|^2}, \tag{6.2}$$

where Ω is the solid angle, M_A the mass of the decaying particle, and $\vec{k}_1$ the three momentum of the pion. For the vector-meson decay the invariant amplitude is

$$\overline{|\mathcal{M}|^2} = \sum_{helicities} \frac{e^2 G_{V\pi\gamma}^2}{m^2} |\varepsilon_{\sigma\lambda\nu\mu} q^\sigma p'^\nu A^\lambda V^\mu|^2 = \frac{3}{2} \frac{e^2 G_{V\pi\gamma}^2}{k^* m^2 m_V^2} \left(m_V^2 - m^2\right)^3, \tag{6.3}$$

which I obtain from the Feynman diagram in Fig. 6.1.

I take from PDG the following values: $m_\omega = 782.57$ MeV, $m_{\rho^0} = 768.5$ MeV, $m_{\rho^\pm} = 766.5$ MeV, $\Gamma_{\rho^0\pi\gamma} = 0.121$ MeV ($G_{\rho^0\pi\gamma} = 0.1161$), $\Gamma_{\rho^\pm\pi\gamma} = 0.068$ MeV ($G_{\rho^\pm\pi\gamma} = 0.0906$), and $\Gamma_{\omega\pi\gamma} = 0.70476$ MeV ($G_{\omega\pi\gamma} = 0.2804$). Thus, only five constants remain unknown. One of them is the cutoff Λ which will be discussed later. The four remaining constants are taken from the analysis of nucleon electromagnetic form factors by Mergell, Meißner, and Drechsel [MMD 96]: $F_{\rho NN} = 2.6$, $K_\rho = 6.1 \pm 0.2$, $F_{\omega NN} = 20.86 \pm 0.25$, and $K_\omega = -0.16 \pm 0.01$, which compare well to the data, including the latest experiments at Jefferson Lab. [Gay 03, Wu 03].

6.2 Masses and Widths of the Nucleon Resonances

I have used three different sets of masses and widths of the nucleon resonances (Table 6.2): First, the PDG values [PDG 04]; second, the unitary multichannel analysis of the processes $\pi N \to N\pi, N\eta, N\pi\pi, N\rho, N\sigma, N\omega$ performed by Vrana, Dytman, and Lee [VDL 00] based upon the the Carnegie-Mellon-Berkeley (CMB) model [CFHK 79]; and third, the speed plot (SP) calculation that I explain below. For the partial decay widths I have two different sets, one from PDG and one from Vrana *et al.*, which lies within the PDG error bars. The Vrana *et al.* set of partial decay widths has been chosen for the SP calculation.

Masses and widths of nucleon resonances can be obtained from πN partial wave analysis using the speed plot technique [Höh 98, TDHKY 01]. First I define the speed by

$$SP\left(W\right) = |dT\left(W\right)/dW|, \tag{6.4}$$

with $W = \sqrt{s}$ and

$$T\left(W\right) = \frac{1}{2i}\left[\mathrm{e}^{2i\delta(W)} - 1\right], \tag{6.5}$$

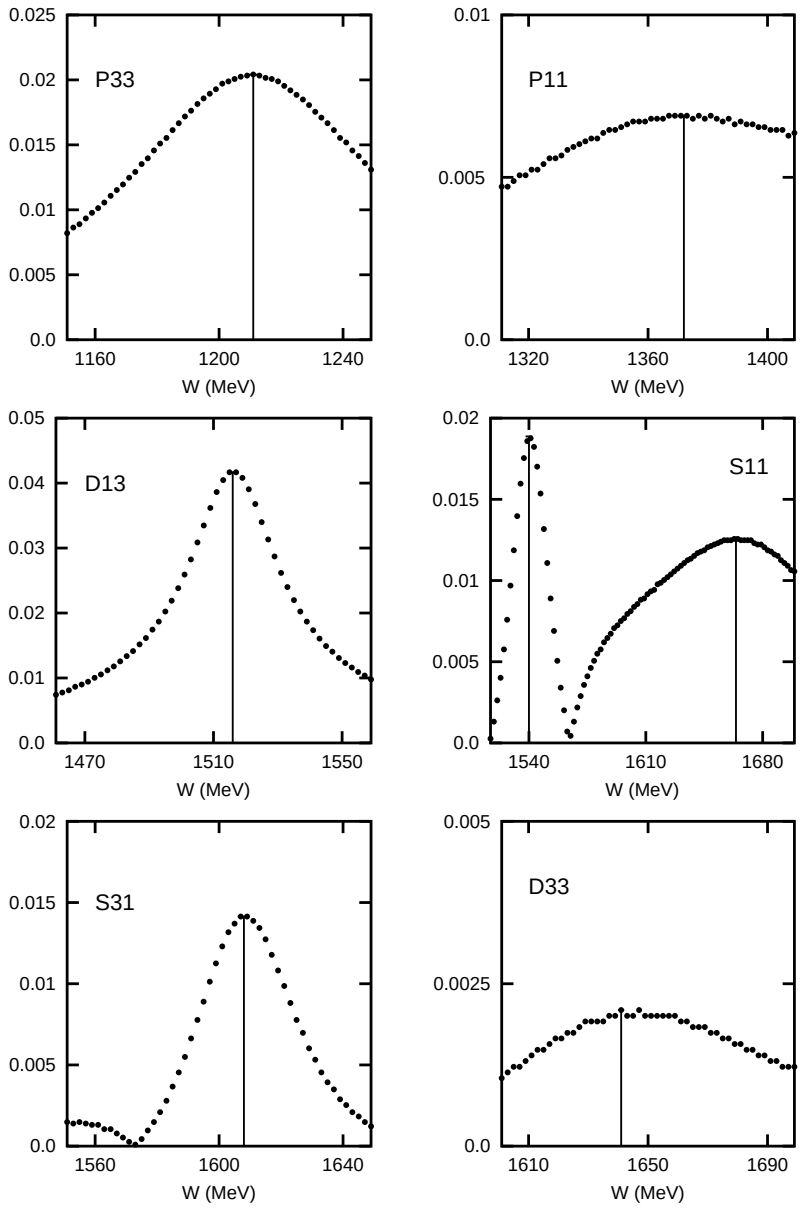

Fig. 6.2. Speed plot of the considered nucleon resonances. Data have been taken from SAID database for πN scattering [SAID].

Table 6.2. Masses, widths, and branching ratios from Refs. [PDG 04, VDL 00] and from the speed plot calculation (see text). Masses and widths in MeV. I have taken $\Gamma_{\pi\pi}/\Gamma = 1-\Gamma_\pi/\Gamma-\Gamma_\eta/\Gamma$. Subscripts PDG, VDL and SP stand for Particle Data Group [PDG 04], Vrana, Dytman, and Lee [VDL 00] and Speed Plot respectively. PDG masses and widths are mean values.

	$\Delta(1232)$	N(1440)	N(1520)	N(1535)	$\Delta(1620)$	N(1650)	$\Delta(1700)$
M_P^*	1210	1365	1510	1505	1607	1660	1660
M_{VDL}^*	1217	1383	1504	1525	1607	1663	1726
M_{SP}^*	1211	1372	1516	1540	1608	1664	1641
Γ_{PDG}	100	210	115	170	115	160	200
Γ_{VDL}	96	316	112	102	148	240	118
Γ_{SP}	98	290	48	107	141	159	955
Γ_π/Γ_{PDG}	1.00	0.65	0.55	0.45	0.25	0.72	0.15
Γ_η/Γ_{PDG}	–	0.00	0.00	0.51	–	0.06	–
$\Gamma_{\pi\pi}/\Gamma_{PDG}$	0.00	0.35	0.45	0.04	0.75	0.22	0.85
Γ_π/Γ_{VDL}	1.00	0.72	0.63	0.35	0.45	0.74	0.05
Γ_η/Γ_{VDL}	–	0.00	0.00	0.51	–	0.06	–
$\Gamma_{\pi\pi}/\Gamma_{VDL}$	0.00	0.28	0.37	0.14	0.55	0.20	0.95

where $T(W)$ is the dimensionless resonance partial wave amplitude and $\delta\,(W)$ its phase.

To calculate masses and widths I have taken phases from the current solution of the SAID (Scattering Analysis Interactive Dial-in) πN partial wave analysis [SAID]. In figure 6.2 I show $SP(W)$ for all the resonances considered in this thesis. The position of the peak provides the pole mass, and the height H provides the width: $\Gamma = 2/H$.

The baryon resonances show up clearly and the calculation is straightforward. The only problem is related to the existence of a background which induces a phase shift in the πN phases. In the region of the peak this phase shift can be considered approximately constant and its effect in $SP(W)$ is negligible.

My fits to photoproduction data shown in the next chapter are clasified according to six sets of parameters which are given in table 7.1. Sets #1 and #4 are based on PDG values for masses and widths; set #2 and set #4 are based on Vrana *et al.* [VDL 00]; and sets #3 and #6 are based on the SP calculation.

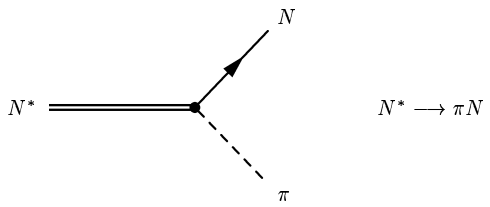

Fig. 6.3. Feynman diagram of the decay of a nucleon resonance into a pion [SAID].

The strong coupling constants (h's) for the resonances are obtained using the partial decay widths of the resonances into one pion. I obtain the decay widths by calculating the Feynman diagram in Fig. 6.3 for each resonance and applying equation (6.2):

$$\Gamma_{\pi}^{\mathrm{S}_{11}} = 3\frac{k^* h^2}{2\pi M^* f_{\pi}^2}\frac{\left[E_{\pi}\left(E_N + M\right) + k^{*2}\right]^2}{2\left(E_N + M\right)}, \tag{6.6}$$

$$\Gamma_{\pi}^{\mathrm{S}_{31}} = \frac{k^* h^2}{2\pi M^* f_{\pi}^2}\frac{\left[E_{\pi}\left(E_N + M\right) + k^{*2}\right]^2}{2\left(E_N + M\right)}, \tag{6.7}$$

$$\Gamma_{\pi}^{\mathrm{P}_{11}} = 3\frac{k^{*3} h^2}{2\pi M^* f_{\pi}^2}\frac{\left(E_N + M + E_{\pi}\right)^2}{2\left(E_N + M\right)}, \tag{6.8}$$

$$\Gamma_{\pi}^{\mathrm{P}_{33}} = \frac{h^2}{3\pi f_{\pi}^2}\frac{k^{*3}}{M^*}\left(E_N + M\right), \tag{6.9}$$

$$\Gamma_{\pi}^{\mathrm{D}_{33}} = \frac{h^2}{3\pi f_{\pi}^2}\frac{k^{*5}}{M^*}\frac{1}{E_N + M}, \tag{6.10}$$

$$\Gamma_{\pi}^{\mathrm{D}_{13}} = \frac{h^2}{\pi f_{\pi}^2}\frac{k^{*5}}{M^*}\frac{1}{E_N + M}, \tag{6.11}$$

where

$$k^* = \frac{1}{2M^*}\left[\left(M^{*2} - M^2 - m_{\pi}^2\right)^2 - 4m_{\pi}^2 M^2\right]^{\frac{1}{2}}, \tag{6.12}$$

$$E_{\pi} = \sqrt{k^{*2} + m_{\pi}^2}, \tag{6.13}$$

$$E_N = \sqrt{k^{*2} + M^2}, \tag{6.14}$$

I choose all the strong coupling constants to be positive, thus the overall sign of the amplitude of each resonance depends on the sign of the electromagnetic coupling constants.

7 Electromagnetic Coupling Constants of the Nucleon Resonances

AT this point, only the electromagnetic coupling constants and the cutoff Λ remain undetermined. The best way to establish them is by fitting pion photoproduction experimental data. Among all the observables (cross section, asymmetries, etc.) for pion photoproduction, the set of data I have chosen is the one given by the current SAID multipole energy independent solution [ABSW 02, ASW 96, AWLR 90a, SAID]. There are two main reasons for this choice. First, electromagnetic multipoles are directly related to the amplitudes and are more sensitive to coupling properties than are other observables. Deficiencies in the model show up much more clearly in multipoles than in any other observable. Second, all the observables can be expressed in terms of the multipoles, thus, if the multipoles are properly fitted by the model, so should be the other observables.

It is lenghtly but straightforward to calculate the electromagnetic multipoles from the invariant amplitudes in chapter 4. The initial state of the process is characterized by a photon with spin $\vec{s}_\gamma$ ($s_\gamma = 1$) and angular momentum $\vec{\ell}$ relative to the nucleon target which couples to a nucleon with spin $\vec{J}_N$ ($J_N = 1/2$) and parity $\Pi_N = 1$ in order to produce a spin $\vec{J}$ and parity Π intermediate state. The multipole expansion of the photon field provides electric (E) and magnetic (M) multipoles with parities $\Pi_\gamma = (-1)^L$ and $\Pi_\gamma = (-1)^{L+1}$ respectively. The following selection rules apply:

$$|L_\gamma - J_N| = |L_\gamma - \frac{1}{2}| \leq J \leq |L_\gamma + \frac{1}{2}| = |L_\gamma + J_N|, \tag{7.1}$$

$$\Pi = \Pi_N \cdot \Pi_\gamma = \Pi_\gamma. \tag{7.2}$$

The final state is composed by a nucleon and a pseudoscalar meson with orbital angular momentum L_π. Selection rules of the process are

$$|L_\pi - J_N| = |L_\pi - \frac{1}{2}| \leq J \leq |L_\pi + \frac{1}{2}| = |L_\pi + J_N|, \tag{7.3}$$

$$\Pi = \Pi_N \cdot \Pi_\pi \cdot (-1)^{L_\pi} = (-1)^{L_\pi + 1}. \tag{7.4}$$

Thus

$$\Pi_\gamma = \Pi = (-1)^{L_\pi + 1}, \tag{7.5}$$

$$L_\gamma \pm \frac{1}{2} = J = L_\pi \pm \frac{1}{2}, \tag{7.6}$$

where the '+' and the '−' are independent. There are two possibilities

$$\text{Electric} : L = L_\pi \pm 1, \tag{7.7}$$

$$\text{Magnetic} : L = L_\pi. \tag{7.8}$$

The multipoles are denoted by $E_{\ell\pm}$ and $M_{\ell\pm}$, where E and M stand for electric and magnetic multipoles respectively, $\ell = L_\pi$ is the relative orbital angular momentum of the final meson-nucleon system, and the '+' and the '−' indicate whether the nucleon spin must be added or substracted.

To calculate the electromagnetic multipoles I first need to define nucleon helicity spinors in the center of mass reference system. In momentum space, I normalise the spinors using the conventions of Ref. [HM 84]:

$$\bar{u}^r(p)\, u^s(p) = 2M\delta_{rs}, \tag{7.9}$$

$$\sum_s u^s(p)\bar{u}^s(p) = \not{p} + M, \tag{7.10}$$

where p is the nucleon four momentum, M the mass of the nucleon, and s and r stand for the spin third component. Under this normalisation, the free Dirac equation solution is:

$$u(p) = \sqrt{E+M}\begin{bmatrix} I \\ \frac{\vec{\tau}\cdot\vec{p}}{E+M} \end{bmatrix}\chi. \tag{7.11}$$

Helicity eigenstates are built to fulfill the following relations:

$$\frac{\vec{\tau}\cdot\vec{p}}{|\vec{p}|}\chi_{initial} = \pm\chi_{initial}, \tag{7.12}$$

for the initial spinor, and

$$\frac{\vec{\tau}\cdot\vec{p}\,'}{|\vec{p}\,'|}\chi_{final} = \pm\chi_{final}, \tag{7.13}$$

for the final spinor. In the center of mass reference system, with helicity defined along the incoming photon, the spinors are

$$u(p)^{\lambda=\frac{1}{2}} = \sqrt{\rho}\begin{bmatrix} 0 \\ 1 \\ 0 \\ \zeta \end{bmatrix}, \tag{7.14}$$

$$u(p)^{\lambda=-\frac{1}{2}} = \sqrt{\rho}\begin{bmatrix} 1 \\ 0 \\ -\zeta \\ 0 \end{bmatrix}; \tag{7.15}$$

for the incoming nucleon and

$$\bar{u}(p')^{\lambda=\frac{1}{2}} = \sqrt{\rho'}\left[-\sin\tfrac{\theta}{2}, \cos\tfrac{\theta}{2}, \zeta'\sin\tfrac{\theta}{2}, -\zeta'\cos\tfrac{\theta}{2}\right], \tag{7.16}$$

$$\bar{u}(p')^{\lambda=-\frac{1}{2}} = \sqrt{\rho'}\left[\cos\tfrac{\theta}{2}, \sin\tfrac{\theta}{2}, \zeta'\cos\tfrac{\theta}{2}, \zeta'\sin\tfrac{\theta}{2}\right]; \tag{7.17}$$

for the outgoing nucleon. Where

$$\rho = E^* + M, \tag{7.18}$$

$$\rho' = E'^* + M, \tag{7.19}$$

$$\zeta = \frac{p^*}{\rho}, \tag{7.20}$$

$$\zeta' = \frac{p'^*}{\rho'}. \tag{7.21}$$

I can now define the helicity amplitudes. Because of parity, among the eight helicity amplitudes, only four of them are independent:

$$H_N \equiv \mathcal{A}_{\frac{1}{2},\frac{1}{2}} \equiv \mathcal{A}_{\frac{1}{2},-\frac{1}{2},1} = -\mathcal{A}_{-\frac{1}{2},-\frac{1}{2}} = -\mathcal{A}_{-\frac{1}{2},\frac{1}{2},-1}, \tag{7.22}$$

$$H_{SF} \equiv \mathcal{A}_{\frac{3}{2},\frac{1}{2}} \equiv \mathcal{A}_{-\frac{1}{2},-\frac{1}{2},1} = \mathcal{A}_{-\frac{3}{2},-\frac{1}{2}} = \mathcal{A}_{\frac{1}{2},\frac{1}{2},-1}, \tag{7.23}$$

$$H_{SA} \equiv \mathcal{A}_{\frac{1}{2},-\frac{1}{2}} \equiv \mathcal{A}_{\frac{1}{2},\frac{1}{2},1} = \mathcal{A}_{-\frac{1}{2},\frac{1}{2}} = \mathcal{A}_{-\frac{1}{2},-\frac{1}{2}-1}, \tag{7.24}$$

$$H_D \equiv \mathcal{A}_{\frac{3}{2},-\frac{1}{2}} \equiv \mathcal{A}_{-\frac{1}{2},\frac{1}{2},1} = -\mathcal{A}_{-\frac{3}{2},\frac{1}{2}} = -\mathcal{A}_{\frac{1}{2},-\frac{1}{2},-1}. \tag{7.25}$$

Subindices stand for: N, non-spin flip; SF, spin flip with photon and initial nucleon having parallel spins; SA, spin flip with photon and initial nucleon having antiparallel spins; and D, double spin flip. In terms of these four independent helicity amplitudes (see chapter 2 for $\mathcal{A}_{\lambda_1,\lambda_2,\lambda_\gamma}$ definition), it is possible to write all the physical observables [AWLR 90a].

On the other hand, the pion photoproduction differential cross section can be written:

$$\frac{d\sigma}{d\Omega} = \sum_{\lambda\mu} |f_{\lambda\mu}(\theta, k)|^2, \tag{7.26}$$

where $\lambda = \lambda_\gamma - \lambda_1$ and $\mu = -\lambda_2$. $f_{\lambda\mu}$ and $\mathcal{A}_{\lambda\mu}$ are related by means of

$$f_{\lambda\mu} = \frac{1}{16\pi}\sqrt{\frac{k^*}{s^* E_\gamma^*}}\mathcal{A}_{\lambda\mu}, \tag{7.27}$$

which relates equation (7.26) with Eq. (2.12) in chapter 2.

If I project $f(\theta, k)$ using the Wigner d-function basis

$$f^j_{\lambda\mu}(k) = \frac{1}{2}\int_{-1}^{1} d(\cos\theta) d^j_{\lambda\mu}(\theta) f_{\lambda\mu}(\theta, k), \tag{7.28}$$

in this expansion

$$f_{\lambda\mu}(\theta,k)=\sum_j(2j+1)d^j_{\lambda\mu}(\theta)f^j_{\lambda\mu}\,(k)\,. \tag{7.29}$$

If I integrate Eq. (7.26) I obtain the optical theorem result:

$$\sigma=4\pi\sum_{\lambda\mu}\sum_j\left(2j+1\right)|f^j_{\lambda\mu}\,(k)\,|^2. \tag{7.30}$$

Wigner d-functions are related to the matrix elements of finite rotations and are used in the calculation of electromagnetic multipoles and helicity amplitudes. The matrix element of a finite rotation can be written

$$\mathcal{D}^j_{\lambda\mu}\equiv\langle j\lambda|D\left(\alpha\theta\gamma\right)|j\mu\rangle. \tag{7.31}$$

I define

$$D\left(\alpha\theta\gamma\right)=\mathrm{e}^{i\gamma J_z}\mathrm{e}^{i\theta J_y}\mathrm{e}^{i\alpha J_z}, \tag{7.32}$$

where α, θ, and γ are the Euler angles.

Given a representation where matrices J_z are diagonal, it holds:

$$\mathcal{D}^j_{\lambda\mu}\left(\alpha\theta\gamma\right)=\mathrm{e}^{i\lambda\gamma}d^j_{\lambda\mu}\left(\theta\right)\mathrm{e}^{i\mu\alpha}, \tag{7.33}$$

where the Wigner d-functions $d^j_{m'm}\left(\theta\right)$ are given by:

$$d^j_{\lambda\mu}\left(\theta\right)=\langle j\lambda|\mathrm{e}^{i\theta J_y}|j\mu\rangle. \tag{7.34}$$

Details on the calculation of d-functions and their relation to Jacobi and Legendre polynomials can be found in Ref. [Edm 74]. From a practical point of view my interest in d-functions is restricted to use them as an eigenfunction basis to project and perform partial wave expansions of amplitudes.

Wigner d-functions verify the following normalisation relation

$$\int_{-1}^{1}d\left(\cos\theta\right)d^j_{\lambda\mu}\left(\theta\right)d^{j'}_{\lambda'\mu'}\left(\theta\right)=\frac{2}{2j+1}\delta_{jj'}\delta_{\lambda\lambda'}\delta_{\mu'\mu}, \tag{7.35}$$

and the symmetry relations:

$$d^j_{\lambda,\mu}\left(\theta\right)=(-1)^{\mu-\lambda}\,d^j_{\mu,\lambda}\left(\theta\right)=d^j_{-\mu,-\lambda}\left(\theta\right). \tag{7.36}$$

I need the explicit expresion up to a certain j. The Wigner d-functions needed in this thesis are

$$d^1_{0,0}\left(\theta\right)=\cos\theta, \tag{7.37}$$

$$d^{1/2}_{1/2,1/2}\left(\theta\right)=\cos\frac{\theta}{2}, \tag{7.38}$$

$$d^{1/2}_{1/2,-1/2}\left(\theta\right)=-\sin\frac{\theta}{2}, \tag{7.39}$$

$$d^1_{1,1}(\theta) = \frac{1+\cos\theta}{2}, \tag{7.40}$$

$$d^1_{1,0}(\theta) = -\frac{\sin\theta}{\sqrt{2}}, \tag{7.41}$$

$$d^1_{1,-1}(\theta) = \frac{1-\cos\theta}{2}, \tag{7.42}$$

$$d^{3/2}_{3/2,3/2}(\theta) = \frac{1+\cos\theta}{2}\cos\frac{\theta}{2}, \tag{7.43}$$

$$d^{3/2}_{3/2,1/2}(\theta) = -\sqrt{3}\frac{1+\cos\theta}{2}\sin\frac{\theta}{2}, \tag{7.44}$$

$$d^{3/2}_{3/2,-1/2}(\theta) = \sqrt{3}\frac{1-\cos\theta}{2}\cos\frac{\theta}{2}, \tag{7.45}$$

$$d^{3/2}_{3/2,-3/2}(\theta) = -\frac{1-\cos\theta}{2}\sin\frac{\theta}{2}, \tag{7.46}$$

$$d^{3/2}_{1/2,1/2}(\theta) = \frac{3\cos\theta-1}{2}\cos\frac{\theta}{2}, \tag{7.47}$$

$$d^{3/2}_{1/2,-1/2}(\theta) = -\frac{3\cos\theta+1}{2}\sin\frac{\theta}{2}. \tag{7.48}$$

If more d-functions are necesary the following recurrence relations can be employed:

– if $j = \mu$

$$d^j_{\lambda j}(\theta) = (-1)^{j-\lambda}\left[\frac{(2j)!}{(j+\lambda)!\,(j-\lambda)!}\right]\left(\cos\frac{\theta}{2}\right)^{j+\lambda}\left(\sin\frac{\theta}{2}\right)^{j-\lambda}. \tag{7.49}$$

– if $j \neq \mu$

$$\begin{aligned} d^j_{\lambda\mu}(\theta) = &\left(\frac{j-\mu}{j-\lambda}\right)^{\frac{1}{2}} d^{j-1/2}_{\mu+1/2,\lambda+1/2}(\theta)\cos\frac{\theta}{2} \\ &- \left(\frac{j+\mu}{j-\lambda}\right)^{\frac{1}{2}} d^{j-1/2}_{\mu-1/2,\lambda+1/2}(\theta)\sin\frac{\theta}{2}. \end{aligned} \tag{7.50}$$

The amplitudes are expanded in partial waves depending on the angular momentum, the parity, and their electric or magnetic character. The helicity amplitudes are related to the multipoles by means of:

$$\begin{aligned} H_N = &\sum_{\ell=0}^{\infty}\frac{1}{\sqrt{2}}\cos\frac{\theta}{2}\left(P'_{\ell+1}-P'_{\ell}\right) \\ &\times\left[(\ell+2)\left(E_{\ell+}-M_{(\ell+1)-}\right)+\ell\left(M_{\ell+}+E_{(\ell+1)-}\right)\right] \\ = &-\sum_{\ell=0}^{\infty}\frac{(\ell+1)}{\sqrt{2}}d^j_{\frac{1}{2}\frac{1}{2}}(\theta) \\ &\times\left[(\ell+2)\left(E_{\ell+}-M_{(\ell+1)-}\right)+\ell\left(M_{\ell+}+E_{(\ell+1)-}\right)\right], \end{aligned} \tag{7.51}$$

$$\begin{aligned} H_{SF} &= \sum_{\ell=0}^{\infty} \frac{1}{\sqrt{2}} \sin\theta \cos\frac{\theta}{2} \left(P''_{\ell+1} - P''_{\ell}\right) \\ &\times \left[E_{\ell+} - M_{\ell+} - E_{(\ell+1)-} - M_{(\ell+1)-}\right] \\ &= \sum_{\ell=0}^{\infty} \frac{(\ell+1)}{\sqrt{2}} \left[\ell\,(\ell+2)\right]^{\frac{1}{2}} d^{j}_{\frac{3}{2}\frac{1}{2}}(\theta) \\ &\times \left[E_{\ell+} - M_{\ell+} - E_{(\ell+1)-} - M_{(\ell+1)-}\right], \end{aligned} \tag{7.52}$$

$$\begin{aligned} H_{SA} &= \sum_{\ell=0}^{\infty} \frac{1}{\sqrt{2}} \sin\frac{\theta}{2} \left(P'_{\ell+1} + P'_{\ell}\right) \\ &\times \left[(\ell+2)\left(E_{\ell+} + M_{(\ell+1)-}\right) + \ell\left(M_{\ell+} - E_{(\ell+1)-}\right)\right] \\ &= -\sum_{\ell=0}^{\infty} \frac{(\ell+1)}{\sqrt{2}} d^{j}_{\frac{1}{2}-\frac{1}{2}}(\theta) \\ &\times \left[(\ell+2)\left(E_{\ell+} + M_{(\ell+1)-}\right) + \ell\left(M_{\ell+} - E_{(\ell+1)-}\right)\right], \end{aligned} \tag{7.53}$$

$$\begin{aligned} H_{D} &= \sum_{\ell=0}^{\infty} \frac{1}{\sqrt{2}} \sin\theta \sin\frac{\theta}{2} \left(P''_{\ell+1} + P''_{\ell}\right) \\ &\times \left[E_{\ell+} - M_{\ell+} + E_{(\ell+1)-} + M_{(\ell+1)-}\right] \\ &= \sum_{\ell=0}^{\infty} \frac{(\ell+1)}{\sqrt{2}} \left[\ell\,(\ell+2)\right]^{\frac{1}{2}} d^{j}_{\frac{3}{2}-\frac{1}{2}}(\theta) \\ &\times \left[E_{\ell+} - M_{\ell+} + E_{(\ell+1)-} + M_{(\ell+1)-}\right], \end{aligned} \tag{7.54}$$

where the following relations have been applied:

$$\sin\theta \cos\frac{\theta}{2} \left(P''_{\ell+1} - P''_{\ell}\right) = -(\ell+1)\left[\ell\,(\ell+2)\right]^{\frac{1}{2}} d^{j}_{\frac{3}{2}\frac{1}{2}}(\theta), \tag{7.55}$$

$$\cos\frac{\theta}{2} \left(P'_{\ell+1} - P'_{\ell}\right) = (\ell+1)\, d^{j}_{\frac{1}{2}\frac{1}{2}}(\theta), \tag{7.56}$$

$$\sin\theta \sin\frac{\theta}{2} \left(P''_{\ell+1} + P''_{\ell}\right) = (\ell+1)\left[\ell\,(\ell+2)\right]^{\frac{1}{2}} d^{j}_{\frac{3}{2}-\frac{1}{2}}(\theta), \tag{7.57}$$

$$\sin\frac{\theta}{2} \left(P'_{\ell+1} + P'_{\ell}\right) = -(\ell+1)\, d^{j}_{\frac{1}{2}-\frac{1}{2}}(\theta), \tag{7.58}$$

where:

$$P'_{\ell} = \frac{d}{d\,(\cos\theta)} P_{\ell}. \tag{7.59}$$

If I project using d-functions, I can eliminate the angular dependence:

$$H_N^\ell = -\frac{1}{\sqrt{2}}\left[(\ell+2)\left(E_{\ell+} - M_{(\ell+1)-}\right) + \ell\left(M_{\ell+} + E_{(\ell+1)-}\right)\right], \tag{7.60}$$

$$H_{SF}^\ell = \frac{1}{\sqrt{2}}\left[\ell\left(\ell+2\right)\right]^{\frac{1}{2}}\left[E_{\ell+} - M_{\ell+} - E_{(\ell+1)-} - M_{(\ell+1)-}\right], \tag{7.61}$$

$$H_{SA}^\ell = -\frac{1}{\sqrt{2}}\left[(\ell+2)\left(E_{\ell+} + M_{(\ell+1)-}\right) + \ell\left(M_{\ell+} - E_{(\ell+1)-}\right)\right], \tag{7.62}$$

$$H_D^\ell = \frac{1}{\sqrt{2}}\left[\ell\left(\ell+2\right)\right]^{\frac{1}{2}}\left[E_{\ell+} - M_{\ell+} + E_{(\ell+1)-} + M_{(\ell+1)-}\right]. \tag{7.63}$$

Defining the helicity amplitudes:

$$A_{\ell+} = -\frac{\sqrt{2}}{4}\left(H_N^\ell + H_{SA}^\ell\right) = \frac{1}{2}\left[(\ell+2)\,E_{\ell+} + \ell M_{\ell+}\right], \tag{7.64}$$

$$A_{(\ell+1)-} = \frac{\sqrt{2}}{4}\left(H_N^\ell - H_{SA}^\ell\right) = \frac{1}{2}\left[(\ell+2)\,M_{(\ell+1)-} - \ell E_{(\ell+1)-}\right], \tag{7.65}$$

$$B_{\ell+} = \frac{\sqrt{2}}{2}\left[\ell\left(\ell+2\right)\right]^{-\frac{1}{2}}\left(H_{SF}^\ell + H_D^\ell\right) = E_{\ell+} - M_{\ell+}, \tag{7.66}$$

$$B_{(\ell+1)-} = \frac{\sqrt{2}}{2}\left[\ell\left(\ell+2\right)\right]^{-\frac{1}{2}}\left(H_{SF}^\ell - H_D^\ell\right) = E_{(\ell+1)-} - M_{(\ell+1)-}. \tag{7.67}$$

The multipoles are

$$E_{\ell+} = \frac{1}{\ell+1}\left[A_{\ell+} + \frac{\ell}{2}B_{\ell+}\right], \tag{7.68}$$

$$M_{\ell+} = \frac{1}{\ell+1}\left[A_{\ell+} - \frac{\ell+2}{2}B_{\ell+}\right], \tag{7.69}$$

$$E_{(\ell+1)-} = -\frac{1}{\ell+1}\left[A_{(\ell+1)-} - \frac{\ell+2}{2}B_{(\ell+1)-}\right], \tag{7.70}$$

$$M_{(\ell+1)-} = \frac{1}{\ell+1}\left[A_{(\ell+1)-} + \frac{\ell}{2}B_{(\ell+1)-}\right]. \tag{7.71}$$

In this thesis I only need the lowest order multipoles. I define:

$$H_{\lambda\mu}^{I,j}(W) = \frac{1}{8W\pi}\int_{-1}^{1} d\left(\cos\theta\right) d_{\lambda\mu}^{j}\left(\theta\right) A_{\lambda\mu}^{I}\left(\theta, W\right), \tag{7.72}$$

where j is the amplitude spin, and $W = \sqrt{s^*}$. $A_{\lambda\mu}^{I}\left(\theta, W\right)$ are the invariant amplitudes in the isospin basis $\left(A^{3/2}, {}_pA^{1/2}, {}_nA^{1/2}\right)$ which relates to the $\left(A^0, A^+, A^-\right)$ basis of chapter 2 through

$$A^{3/2} = A^+ - A^-, \tag{7.73}$$

$${}_pA^{1/2} = \frac{1}{3}A^+ + \frac{2}{3}A^- + A^0, \tag{7.74}$$

$${}_nA^{1/2} = -\frac{1}{3}A^+ - \frac{2}{3}A^- + A^0. \tag{7.75}$$

Under this decomposition Eq. (2.17) becomes:

$$\mathcal{M} = \chi_2^\dagger \left(\mathcal{T}_j^+ \, {}_pA^{1/2} + \mathcal{T}_j^- \, {}_nA^{1/2} + \mathcal{T}_j^{3/2} A^{3/2} \right) \pi_j \chi_1, \tag{7.76}$$

where

$$\mathcal{T}_j^+ = \frac{1}{2}\tau_j \left(1 + \tau_3\right), \tag{7.77}$$

$$\mathcal{T}_j^- = \frac{1}{2}\tau_j \left(1 - \tau_3\right), \tag{7.78}$$

$$\mathcal{T}_j^{3/2} = \delta_{j3} - \frac{1}{3}\tau_j\tau_3; \tag{7.79}$$

and the physical amplitudes are:

$$A\left(\gamma p \to p\pi^0\right) = {}_pA^{1/2} + \frac{2}{3}A^{3/2}, \tag{7.80}$$

$$A\left(\gamma n \to n\pi^0\right) = -{}_nA^{1/2} + \frac{2}{3}A^{3/2}, \tag{7.81}$$

$$A\left(\gamma n \to p\pi^-\right) = \sqrt{2}\left({}_nA^{1/2} + \frac{1}{3}A^{3/2} \right), \tag{7.82}$$

$$A\left(\gamma p \to n\pi^+\right) = \sqrt{2}\left({}_pA^{1/2} - \frac{1}{3}A^{3/2} \right). \tag{7.83}$$

The lowest order multipoles are [AWLR 90a, BDW 67, CGLN 57, Wal 69]:

$$E_{0+}^I = \frac{\sqrt{2}}{4}\left[H_{1/2,1/2}^{I,1/2} + H_{1/2,-1/2}^{I,1/2} \right], \tag{7.84}$$

$$M_{1-}^I = -\frac{\sqrt{2}}{4}\left[H_{1/2,1/2}^{I,1/2} - H_{1/2,-1/2}^{I,1/2} \right], \tag{7.85}$$

$$\begin{aligned} E_{1+}^I = & \frac{\sqrt{2}}{8}\left[\left(H_{1/2,1/2}^{I,3/2} + H_{1/2,-1/2}^{I,3/2} \right) \right. \\ & \left. - \frac{1}{\sqrt{3}}\left(H_{3/2,1/2}^{I,3/2} + H_{3/2,-1/2}^{I,3/2} \right) \right], \end{aligned} \tag{7.86}$$

$$\begin{aligned} M_{1+}^I = & \frac{\sqrt{2}}{8}\left[\left(H_{1/2,1/2}^{I,3/2} + H_{1/2,-1/2}^{I,3/2} \right) \right. \\ & \left. + \sqrt{3}\left(H_{3/2,1/2}^{I,3/2} + H_{3/2,-1/2}^{I,3/2} \right) \right], \end{aligned} \tag{7.87}$$

$$\begin{aligned} E_{2-}^I = & \frac{\sqrt{2}}{8}\left[\left(H_{1/2,1/2}^{I,3/2} - H_{1/2,-1/2}^{I,3/2} \right) \right. \\ & \left. + \sqrt{3}\left(H_{3/2,1/2}^{I,3/2} - H_{3/2,-1/2}^{I,3/2} \right) \right], \end{aligned} \tag{7.88}$$

$$M_{2-}^{I} = -\frac{\sqrt{2}}{8}\left[\left(H_{1/2,1/2}^{I,3/2} - H_{1/2,-1/2}^{I,3/2}\right) - \frac{1}{\sqrt{3}}\left(H_{3/2,1/2}^{I,3/2} - H_{3/2,-1/2}^{I,3/2}\right)\right]. \tag{7.89}$$

Another issue to take into account is unitarity. Models below the two pion production threshold fulfill Watson's theorem to achieve unitarity using either πN scattering phases [DHKT 99], dynamical models [FA 03, NBL 90, SL 96, SL 01, PT 04] or K matrix [DMW 91]. Beyond the two pion production limit, implementation of unitarity is unclear and usually relies on experimental data and/or extensions of the methods applied below the two pion threshold.

I would like to note that, although my calculation seems to be at tree-level, it is not quite so due to the inclusion of the width and the form factors, which effectively take into account higher order diagrams and structure effects. If I perform a truly tree-level calculation – straightforwardly from amplitudes of chapter 4 – I would find out that all the amplitudes are real and that it would be impossible to fulfill the unitarity condition $\mathcal{S}\mathcal{S}^{\dagger} = 1$, where $\mathcal{S}$ is the scattering matrix. In an effective Lagrangian perturbative model, unitarity should be restored by the inclusion of higher order diagrams. In this thesis, however, I adopt a phenomenological point of view. The main higher order effects can be taken into account including a width in the propagator, (which amounts to dress the propagator), and including effectively final state interactions (FSI) as I describe in chapter 3.5. Once the width is included, unitarity restoration may be achieved through FSI. I can assume that it is possible to isolate the FSI effects by factorizing the multipoles $\mathcal{M}$ in the following way:

$$\mathcal{M}^{I,\ell,\Pi} = |\mathcal{M}^{I,\ell,\Pi}|\mathrm{e}^{\delta_{width}} F^{I,\ell,\Pi}, \tag{7.90}$$

where $F^{I,\ell,\Pi}$ is a phase factor that takes into account FSI, and ℓ stands for orbital angular momentum, Π for parity, and I for isospin:

$$F^{I,\ell,\Pi} = \mathrm{e}^{i\delta_{FSI}^{I,\ell,\Pi}}. \tag{7.91}$$

Then, the absolute value of the multipoles must be well reproduced by the model and only the phases of the multipoles remain unknown. I am interested in the bare values of the coupling constants, so the best choice is to use directly the experimental phases. Hence, the multipole phase can be written as:

$$\delta^{I,\ell,\Pi} = \delta_{width} + \delta_{FSI}^{I,\ell,\Pi}, \tag{7.92}$$

where I call δ_{width} to the phase given by the calculated amplitudes. Comparison with experimental phase shifts ($\delta^{I,\ell,\Pi}$) provides me with the unknown final state interaction phase shifts $\delta_{FSI}^{I,\ell,\Pi}$. Phases $\delta^{I,\ell,\Pi}$ are taken

Table 7.1. Specifications of the parameter sets. Masses, widths, and Λ are in GeV. The coupling constants for the vector mesons are dimensionless. I provide also the $\chi^2/\chi^2_{\rm PDG}$ in order to compare fits.

Set	#1	#2	#3	#4	#5	#6
Masses & Widths	PDG	Vrana	SP	PDG	Vrana	SP
δ_{FSI}	Yes	Yes	Yes	No	No	No
$\chi^2/\chi^2_{\rm PDG}$	1	0.53	0.60	9.30	5.57	4.56
Λ	1.121	1.050	1.040	1.494	0.951	0.962
K_ρ	6.30	6.30	6.30	6.30	5.90	5.90
$F_{\omega NN}$	21.11	21.11	21.11	20.61	21.11	21.11
K_ω	-0.17	-0.17	-0.17	-0.15	-0.17	-0.17
M^* [Δ(1232)]	1.209	1.215	1.209	1.210	1.215	1.209
Γ [Δ(1232)]	0.102	0.098	0.100	0.102	0.094	0.099
M^* [N(1440)]	1.385	1.381	1.370	1.385	1.381	1.370
Γ [N(1440)]	0.160	0.318	0.292	0.260	0.314	0.288
M^* [N(1520)]	1.505	1.502	1.514	1.505	1.502	1.514
Γ [N(1520)]	0.110	0.110	0.050	0.110	0.110	0.050
M^* [N(1535)]	1.495	1.527	1.542	1.495	1.523	1.538
Γ [N(1535)]	0.250	0.104	0.109	0.099	0.100	0.109
M^* [Δ(1620)]	1.590	1.605	1.606	1.620	1.605	1.606
Γ [Δ(1620)]	0.100	0.150	0.143	0.100	0.150	0.143
M^* [N(1650)]	1.680	1.665	1.666	1.640	1.665	1.666
Γ [N(1650)]	0.150	0.238	0.157	0.150	0.242	0.157
M^* [Δ(1700)]	1.620	1.728	1.639	1.620	1.728	1.639
Γ [Δ(1700)]	0.250	0.120	0.957	0.250	0.120	0.957

from the current energy dependent multipole solution of SAID analysis [AWLR 90a, ASW 96, ABSW 02, SAID]. For each set of masses and widths, I obtain two types of fits, one with and one without SAID phases.

In order to fit the data and determine the best parameters of the resonances I have written a genetic algorithm combined with the `E04FCF` routine from NAG libraries [NAG]. Although genetic algorithms are computationally more expensive (in terms of computational effort) than other algorithms, it is much less likely for them to get stuck at local minima than for other methods,

Table 7.2. Coupling constants of the resonances. The E2/M1 Ratio (EMR) of $\Delta(1232)$ is also given. All magnitudes are dimensionless.

			#1	#2	#3	#4	#5	#6
$\Delta(1232)$	P_{33}	h	0.764	0.721	0.757	0.759	0.706	0.753
		g_1	6.061	5.574	5.630	6.254	5.382	4.984
		g_2	2.414	1.187	1.123	4.032	7.253	7.696
		G_E^Δ	-0.152	-0.076	-0.071	-0.255	-0.466	-0.485
		G_M^Δ	6.213	5.650	5.701	6.509	5.848	5.469
		EMR	-2.45%	-1.35%	-1.24%	-3.92%	-7.97%	-8.87%
N(1440)	P_{11}	h	0.213	0.304	0.303	0.272	0.302	0.300
		g^p	0.255	-0.269	-0.247	0.255	-0.164	0.017
		g^n	-0.125	0.273	0.234	-0.125	0.096	-0.128
N(1520)	D_{13}	h	0.560	0.567	0.366	0.560	0.567	0.360
		g_1^p	-5.753	-4.848	-5.607	-5.498	-0.580	-2.348
		g_1^n	1.217	2.829	1.982	0.301	-1.503	0.105
		g_2^p	-0.861	-0.645	-0.520	-0.920	-0.986	-0.691
		g_2^n	1.462	0.960	0.979	1.674	2.731	2.174
N(1535)	S_{11}	h	0.132	0.079	0.078	0.083	0.078	0.079
		g^p	0.219	0.078	0.028	0.435	0.230	0.084
		g^n	-0.102	-0.127	-0.080	-0.164	-0.195	-0.129
$\Delta(1620)$	S_{31}	h	0.133	0.159	0.155	0.126	0.159	0.155
		g	-0.154	-0.324	-0.308	-0.063	0.008	0.044
N(1650)	S_{11}	h	0.102	0.132	0.107	0.110	0.134	0.107
		g^p	0.113	-0.167	0.025	0.117	0.074	0.127
		g^n	0.018	0.411	0.324	0.019	0.281	0.056
$\Delta(1700)$	D_{33}	h	0.285	0.149	0.528	0.285	0.149	0.528
		g_1	-3.513	0.663	-11.875	-3.996	-19.642	-26.531
		g_2	1.871	0.548	-2.392	2.000	3.701	7.293

namely gradient based minimisation. Thus, in a multiparameter minimisation like the one I face here it is probably the best possibility to search for the minimum. A detailed explanation on the genetic algorithm used to assess the parameters can be found in chapter 8.

The function to minimise is the χ^2 defined as

$$\chi^2 = \sum_j \frac{\left(\mathcal{M}_j^{exp} - \mathcal{M}_j^{th}\right)^2}{\left(\Delta\mathcal{M}_j^{exp}\right)^2}, \tag{7.93}$$

where $\mathcal{M}^{exp}$ stands for the current energy independent extraction of the multipole analysis of SAID up to 1 GeV for E_{0+}, M_{1-}, E_{1+}, M_{1+}, E_{2-}, and M_{2-} multipoles in the three isospin channels $I = \frac{3}{2}, p, n$ for the $\gamma p \to \pi^0 p$ process. $\Delta\mathcal{M}^{exp}$ is the error and $\mathcal{M}^{th}$ is the multipole given by the model which depends on the parameters. These parameters are the cutoff Λ and the electromagnetic coupling constants in Table 7.2, which are related to the helicity amplitudes A_λ^I of the resonances in Table 7.3. The connection between my amplitudes and the helicity amplitudes of the resonances as they are found in Ref. [PDG 04] is straightforward. This connection is necessary in order to relate the coupling constants to the usual partial wave analyses. To perform this connection the isospin decomposition $\left(A^\Delta, A^p, A^n\right)$ is needed instead of the one in chapter 2. Both are related in the following way:

$$A^\Delta = \sqrt{\frac{2}{3}}\left(A^+ - A^-\right), \tag{7.94}$$

$$A^p = -\frac{1}{\sqrt{3}}\left(A^+ + 2A^- + 3A^0\right), \tag{7.95}$$

$$A^n = \frac{1}{\sqrt{3}}\left(A^+ + 2A^- - 3A^0\right). \tag{7.96}$$

And the helicity amplitudes are given by [AWLR 90b, GM 93]

$$A_\lambda^I d_{\lambda\mu}^j(\theta) = \frac{i}{8\pi(2j+1)}\sqrt{(2j+1)\frac{2\pi}{s^*}\frac{k^*}{q^*}\frac{M^*}{M}\frac{\Gamma^2}{\Gamma_\pi}}A^I_{\lambda_1\lambda_2\lambda_\gamma}, \tag{7.97}$$

where λ, μ, j, and $d_{\lambda\mu}^j(\theta)$ have the same meaning as in the electromagnetic multipoles calculation; Γ is the total decay width and Γ_π the pion-nucleon decay width of the resonance as defined in chapter 6.2. k^* and q^* are the pion and the photon momenta in the c.m. system. I define the kinematical coefficients:

$$q^* = \frac{M^{*2} - M^2}{2M^*}, \tag{7.98}$$

$$\xi = \frac{q^*}{\sqrt{q^{*2} + M^2} + M}, \tag{7.99}$$

$$T = \frac{1}{4}\frac{M^*}{M(M+M^*)}\frac{q^*}{\sqrt{M\xi}}, \tag{7.100}$$

to obtain finally the following results:

Resonance S_{11}

$$A_{1/2}^{p,n}(S_{11}) = \frac{1}{\sqrt{2}}\frac{eg^{p,n}}{M}\sqrt{\frac{\xi}{M}}(M + M^*). \tag{7.101}$$

Table 7.3. Helicity amplitudes in $\mathrm{GeV}^{-1/2}$ for the different sets.

			#1	#2	#3	#4	#5	#6
$\Delta(1232)$	P_{33}	$A^{\Delta}_{1/2}$	-0.129	-0.123	-0.123	-0.129	-0.101	-0.090
		$A^{\Delta}_{3/2}$	-0.247	-0.225	-0.224	-0.263	-0.248	-0.231
N(1440)	P_{11}	$A^{p}_{1/2}$	-0.061	0.064	0.058	-0.061	0.039	-0.004
		$A^{n}_{1/2}$	0.030	-0.065	-0.055	0.030	-0.023	0.030
N(1520)	D_{13}	$A^{p}_{1/2}$	-0.020	-0.020	-0.034	-0.015	0.027	0.006
		$A^{n}_{1/2}$	-0.050	-0.013	-0.022	-0.068	-0.121	-0.092
		$A^{p}_{3/2}$	0.161	0.129	0.136	0.161	0.095	0.092
		$A^{n}_{3/2}$	-0.128	-0.118	-0.107	-0.128	-0.190	-0.163
N(1535)	S_{11}	$A^{p}_{1/2}$	0.060	0.022	0.008	0.119	0.065	0.024
		$A^{n}_{1/2}$	-0.028	-0.036	-0.023	-0.045	-0.055	-0.037
$\Delta(1620)$	S_{31}	$A^{\Delta}_{1/2}$	0.038	0.081	0.077	0.016	-0.002	-0.011
N(1650)	S_{11}	$A^{p}_{1/2}$	0.037	-0.054	0.008	0.037	0.024	0.041
		$A^{n}_{1/2}$	0.006	0.133	0.105	0.006	0.091	0.018
$\Delta(1700)$	D_{33}	$A^{\Delta}_{1/2}$	0.109	0.015	0.222	0.119	0.406	0.573
		$A^{\Delta}_{3/2}$	0.063	0.055	0.057	0.063	-0.156	0.006

Resonance $\mathbf{S_{31}}$

$$A^{\Delta}_{1/2}(\mathrm{S}_{31}) = -\frac{1}{\sqrt{3}}\frac{eg}{M}\sqrt{\frac{\xi}{M}}\,(M+M^*)\,. \tag{7.102}$$

Resonance $\mathbf{P_{11}}$

$$A^{p,n}_{1/2}(\mathrm{P}_{11}) = -\frac{1}{\sqrt{2}}\frac{eg^{p,n}}{M}\sqrt{\frac{\xi}{M}}\,(M+M^*)\,. \tag{7.103}$$

Resonance $\mathbf{P_{33}}$

$$A^{\Delta}_{1/2}(\mathrm{P}_{33}) = -eT\sqrt{\frac{1}{2}}\,[g_1-\xi g_2]\,, \tag{7.104}$$

$$A^{\Delta}_{3/2}(\mathrm{P}_{33}) = -eT\sqrt{\frac{3}{2}}\,[g_1+\xi g_2]\,. \tag{7.105}$$

Resonance $\mathbf{D_{33}}$

$$A^{\Delta}_{1/2}\,(\mathrm{D}_{33}) = eT\frac{\sqrt{2}}{2}\,[g_2 - \xi g_1]\,, \tag{7.106}$$

$$A^{\Delta}_{3/2}\,(\mathrm{D}_{33}) = eT\sqrt{\frac{3}{2}}\,[g_2 + \xi g_1]\,. \tag{7.107}$$

Resonance $\mathbf{D_{13}}$

$$A^{p,n}_{1/2}\,(\mathrm{D}_{13}) = -eT\frac{3}{2\sqrt{3}}\,[g^{p,n}_2 - \xi g^{p,n}_1]\,, \tag{7.108}$$

$$A^{p,n}_{3/2}\,(\mathrm{D}_{13}) = -eT\frac{3}{2}\,[g^{p,n}_2 + \xi g^{p,n}_1]\,. \tag{7.109}$$

The minimisation procedure applied is the one presented in Fig. 7.1: First the genetic algorithm has been run and when the convergence conditions were accomplished, the `E04FCF` routine was used for fine tunning. I use the genetic algorithm solution as the initial value for the `E04FCF` routine from NAG libraries [NAG]. This `E04FCF` routine implements an algorithm that allows to find an unconstrained minimum of a sum of squares:

$$\text{Minimise } F(x_1 \ldots x_n) = \sum_{j=1}^{m} |f_j\,(x_1 \ldots x_n)\,|^2, \tag{7.110}$$

of m nonlinear functions in n variables ($m \geq n$). This algorithm does not require to know derivatives. From a starting point $x^{(1)}_1 \ldots x^{(1)}_n$ (in my case supplied by the genetic algorithm) the routine applies Newton method in order to reach the minimum. The Newton method uses a finite-difference approximation to the Hessian matrix to define the search direction.

It is a very accurate and fast converging algorithm once I have an initial solution close to the minimum I seek. Thus it is perfect for my fine tunning purpose. If I try to solve the optimisation problem by means of the `E04FCF` routine alone it shows completely useless and no reliable results are obtained because it gets stuck in the first local minimum found [IJR 04].

The code has been run many times with different seeds in order to ensure that the minimum was not local. I have taken into account 763 data for the real part of the multipoles and the same amount for the imaginary part. Thus, 1526 data points have been used in the fits.

In Tables 7.1, 7.2, and 7.3 I show results for the six different sets and provide the reader with all the parameters of the model. Table 7.1 shows masses and widths, the cutoff Λ, as well as the vector-meson parameters K_ρ, $F_{\omega NN}$, and K_ω, for each set. Table 7.2 provides all the coupling constants of the resonances as well as the the E2/M1 Ratio (EMR) of the $\Delta(1232)$ resonance. Table 7.3 contains the helicity amplitudes of the resonances which can be compared to those in other references such as [DMW 91, FM 97, GM 93, PDG 04].

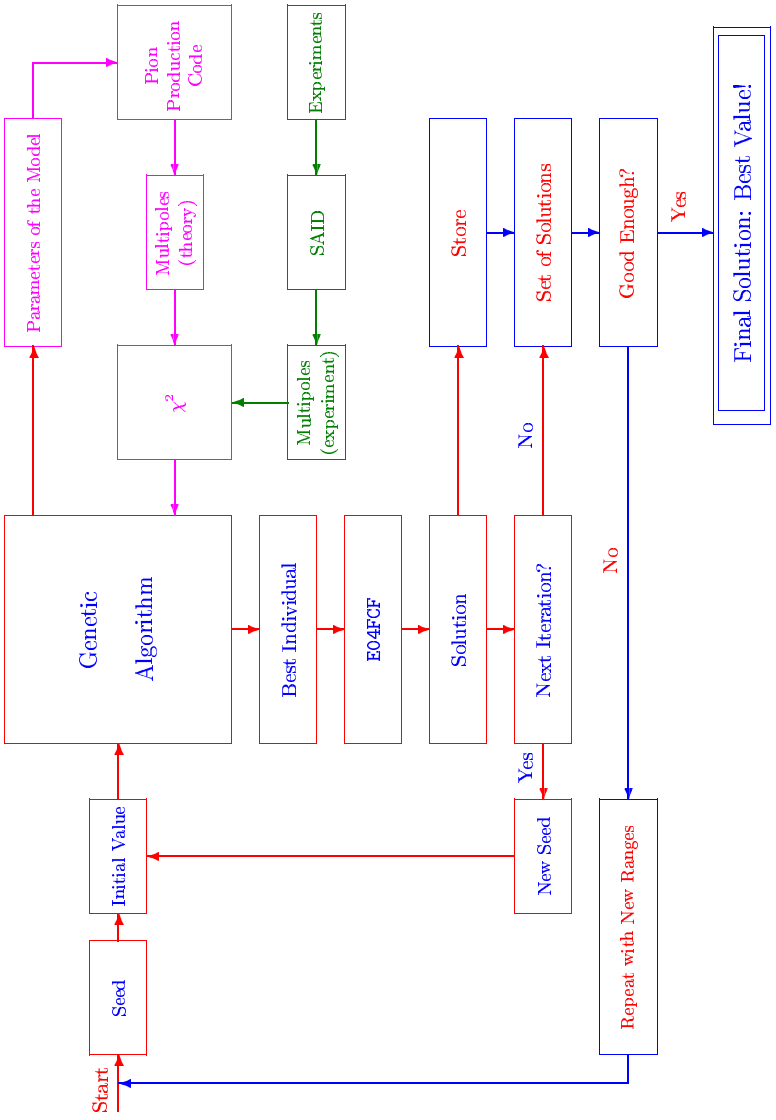

Fig. 7.1. Minimisation scheme applied to assess the values of the resonance parameters.

8 Genetic Algorithms

Britannica Encyclopædia [Britannica] provides the following definition for evolution:

> "theory in biology postulating that the various types of plants, animals, and other living things on Earth have their origin in other preexisting types and that the distinguishable differences are due to modifications in successive generations."

Following this definition it is possible to think about evolution in a simplified way and implement a mathematical model for it. I can consider evolution as an optimisation scheme where the different species evolve to optimal adaptation to the surrounding environment. Thus, evolution is an "algorithm" that searchs for best solutions creating a set of individuals (a generation), it decides which individuals are the best fit ones, and, by means of crossover, keeps the good genetic characteristics for the next generation – that will be closer to the optimal solution – and removes the individuals with less fit. Thus, Nature provides an optimisation scheme that has been used as the basis of genetic algorithms (GAs). During the last years these algorithms have been exploited to solve optimisation problems in different fields such as physics, chemistry, biology, engineering, and economy. In an optimisation problem the function to minimise plays the role of environment in Nature, a set of parameters to play the role of an individual, and a set of individuals that plays the role of a generation.

There are three different kinds of optimization strategies [Gol 89]:

1. Calculus-based methods, divided in two types.
   a) Indirect: I solve the equations obtained from setting the gradient to zero. This technique requires the function to be minimised to be smooth and requires the knowledge of the first derivatives.
   b) Direct: This method is based upon the hillclimbing idea. I climb the function in the steepest direction until I find a local optima. The `E04FCF` routine from NAG libraries I use for fine tunning is based upon this method.

   These methods are local and the hillclimbing strategy depends heavily on the initial point chosen to start climbing. They also require smoothness of the objective function and quite often also the existence of derivatives.

These methods are excellent in academic problems, but not in many practical ones as the one I face in this thesis.
2. Enumerative. In this case, every point in a discretization version of the parameter space is explored. If the search space is very small this method is succesful, but if not, the algorithm is useless because of efficiency and time.
3. Stochastic. There are several kinds of stochastic search methods and among them are GAs. In these methods, a certain randomness is intrinsic to the search. However, this does not mean that the search is directionless. For example, in GAs, the evaluation function and criteria to build up the generations provide strong guidance to the algorithm.

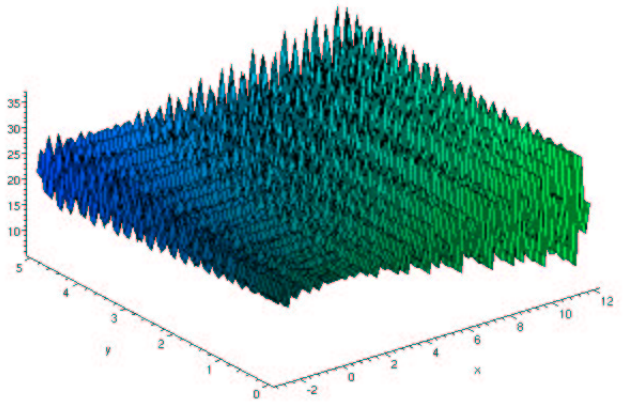

Fig. 8.1. Plot of a function which has so many local optima that a hillclimbing method to search for global optimum is useless.

In order to understand how a GA works compared to other methods it is useful the following example. Imagine that you want to know which one is the highest mountain in Himalaya. Hillclimbing methods are like dropping a climbing-loving kangaroo in the middle of Himalaya. As soon as you leave it, it starts climbing, so it is going to reach quickly the top of a certain peak, but nothing guarantees that the peak is Mount Everest. A GA works in a quite different way. It is like parachuting a lot of kangaroos into the Himalayas at random places. The kangaroos do not know what they are doing, they just wander in the area, mix with other kangaroos, and make more kangaroos. But every certain years I retire the kangaroos living at low altitudes and I hope the ones at higher altitudes will multiply. After several generations of kangaroos, only the best adapted to the highest altitude will remain in Himalaya, and at the very end only the ones on the top of Mount Everest (also perhaps the ones on the top of Mount K2) will stay [Mic 99].

From this example it stems clearly why a hillclimbing method would fail to find the optimum in a function like the one in Fig. 8.1 and a GA might have high chances of success. The main properties of GAs compared to hillclimbing methods are [Gol 89]:

- GAs do not work directly with the parameters. They work with a codification (an encoding scheme) of the parameters (the chromosome).
- Whereas most methods employ a single solution which evolves to reach the local optimum, GAs work on a population of many possible solutions simultaneously.
- GAs only need the objective function to determine how fit an individual is. Neither derivatives nor other auxiliary knowledge are required.
- GAs use probabilistic rules to evolve.

Instead of describing how GAs work from a general point of view I prefer to describe how the GA used in this thesis works and use it as a paradigm [Udi 03a, Udi 03b]. The code follows the scheme in Fig. 8.2.

1. I provide the first generation consisting of individuals randomly generated with reasonable values of the parameters.
2. The individuals are ordered according to the "fitness" function, in my case the χ^2 value. This is called "scaling of the population" and determines the probability that an individual has to mate and survive. I provide a 0.8 probability to the worst individual and 1.0 to the best. In order to keep genetic diversity it is good to avoid the best and the worst individuals having too different surviving probability. If I do not care about genetic diversity, the appearance of a very fit individual would make the forthcoming offsprings to collapse to that individual characteristics, with a loss of the good optimisation properties of GAs. Another important technique to maintain diversity is "mutation", which is discussed in a forthcoming paragraph.
3. After scaling, individuals are classified in two sets:
   a) A set consisting of a quarter of individuals, the top best quartile, that will be kept for the next generation.
   b) The remaining three quarters of the population.
4. I generate the offsprings in the following way:
   - 25% of the individuals are taken from the most fit ones of the previous generation
   - Another 25% is selected through fight among all the individuals (tournament). The fight depends on probability, and in the least favourable case the winning probability of an individual is 15%. Winning probabilities are computed accordingly to the fitness of each contender.
   - Another 25% is obtained by means of half-elitist crossover. It means that I mate an individual from the best 25% of the previous generation with an individual which was in the remaining 75%. Both individuals are selected randomly.

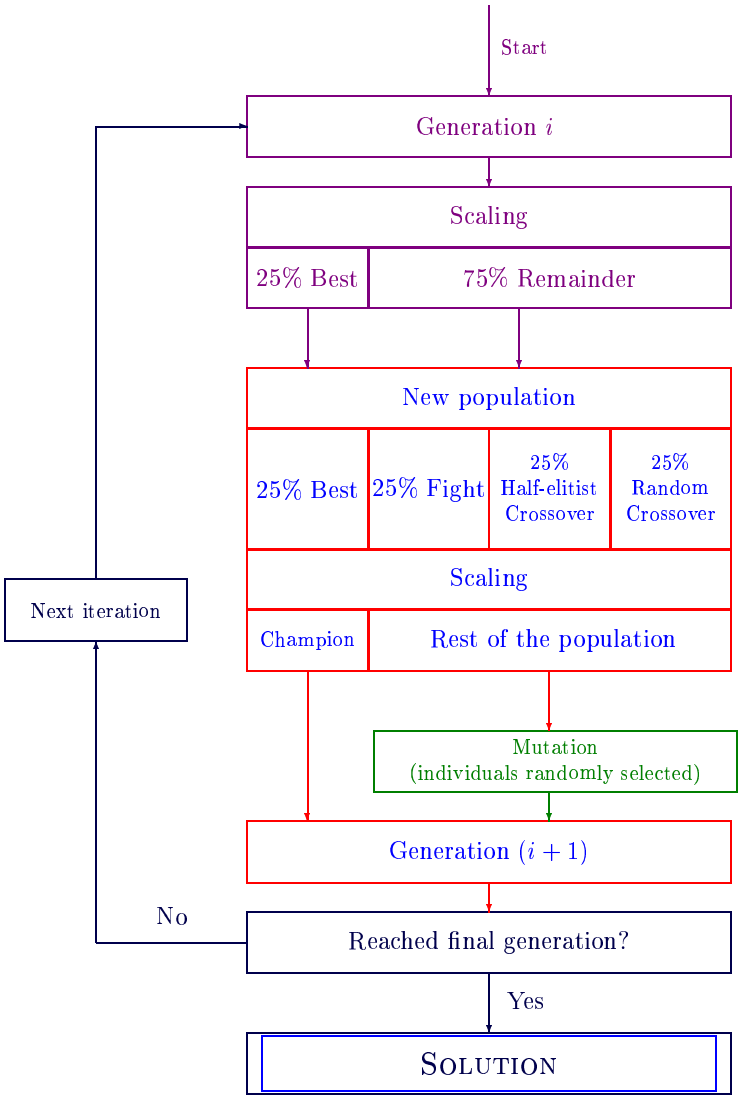

Fig. 8.2. Scheme of the genetic algorithm.

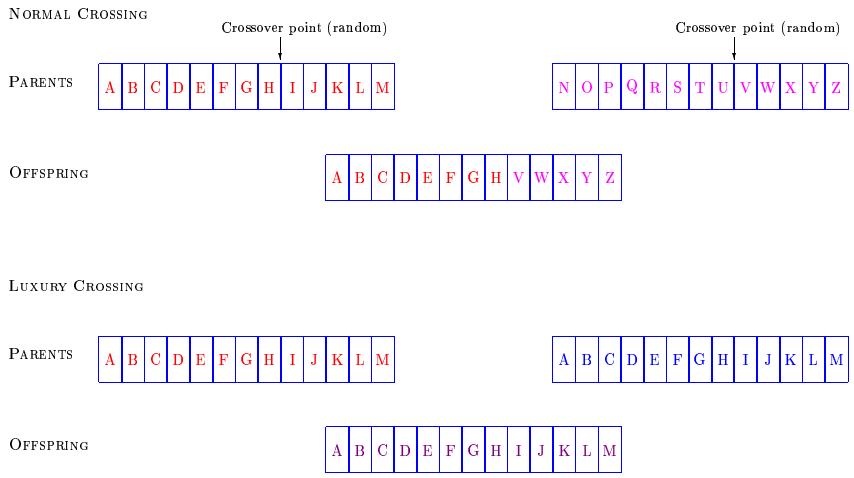

Fig. 8.3. Schemes of the crossovers used in the genetic algorithm to generate the offspring. In the upper figure I present the "normal" crossing, where parents are split in two parts and the first part from one parent is combined with the second from the other to generate the offspring. In the lower figure the "luxury" crossing is shown. The offspring is weighed average of both individuals with a weight $r \cdot 100\%$ from one parent and a weight $(1 - r) \cdot 100\%$ from the other, being r a random number within 0 and 1.

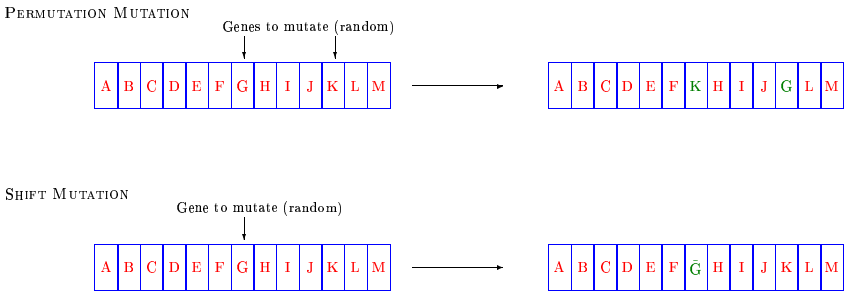

Fig. 8.4. Schemes of the mutations used in the genetic algorithm. The upper figure (permutation mutation) shows the exchange of two genes randomly selected. The lower figure (shift mutation) represents a small change in a gene.

- The remaining 25% of the offsprings is generated mating individuals selected randomly without restrictions.

In Fig. 8.3 I show the two different kinds of crossover I apply. For the "normal crossing" I select randomly a crosover point for the parents. I split each chromosome of the parents in two pieces. I take the second piece of the second parent and I attatch it to the first piece of the first parent. In this way I obtain an individual that is a mixture of the original ones. The second kind of crossover is the one I call "luxury crossover". I choose randomly a number r between 0 and 1, and the offspring is calculated weighting the parents with this probability. Half of the crossovers done are "normal" and the other half are "luxury". The kind of crossover to apply is selected randomly.

5. I evaluate the new population in order to obtain the best fit individual. This individual is called the "champion" and will be stored. Among the rest of the population I select individuals to mutate. Fig. 8.4 shows two types of mutation I have applied. The "permutation mutation" exchanges two genes selected randomly. The "shift mutation" changes the value of a gene in a small quantity. The amount of change is random within a range. Often, the crossover operator and selection method are too effective and they end up driving the genetic algorithm towards a population of individuals that are almost exactly the same. When the population consists of similar individuals the likelihood of finding new solutions typically decreases. The mutation operator introduces an amount of randomness to the search. It can help the search to keep diversity and to find solutions that crossover alone might not discover.
6. Finally, I have built up the new generation. If I have not reached the limit of generations, I run the algorithm again with the offspring as initial population. For the last computed generation, I choose the best individual as solution. If enough generations have been run, most of the individuals will have close values.

I have run the algorithm thirty times. In Fig. 8.5 I provide a sample of how the the process of optimum search evolves (set #2 calculation). The upper figure shows the evolution of each time the algorithm has been run. In spite of the fact that the convergence is accomplished quickly I decided to keep the algorithm running in order let mutation find other possible minima and to ensure that the absolute minimum was reached. When a jump in the χ^2/χ^2_{min} happens it is due to the appearance of a very good new individual due to either crossover of good individuals or to mutation. Each minimisation takes the algorithm 3.3 hours to calculate the minimum in a machine equivalent to a Pentium at 4 GHz. In the lower panel, the effect of NAG routine is appreciated. It is also shown how alike are the different minima obtained in each evaluation.

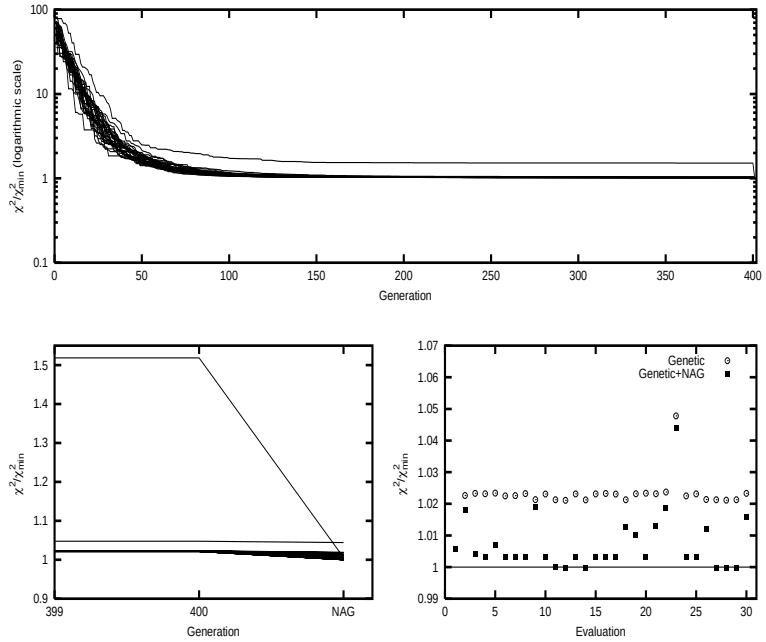

Fig. 8.5. Evolution of the minimisation. The upper figure shows the evolution of the χ^2/χ^2_{min} with the generations of the genetic algorithm in a logarithm scale. The lower-left figure shows the effect of the fine tunning performed by the `E04FCF` routine in the χ^2/χ^2_{min}. The lower-right figure shows the minima obtained each time the algorithm has been run (the χ^2/χ^2_{min} obtained for the first evaluation is out of the scale).

Part III

Results

9 Analysis of the Electromagnetic Multipoles

AS has been previously explained, in order to determine the parameters of the resonances and the cutoff value I have used data for electromagnetic multipoles. In this section I discuss the results obtained for multipoles as well as the quality of the different fits.

9.1 Electromagnetic Multipoles

Effective Lagrangian models, like the one presented here, are more complicated than Breit-Wigner models such as MAID [DHKT 99]. The latter are simple and describe accurately experimental observables, but do not provide much information about properties of the resonances such as the strength of the couplings. Breit-Wigner treatment of resonances can be considered naive because each resonance contributes only to the multipole with its same angular momentum quantum number and thus there is no background from resonances, what is very different from Lagrangian models where, for a given resonance, the direct term contributes only to a single spin-isospin channel, while the crossed term contributes to different spin-isospin channels as background, and then one resonance does indeed affect to the determination of the parameters of other resonances. Contributions from crossed terms to the background cannot be neglected and there are resonant contributions to several multipoles. For instance, N(1520) contributes to $E_{2-}^{p,n}$ and $M_{2-}^{p,n}$, as expected for a D_{13} isobar, but on the other hand, it also contributes strongly to M_{1+}^{p}. The background of Breit-Wigner models is much simpler because it only has contributions from Born terms and vector mesons (ρ and ω).

Figures 9.1, 9.2, and 9.3 show the comparison of the six different sets of Table 7.1 to experimental data from SAID database [SAID]. Without FSI at low energies, I get nice fits to some of the multipoles: $M_{1+}^{3/2}$, $E_{2-}^{3/2}$, and E_{2-}^{p}. With increasing energy there is a breakdown of the model which calls for further improvements. The major ingredient that lacks the model is FSI, which I introduce phenomenologically as described in section 7. Indeed, the fits are greatly improved – specially the fits of the imaginary parts of the multipoles – when FSI are included, as it stems from the comparison of the χ^2 (Table 7.1). The experimental data are quite well reproduced by theory with better quality for the low energy region than for the high energy (900

MeV and further), where some of the fits start to deviate from the data increasingly with energy (i.e. $\mathrm{Im}\left[M^p_{1+}\right]$ and $\mathrm{Im}\left[E^n_{0+}\right]$). In this section I focus on fits that include FSI, except in the case in which comparison with non-FSI sets provides relevant information.

Despite of the difference between SP and Vrana *et al.* masses and widths, the curves that I obtain for sets #2 and #3 are very close to each other (so are their χ^2, see Table 7.1), sometimes undistinguishable, except for some high order multipoles as $\mathrm{Im}\left[M^p_{2-}\right]$. Curves from set #1 do not reproduce data as well as #2 and #3 do and the χ^2 is almost twice as large due to the additional restrictions in the values of the parameters.

If I go through the multipoles in detail, it is convenient to start with $E^{3/2}_{1+}$ and $M^{3/2}_{1+}$ (both in Fig. 9.1) which provide information about the most important low-lying nucleon resonance, the $\Delta(1232)$. These multipoles are of great interest at present and a lot of experimental effort has been put in the study of the $\Delta(1232)$ in the last years [Bel 99, Bla 01]. The $M^{3/2}_{1+}$ presents a quite simple structure which is very well reproduced by all my sets and is not affected by FSI. That is why all sets are quite similar. Sets #1, #4, and #5 overestimate the multipole peaks which will cause an overestimation of the cross section as will be seen in section 12. The situation is much more complicated for the $E^{3/2}_{1+}$, where the FSI are critical, as can be inferred when I compare data to sets with and without FSI and check the strong differences among them. For these multipoles, data cannot be well reproduced without the inclusion of δ_{FSI}. When the latter is included the multipoles show an abrupt change at $\sqrt{s} = 1.249$ GeV. This behaviour is also seen in experimental data.

The multipoles M^p_{1-} and M^n_{1-} are closely related to the N(1440) resonance. If I focus on sets #2 and #3, when δ_{FSI} is included the fits look quite well except for the real part of the M^n_{1-} (second figure of the left panel in Fig. 9.3) where a serious discrepancy between theory and data is found in the $0.2 - 0.5$ GeV energy range. Also, a rather odd behaviour in the M^p_{1-} is found between 0.3 and 0.4 GeV (see Fig. 9.2), where no experimental data are available. For these multipoles related to N(1440) resonance, background and resonant contributions are not well established. As a consequence, the parameters of the P_{11} resonance cannot be well determined. These multipoles also show the importance of FSI in the model in order to determine the properties of the resonances because of the large discrepancies among fits with and without δ_{FSI}. However, if I focus on sets #1 and #4, FSI do not seem so important when the PDG values are used. Actually, set #4 provides better results than set #1 except for the high energy region of $\mathrm{Re}\left[M^p_{1-}\right]$ and $\mathrm{Re}\left[M^n_{1-}\right]$. More research on the properties of this resonance (and of its role in nuclear medium) has to be done in forthcoming years [KS 03].

Resonance N(1520) contributes mainly to $E^{p,n}_{2-}$ and $M^{p,n}_{2-}$ due to its angular momentum and isospin. It also contributes sizeably to other multipoles. The s-channel contributes to M^p_{1+} and its crossed term to $\mathrm{Im}\left[M^{3/2}_{1-}\right]$ as back-

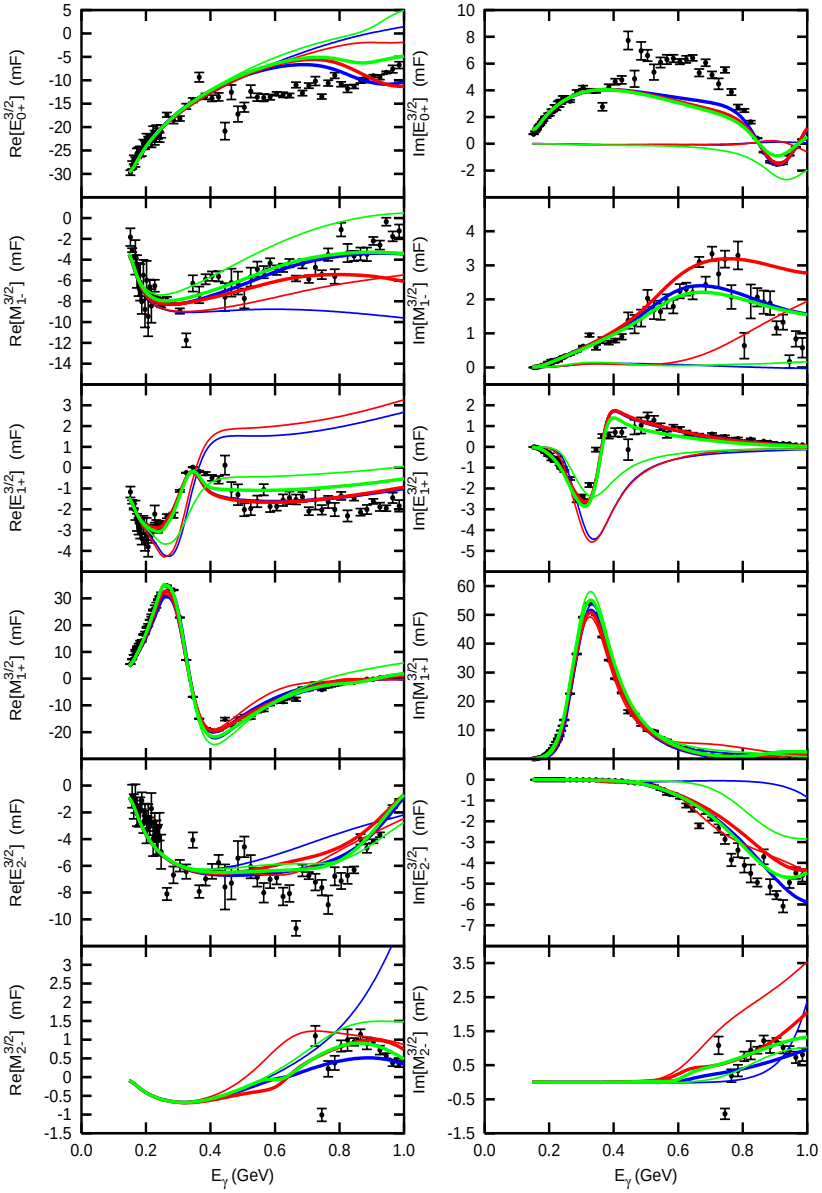

Fig. 9.1. Electromagnetic multipoles for the isospin-3/2 channel. Data have been taken from Ref. [SAID]. Photon energy is given in the laboratoy frame. Curves conventions: thick green set #1; thick blue set #2; thick red set #3; thin green set #4; thin blue set #5; thin red set #6.

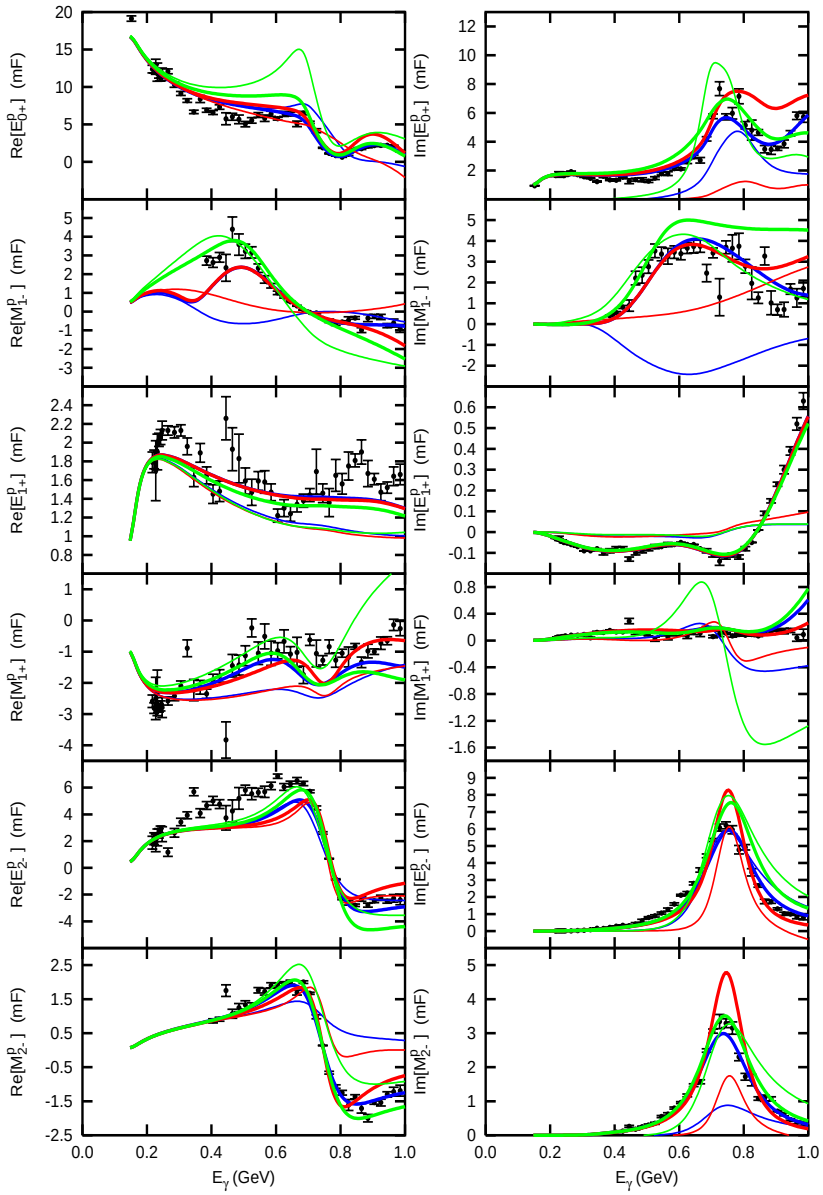

Fig. 9.2. Electromagnetic multipoles for the isospin-1/2 proton channel. Same conventions as in Fig. 9.1 apply. Data have been taken from Ref. [SAID]

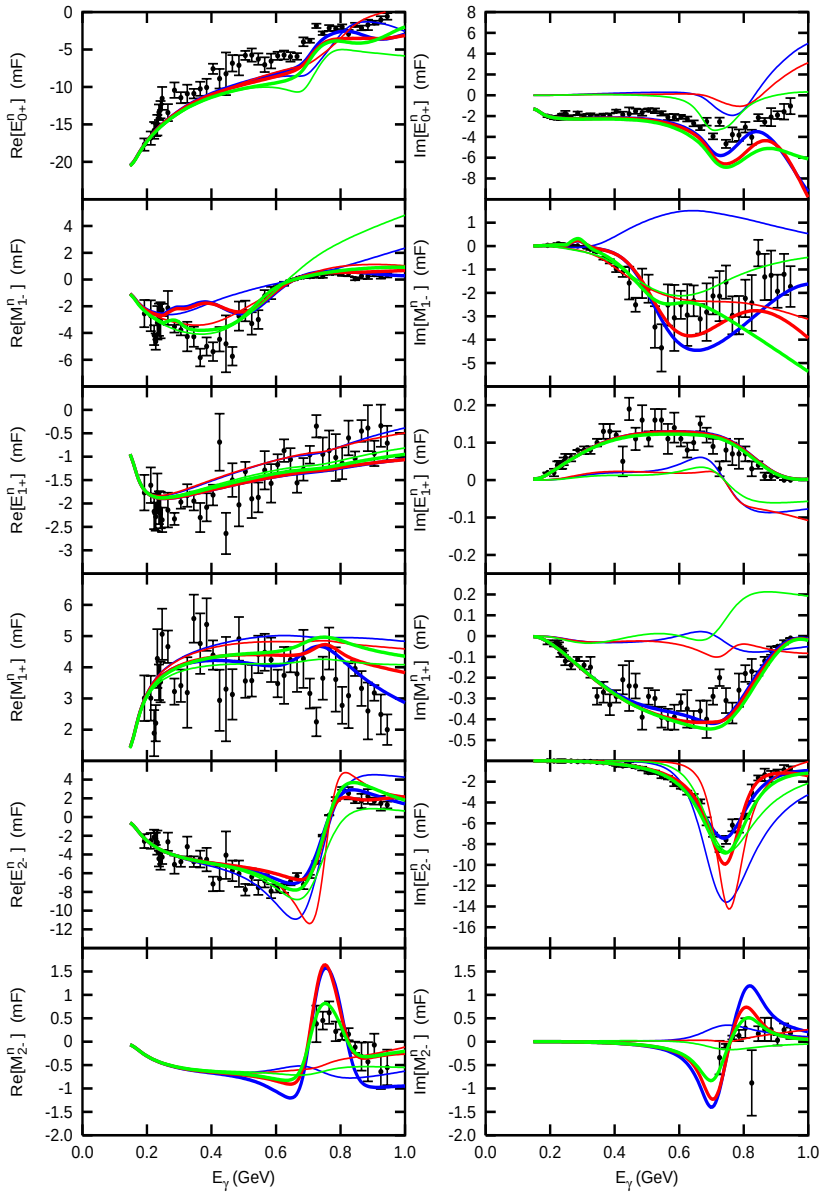

Fig. 9.3. Electromagnetic multipoles for the isospin-1/2 neutron channel. Same conventions as in Fig. 9.1 apply. Data have been taken from Ref. [SAID]

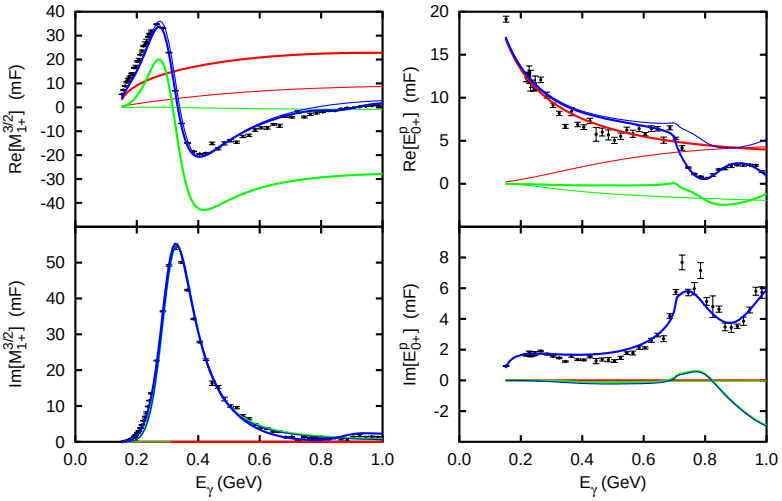

Fig. 9.4. Examples of various contributions to the multipoles. Left panel shows the $M_{1+}^{3/2}$ multipole, right panel the E_{0+}^{p} multipole. Data have been taken from Ref. [SAID]. All the curves have been obtained using set #2 parameters. Thick green: Born terms contribution; thin green: vector-meson contributions; thick red: direct terms contribution from resonances; thin red: crossed terms contribution from resonances; thin blue: full calculation without FSI; thick blue: full calculation with FSI.

ground. It also has small contributions to the background of other multipoles. Considering set #2 and multipoles $E_{2-}^{p,n}$ and $M_{2-}^{p,n}$, the agreement is excellent except where there are few experimental data. Set #3 overestimates the peak of the resonance in the multipoles and so will do for the cross section.

$E_{0+}^{3/2,p,n}$ multipoles get contributions from Born terms and vector mesons mainly. Resonances N(1535), $\Delta(1620)$, and N(1650) only contribute in the high energy region, where they acquire great importance defining the shape of the multipoles. For example, the cusp peak that shows up in $\mathrm{Im}\left[E_{0+}^{p,n}\right]$ (Figs. 9.2 and 9.3) is due to the structure of the phenomenological width – Eq. (3.71) – and to the inclusion of the partial decay width Γ_η/Γ in N(1535) resonance. Multipoles $E_{0+}^{p,n}$ are well reproduced by sets #2 and #3, except in the high energy region for $\mathrm{Im}\left[E_{0+}^{n}\right]$. The multipole $E_{0+}^{3/2}$ (Fig. 9.1) is not so well reproduced in the intermediate energy region ($0.4 - 0.8$ GeV), with an overestimation of the real part and an underestimation of the imaginary part. This indicates that the prediction of the model is correct for the absolute values of the multipoles and that there may be a problem with the phases.

Only one resonance remains to be commented, $\Delta(1700)$, which is associated mainly to multipoles $E_{2-}^{3/2}$ and $M_{2-}^{3/2}$. As one can see in Fig. 9.1, when

enough data points are available the fits are good, yet the large ambiguities in the mass and width of this resonance make somewhat unreliable the determination of its coupling constants and its contribution to the observables (see Table 7.2). Further research on the properties of this resonance is necessary.

In figure 9.4 I show two examples of the various contributions to the multipoles using the coupling constants of set #2. It is clear that, without FSI the Born terms and vector mesons do not contribute to the imaginary part of the multipoles and represent a background — it has to be noticed that when the FSI are included, they do contribute to both real and imaginary parts of the multipole. Left panel shows the multipole $M_{1+}^{3/2}$, whose main contribution is the $\Delta(1232)$. In this multipole, FSI are not important and curves with and without SAID phases differ little. Thus, the phenomenological width included is enough to describe accurately the multipole and its structure is quite simple. However, the situation is different for the multipole E_{0+}^{p} which exhibits a more complex structure because its dominant contribution comes from Born terms and vector mesons. In the absence of FSI, the imaginary part of this multipole is practically zero up to 0.8 GeV. The inclusion of FSI makes Born and vector mesons contribute to the imaginary part too, improving agreement with data.

I have not considered spin-5/2 resonances in the model. This will be required in order to extend the model to multipoles of higher angular momentum. For the energy range considered here, their contribution is expected not to be important, although their contribution to the background could improve the agreement with data.

9.2 E2/M1 Ratio of the $\Delta(1232)$

From general symmetry principles, the emission of a photon by a spin-3/2 system that becomes spin-1/2, involves transverse electric quadrupole (E2) and magnetic dipole (M1) multipolarities. Likewise, this is the case of the absorption of a real photon by a spin-1/2 to reach spin-3/2. In the absence of knowledge of the internal structure of the system, an estimate of the ratio between the two multipolarities can be made by resorting to Weisskopf [BW 91] units for multipole strengths in nuclear systems. For the excitation of a nucleon into a $\Delta(1232)$ ($\gamma + N \to \Delta$) this estimate gives

$$R_W = \sqrt{\left(\frac{S_{\rm E2}}{S_{\rm M1}}\right)} = 1.07 \cdot 10^{-3} R_0^2 \left(M_\Delta - M_N\right), \tag{9.1}$$

with the nucleon radius R_0 in fm and the mass difference in MeV. In what follows I refer to this value as the Weisskopf ratio (R_W). Taking a radius $R_0 = 0.875$ [PDG 04] and a mass difference $(M_\Delta - M_N) \simeq 270$ one gets $R_W \simeq 0.22$.

Within the quark model, a single quark spin flip is the standard picture for the photoexcitation of the nucleon into a Δ, assuming spherically symmetric ($L = 0$) radial wave functions of both parent and daughter. Under these premises, an E2 transition cannot take place, as it was first noticed by Becchi and Morpurgo in their 1965 paper [BM 65], where they concluded that a value of the E2/M1 ratio (EMR) much smaller than R_W should be considered as a test of the model. As early as 1963 values of EMR small but different from zero were reported in the literature [GS 63a, GS 63b] which was supported by further experiments later on [Bec 97, Bla 01, DMW 86, Mol 96, Pei 96, Wis 99]. A non-vanishing E2 multipolarity evokes a deformed nucleon picture [Gla 79]. In an extreme rotational model approximation the nucleon could be considered as the head of a $K^\pi = \frac{1}{2}^+$ rotational band ($\frac{1}{2}^+, \frac{3}{2}^+, \frac{5}{2}^+, \dots$), in analogy to rotational nuclear bands. In this picture the electromagnetic current and multipoles for the transition between the members of the band can be parametrized in terms of intrinsic single particle and collective multipoles [Moy 86]. In particular, the E2 multipole for the transition ($\gamma + N \rightarrow \Delta$) would be given in terms of the intrinsic quadrupole moment (Q_0) by the relation [BM 98, Moy 86]

$$\mathcal{M}\,(\mathrm{E2}) = \langle \frac{1}{2}\frac{1}{2}20|\frac{3}{2}\frac{1}{2}\rangle \sqrt{\frac{5}{8\pi}} Q_0 = 0.282 Q_0. \tag{9.2}$$

In turn, Q_0 would be related to the spectroscopic quadrupole moment of the Δ by

$$Q_0 = -5 Q_\Delta. \tag{9.3}$$

Hence, the relationship between the static $\Delta(1232)$ quadrupole moment and the E2 multipole for the $N \rightarrow \Delta$ transition is

$$\mathcal{M}\,(\mathrm{E2}, N \rightarrow \Delta) = -\frac{5}{\sqrt{4\pi}} Q_\Delta. \tag{9.4}$$

Within this picture, a negative (positive) static quadrupole moment implies a prolate (oblate) intrinsic deformation, which is not always well stated in the literature.

Over the last few years much effort has been invested in the determination of quadrupole deformation in the nucleon [BH 91, KS 03]. Because the spin of the nucleon is 1/2, a possible intrinsic quadrupole deformation is not directly observable and its study requires research on its lowest-lying excitation – $\Delta(1232)$ – and its decay through pion emission. Hints on the possible deformation will be deduced via the EMR. In the context of the quark model, De Rújula, Georgi, and Glashow [RGG 75] were the first to suggest a tensor force arising from one-gluon exchange and leading to d-state admixtures. On the other hand Buchmann and collaborators [BHF 97] pointed out that a non-zero E2 transition could be due to one-gluon or meson-exchange

currents. While debate on the physical interpretation of the EMR may still be far from closed, a more precise determination of the EMR value is both possible and mandatory.

In order to extract the EMR from experiment, a realistic model of the reaction must be employed that takes into account the FSI of the outgoing pion as well as the relevant symmetries. Only then can the ratio deduced from the experimental data be compared to the predictions of nucleonic models — namely, quark models [BHF 97, BM 65, Fae 00], skyrme models [WW 87], and lattice QCD [Ale 05, LDW 93]. Theoretical interest in this topic has been strongly renewed and either new or well-known approaches have been (re)investigated with the latest theoretical advances such as new dynamical models [PT 04, SL 01] and non-pathological spin-3/2 treatments [FMU 06a, PT 04]. A complete account of the experimental and theoretical work done on this topic goes well beyond the scope of this thesis. For a review of the subject I refer the reader to Ref. [KS 03].

A key point in the extraction of the EMR is the reaction model used for the analysis of data. Reaction models have to be developed carefully in order to consider the underlying physics and to minimize model dependencies as well as theoretical uncertainties. Ambiguities in the contribution of the background terms, unitarization, or even formal elements (such as the recently improved spin-3/2 description or the crossing symmetry) can spoil the determination of the parameters of the resonances. This is so even for a well isolated resonance as is the $\Delta(1232)$. A determination of the $\Delta(1232)$ parameters requires one to study the photoproduction reaction not only in the first resonance region, as commonly has been done, but in further kinematical regions in order to keep under control the high energy behavior of the resonance contribution. For example, in a Breit-Wigner model, the inclusion of Regge poles, which take into account heavy meson exchanges, does affect the determination of the $\Delta(1232)$ coupling constants because of the modification of the tail of the resonance [Azn 03].

Table 9.1. Intrinsic (or bare) EMR (from Eq. (9.6)) and parameters of $\Delta(1232)$ for the two fits considered. M_Δ is the mass, $A^\Delta_{1/2}$ and $A^\Delta_{3/2}$ are the helicity amplitudes, G^Δ_E is the electric form factor, and G^Δ_M is the magnetic form factor.

	Set #2	Set #3
M_Δ (MeV)	1215 ± 2	1209 ± 2
$A^\Delta_{1/2}$ ($\mathrm{GeV}^{-1/2}$)	-0.123 ± 0.003	-0.123 ± 0.003
$A^\Delta_{3/2}$ ($\mathrm{GeV}^{-1/2}$)	-0.225 ± 0.005	-0.224 ± 0.004
G^Δ_E	-0.076 ± 0.042	-0.071 ± 0.042
G^Δ_M	5.650 ± 0.070	5.701 ± 0.071
EMR	$(-1.35 \pm 0.74)\,\%$	$(-1.24 \pm 0.74)\,\%$

Caution must be taken with the various definitions of EMR employed in the literature. It should be distinguished between the intrinsic EMR of the $\Delta(1232)$ and the directly measured value which is often called *physical* or *dressed* EMR value [PT 04, SL 01] and which is obtained as the ratio between the imaginary parts of $E_{1+}^{3/2}$ and $M_{1+}^{3/2}$ at the E_γ value at which $\mathrm{Re}\left[M_{1+}^{3/2}\right] = 0 = \mathrm{Re}\left[E_{1+}^{3/2}\right]$. Since all the reaction models are fitted to the experimental electromagnetic multipoles, they generally reproduce the physical EMR value. This is also the case in my model, where I get

$$\mathrm{EMR}^{\mathrm{exp}} = \frac{\mathrm{Im}\left[E_{1+}^{3/2}\right]}{\mathrm{Im}\left[M_{1+}^{3/2}\right]} = (-3.9 \pm 1.1)\,\% \tag{9.5}$$

for 328 MeV $\leq E_\gamma \leq$ 343 MeV. This value compares well with the value obtained by LEGS Collaboration at Brokhaven National Laboratory in Ref. [Bla 01], $\mathrm{EMR}^{\mathrm{exp}} = (-3.07 \pm 0.26\ (\mathrm{stat.+syst.}) \pm 0.24\ (\mathrm{model}))\,\%$, and is somewhat higher than the PDG value, $\mathrm{EMR}^{\mathrm{exp}} = (-2.5 \pm 0.5)\,\%$.

However, this measured EMR value is not easily computed with the theoretical models of the nucleon and its resonances. Instead, in order to compare to models of nucleonic structure, it is better to extract the *bare* EMR value of $\Delta(1232)$ which is defined as:

$$\mathrm{EMR} = \frac{G_E^\Delta}{G_M^\Delta} = -\frac{(M_\Delta - M)\, g_2}{2\,(M_\Delta + M)\, g_1 + (M_\Delta - M)\, g_2} \times 100\%. \tag{9.6}$$

This depends only on the intrinsic characteristics of the $\Delta(1232)$ and can thus be compared directly to predictions from nucleonic models. It is not, however, directly measurable but must be inferred (in a model dependent way) from reaction models.

The connection between both definitions of EMR values is straightforward when FSI are neglected as can be found in the paper by Jones and Scadron [JS 81]. In my formalism, both values can be connected from the definitions of the electromagnetic multipoles [FMU 06a] and their connection to the $\gamma + N \to \Delta$ transition Lagrangian. In my calculation, the numerical differencies between the dressed and the bare EMR values are attributed to FSI.

In Table 9.1 I quote my extracted bare EMR values obtained from Eq. (9.6) together with the mass, helicity amplitudes, and electromagnetic form factors at the photon point of the $\Delta(1232)$.

In my calculations I have considered the pole mass of the resonance instead of the Breit-Wigner mass [FA 03, PT 04, SL 01]. One must be aware of the fact that electromagnetic coupling constants are very sensitive to the mass and that the width of the $\Delta(1232)$ and the multipoles vary rapidly in the region around the peak of the $\Delta(1232)$. Thus, a variation in the mass of the resonance affects the determination of the EMR value. This is also seen in

Table 9.2. Comparison of EMR values from nucleonic models and EMR values extracted from data predicted through several reaction models (see text).

Physical EMR, experiments	EMR	Ref.
LEGS Collaboration	$(-3.07 \pm 0.26 \pm 0.24)\,\%$	[Bla 01]
Particle Data Group	$(-2.5 \pm 0.5)\,\%$	[PDG 04]
Physical EMR, reaction models		
Fuda and Alharbi	-2.09%	[FA 03]
Pascalutsa and Tjon	$(-2.4 \pm 0.1)\%$	[PT 04]
Sato and Lee	-2.7%	[SL 01]
This Thesis (average)	$(\mathbf{-3.9 \pm 1.1})\,\%$	[FMU 06b]
Extractions of bare EMR, reaction models		
Davidson, Mukhopadhyay, and Wittman	-1.45%	[DMW 91]
Garcilazo and Moya de Guerra	-1.42%	[GM 93]
Pascalutsa and Tjon	$(3.8 \pm 1.6)\%$	[PT 04]
Sato and Lee	-1.3%	[SL 01]
Vanderhaeghen *et al.*	-1.43%	[VHRW 95]
This Thesis (average)	$(\mathbf{-1.30 \pm 0.52})\,\%$	[FMU 06b]
Bare EMR, predictions from nucleonic models		
Non-relativistic quark model	0%	[BM 65]
Constituent quark model	-3.5%	[BHF 97]
Skyrme model	$(-3.5 \pm 1.5)\%$	[WW 87]
Lattice QCD (Leinweber *et al.*)	$(3 \pm 8)\%$	[LDW 93]
Lattice QCD (Alexandrou *et al.*)		[Ale 05]
($Q^2 = 0.1$ GeV^2, $m_\pi = 0$)	$(-1.93 \pm 0.94)\%$	
($Q^2 = 0.1$ GeV^2, $m_\pi = 370$ MeV)	$(-1.40 \pm 0.60)\%$	

Table 9.1. Out of the two results given in Table 9.1 I adopt as my final result the average value for the bare EMR= $(-1.30 \pm 0.52)\,\%$.

In Table 9.2 I compare my average EMR [FMU 06b] values (bare and dressed) to the ones extracted by other authors using other models for pion photoproduction, as well as to predictions of nucleonic models. My bare result is similar to that from Ref. [SL 01]. However, it disagrees with the bare value derived with the dynamical model of Pascalutsa and Tjon [PT 04], where a positive deformation of the $\Delta(1232)$ (EMR= $(3.8 \pm 1.6)\,\%$) is inferred. I compare to their model because, together with the one I employ in this work, they were the only available models that include non-pathological $\Delta(1232)$

Lagrangians. The discrepancy is not so worrysome if I recall that dynamical models have ambiguities in the determination of the bare value of EMR [WWA 96] that is highly model dependent as it stems from the comparison among different dynamical models, namely Refs. [FA 03, PT 04, SL 01]. More recently [PV 05] the dependence of the effective chiral perturbation theory on the small expansion parameters was fully exploited to reconcile the (bare) lattice QCD calculations with the physical EMR values.

In conclusion, the bare EMR value derived from the multipole experimental data with my realistic ELA model is compatible with some of the predictions of the nucleonic models. In particular it agrees very well with the latest lattice QCD calculations [Ale 05] and suggests the need for further improvements in quark models. The comparison of my extracted EMR value to R_W is indicative of a small oblate deformation of the $\Delta(1232)$. In my work we show that an ELA which takes into account FSI is also able to reconcile the physical EMR value with the lattice QCD calculations prediction for EMR. I consider that my picture and that of Ref. [PV 05] are complementary. Thus, both pictures will help to understand the issue of the $\Delta(1232)$ deformation as well as the properties of other resonances.

10 Results at Threshold Energy

SPECIAL attention has to be paid to the behaviour of the model at low/threshold energy, because, in the low energy limit, cross sections and multipoles are predicted by Low Energy Theorems (LET) [Ber 91, NKF 90] and Chiral Perturbation Theory (ChPT) [BKM 92, BKM 95]. Owing to the change in the spin-3/2 coupling scheme, the threshold energy results change substantially when compared to previous works. In particular, in Ref. [GM 93], that employed the off-shell formalism, it was found that the contributions from resonances, direct and crossed terms, were of great importance in order to explain the reduced cross section at threshold and the low energy behavior of the cross section. These contributions were particularlly important in neutral processes, mainly because of $\Delta(1232)$, and represented practically the total contribution to the $n\pi^0$ production channel [Fer 03]. However, in the present calculation I obtain a zero contribution to the reduced cross section at threshold from both direct and crossed resonance terms. The reason for such a change is the spin-3/2 coupling scheme used in the present thesis, which has no spurious spin-1/2 sector. The reduced differential cross section at threshold is proportional to the E_{0+} multipole [BKM 92], which is a spin-1/2 one. Thus, at threshold, any contribution of the direct channel from spin-3/2 resonances is a contamination which unveils a pathology in the model. This is the case of models based upon the traditional spin-3/2 formalism explained in chapter 3.4.1, as the one used in Ref. [GM 93]. This result is independent on the phenomenology of the decay width and on the form factors. Therefore, I conclude that, at threshold, only Born terms (Fig. 3.1) and vector mesons (Fig. 3.2, diagram (e)) contribute, as the spin-1/2 resonances are at much higher energy. In Table 10.1 I present results for the reduced cross section at threshold for the four different processes and I find a good agreement with experimental values. Tiny differencies are found with various parameter sets (#1 to #6) that use different cutoff Λ and small variations in the vector-meson parameters.

Table 10.1. Reduced cross section at threshold $\frac{q^*}{k^*}\frac{d\sigma}{d\Omega}$ in μb/sr. Experimental data have been taken from Ref. [GM 93].

Sets	#1	#2	#3	#4	#5	#6	Experiment
$\gamma p \to p\pi^0$	0.0984	0.0998	0.0998	0.0949	0.1023	0.1020	0.094 ± 0.017
$\gamma n \to n\pi^0$	0.0046	0.0045	0.0045	0.0049	0.0044	0.0044	
$\gamma n \to p\pi^-$	18.92	18.93	18.93	18.91	18.95	18.95	20.4 ± 0.7
							20.0 ± 0.3
							19.7 ± 1.4
$\gamma p \to n\pi^+$	14.51	14.50	14.50	14.52	14.48	14.49	15.4 ± 0.5
							15.6 ± 0.5

11 Differential Cross Sections and Asymmetries

THE polarised differential cross section can be expressed in terms of six observables

$$\frac{d\sigma^{pol.}}{d\Omega} = \sigma(\theta) \times \mathcal{F}(P, T, \Sigma, G, H), \tag{11.1}$$

where $\sigma(\theta)$ is the unpolarised differential cross section and P, T, Σ, G, and H are asymmetries. In this section I show results for the differential cross sections together with results for this five asymmetries. Details on the definition of these quantities can be found in Refs. [ALR 90, BDS 75, Bus 79, Bus 80, Ros 54, Wal 69].

The recoil nucleon polarisation P is the polarisation of the nucleon along the direction $\vec{q} \wedge \vec{k}/|\vec{q} \wedge \vec{k}|$ for photon helicity $\lambda_\gamma = 1$ (for $\lambda_\gamma = -1$ the same value for the asymmetry holds).

T stands for the polarised target asymmetry, experimentally defined by

$$T(\theta) = \frac{\sigma_+ - \sigma_-}{\sigma_+ + \sigma_-}, \tag{11.2}$$

where σ_+ and σ_- are the differential cross sections for target nucleon polarised up and down in the direction $\vec{q} \wedge \vec{k}/|\vec{q} \wedge \vec{k}|$.

Σ is the polarised photon beam asymmetry

$$\Sigma(\theta) = \frac{\sigma_\perp - \sigma_\parallel}{\sigma_\perp + \sigma_\parallel}, \tag{11.3}$$

where $\sigma_\perp$ and $\sigma_\parallel$ are the differential cross sections for photons with perpendicular and parallel polarisations to the reaction plane.

G and H are related to double polarisation measurements (see Fig. 11.1 to follow their definitions). For the G asymmetry the target nucleon is polarised along z axis and the photon is linearly polarised at angle $\frac{\pi}{4}$ rad ($-\frac{\pi}{4}$ rad) to the reaction plane (the polarisation vector belongs to the xy plane). For the H asymmetry the target nucleon is polarised perpendicularly to the x axis and the photon has the same polarisation than for the G asymmetry.

Table 11.1 shows the number of experimental data available up to 1 GeV for all the four one pion photoproduction processes.

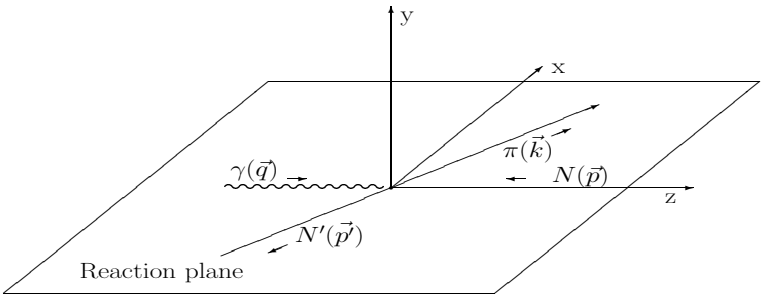

Fig. 11.1. Kinematics for the photoproduction process.

Table 11.1. Number of data points in the SAID database up to 1 GeV, Ref. [SAID].

Observable	$\gamma p \to \pi^0 p$	$\gamma n \to \pi^0 n$	$\gamma p \to \pi^+ n$	$\gamma n \to \pi^- p$
$\sigma\,(\theta)$	5119	120	3868	1686
$P\,(\theta)$	363	0	163	82
$\Sigma\,(\theta)$	530	0	780	154
$T\,(\theta)$	251	0	585	89
$G\,(\theta)$	0	0	32	0
$H\,(\theta)$	0	0	89	0
σ	500	0	70	98

The asymmetries are of great interest in the search for *missing* resonances which do not show up so clearly in other observables [DGL 02]. The formulae relating the amplitudes with the asymmetries will be presented in the forthcoming paragraphs. I provide a wide sample of figures in order to have a broad outlook of the comparison of the model with the data whenever available.

The FSI treatment described in chapter 7 has been applied only to the $\gamma p \to \pi^0 p$ process. For the other three pion production processes, no FSI phases have been included because I have no means to determine them from the available data. I calculate the observables for these processes for the six sets of coupling constants obtained by fitting $\gamma p \to \pi^0 p$ multipoles, given in Tables 7.1 and 7.2. Thus, these calculations have no adjustable parameters. As I shall see in what follows, an overall good agreement with data is found. As the energy increases, differences among the curves obtained with the different sets of parameters show up more. The comparison with the data favours the sets of coupling constants obtained using FSI.

11.1 $\gamma p \to \pi^0 p$

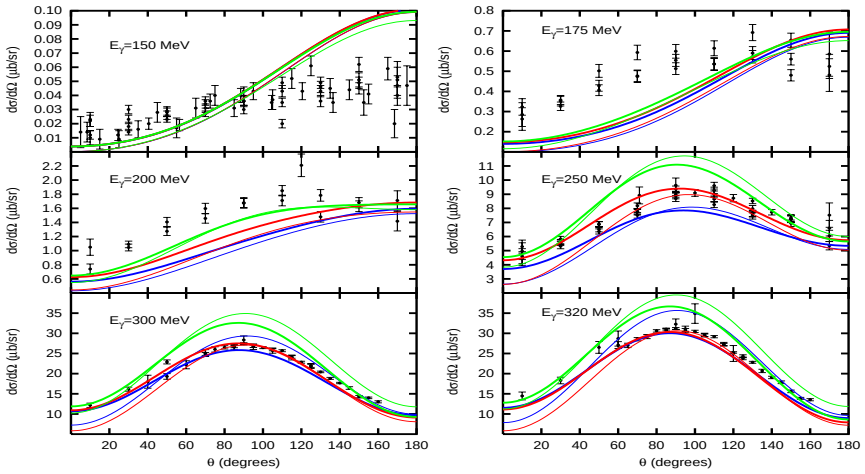

Fig. 11.2. Differential cross section in μb/sr of the $\gamma p \to \pi^0 p$ reaction for different photon energies in the laboratory frame. θ is the pion scattering angle in the center of mass reference frame. The data have been taken from reference [SAID] and are within the range $E_\gamma \pm 1$ MeV. Curve conventions: thick green, set #1; thick blue, set #2; thick red, set #3; thin green, set #4; thin blue, set #5; thin red, set #6.

First I consider the process $\gamma p \to \pi^0 p$, for which the experimental database has been largely increased in the last ten years mainly thanks to the experimental programs developed at Mainz (MAMI) and Brookhaven (LEGS). For this process the amount of experimental information is much larger than for any other pion photoproduction process. Even so, the database on asymmetries is not yet large enough and more measurements are needed in order to fill in the existing gaps. Figs. 11.2 and 11.3 show theoretical curves for the differential cross sections compared to experimental data. Differential cross sections have been calculated using equations from chapter 2 and amplitudes from chapter 4.

I recall that among the eight helicity amplitudes, only four of them are independent

$$H_N = \mathcal{A}_{1/2,-1/2,1} = -\mathcal{A}_{-1/2,1/2,-1}, \tag{11.4}$$

$$H_{SF} = \mathcal{A}_{-1/2,-1/2,1} = \mathcal{A}_{1/2,1/2,-1}, \tag{11.5}$$

$$H_{SA} = \mathcal{A}_{1/2,1/2,1} = \mathcal{A}_{-1/2,-1/2,-1}, \tag{11.6}$$

$$H_D = \mathcal{A}_{-1/2,1/2,1} = -\mathcal{A}_{1/2,-1/2,-1}, \tag{11.7}$$

and that in terms of these four independent helicity amplitudes, it is possible to define every physical observable [AWLR 90a]. In particular, the five asym-

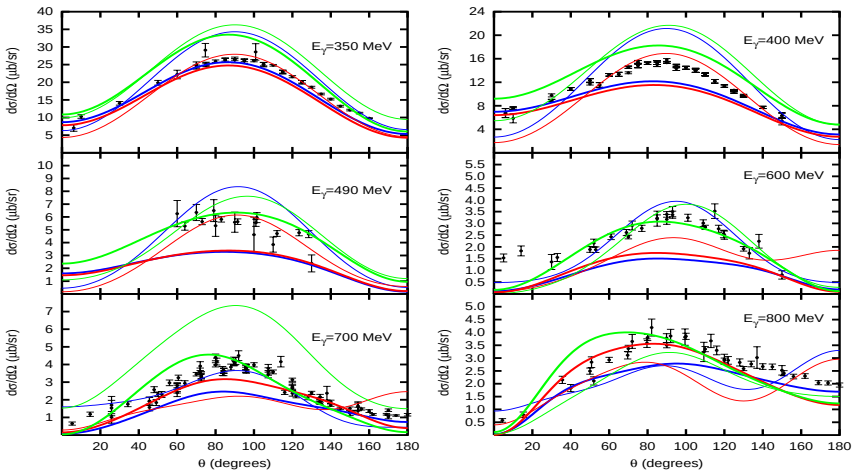

Fig. 11.3. Same as in Fig. 11.2. Experimental data are within the range $E_\gamma \pm 3$ MeV.

metries previously mentioned can ve expressed in terms of these independent helicity amplitudes.

Focusing on sets with δ_{FSI} phases, the fits are qualitatively good in the whole energy region, and even quantitatively in the range $250 - 400$ MeV. Asymmetries are well predicted in almost the whole energy range.

In Fig. 11.4 I provide recoil nucleon polarisation asymmetries (P) defined by

$$\sigma(\theta) P(\theta) = -\frac{1}{64\pi^2 s^*} \frac{k^*}{E_\gamma^*} \mathrm{Im}\left[H_{SF} \bar{H}_D + H_N \bar{H}_{SA}\right], \tag{11.8}$$

where the bar over the helicity amplitudes H_j stands for complex conjugate and $\sigma(\theta)$ for the differential cross section given by Eq. (2.12). Up to 600 MeV, data are well reproduced by sets with FSI. Above this energy, data are reproduced qualitatively but not quantitatively.

In Fig. 11.5 I present the polarised target asymmetry (T) given by equation

$$\sigma(\theta) T(\theta) = \frac{1}{64\pi^2 s^*} \frac{k^*}{E_\gamma^*} \mathrm{Im}\left[H_{SF} \bar{H}_N + H_D \bar{H}_{SA}\right]. \tag{11.9}$$

Up to 400 MeV the six curves are very similar. For 500 and 580 MeV the sets with phases provide good results and the sets without phases do not. The high energy region (700 and 800 MeV) is not well reproduced in general.

Polarised beam asymmetry (Σ) is well predicted in the whole energy range by sets with FSI (Fig. 11.6). Even sets without FSI provide good results

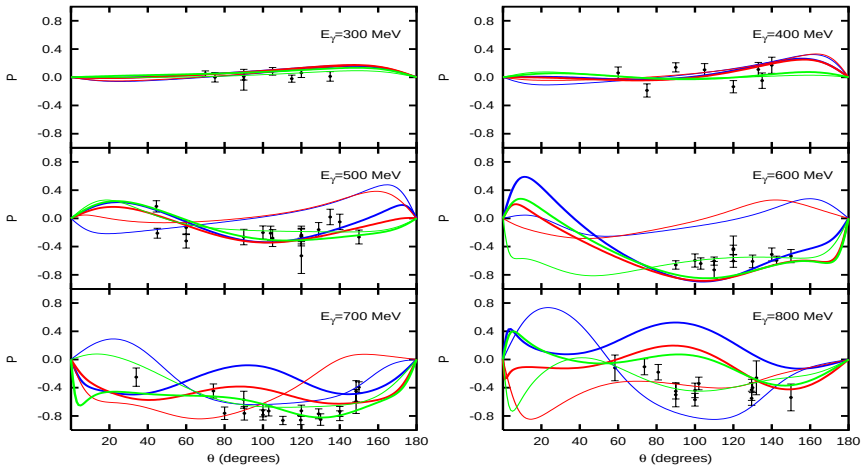

Fig. 11.4. Recoil nucleon polarisation of the $\gamma p \to \pi^0 p$. Photon energy in the laboratory frame. Pion angle in the center of mass reference system. Experimental data are within the range $E_\gamma \pm 3$ MeV. Conventions for the curves are as in Fig. 11.2.

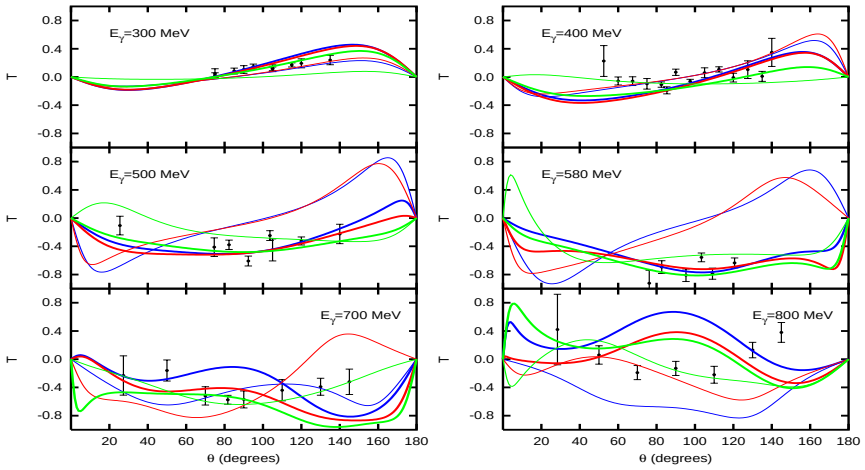

Fig. 11.5. Polarised target asymmetry of the $\gamma p \to \pi^0 p$ reaction. Experimental data are within the range $E_\gamma \pm 3$ MeV. Same conventions as in Fig. 11.4.

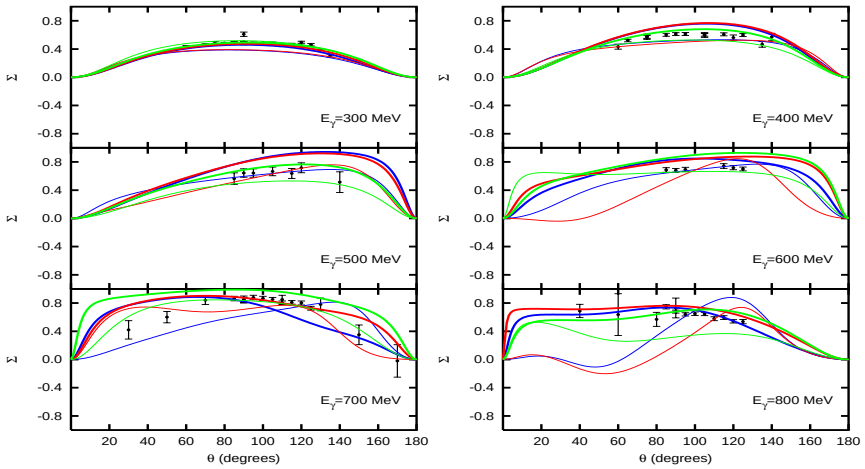

Fig. 11.6. Photon beam asymmetry of the $\gamma p \to \pi^0 p$ reaction. Experimental data are within the range $E_\gamma \pm 3$ MeV. Same conventions as in Fig. 11.4.

except in the very high energy region (800 MeV). Helicity amplitudes are related to Σ through

$$\sigma(\theta)\,\Sigma(\theta) = \frac{1}{64\pi^2 s^*}\frac{k^*}{E_\gamma^*}\mathrm{Re}\left[H_{SF}\bar{H}_{SA} - H_N\bar{H}_D\right]. \tag{11.10}$$

In short, compared to data, good agreement is obtained for energies below 800 MeV. Beyond that energy some observables (v.g. Σ) are also reasonably well described

In the energy region considered here there are no experimental data on the other two asymmetries G and H. These asymmetries are expressed in terms of helicity amplitudes by means of the following equations

$$\sigma(\theta)\,G(\theta) = -\frac{1}{64\pi^2 s^*}\frac{k^*}{E_\gamma^*}\mathrm{Im}\left[H_{SF}\bar{H}_{SA} + H_N\bar{H}_D\right], \tag{11.11}$$

$$\sigma(\theta)\,H(\theta) = -\frac{1}{64\pi^2 s^*}\frac{k^*}{E_\gamma^*}\mathrm{Im}\left[H_{SF}\bar{H}_D + H_{SA}\bar{H}_N\right]. \tag{11.12}$$

I have also calculated these asymmetries and my results are presented in Figs. 11.7 and 11.8.

11.2 $\gamma n \to \pi^0 n$

The situation for the $\gamma n \to \pi^0 n$ process is quite different from the previous case. The amount of experimental information is very small: No asymmetry

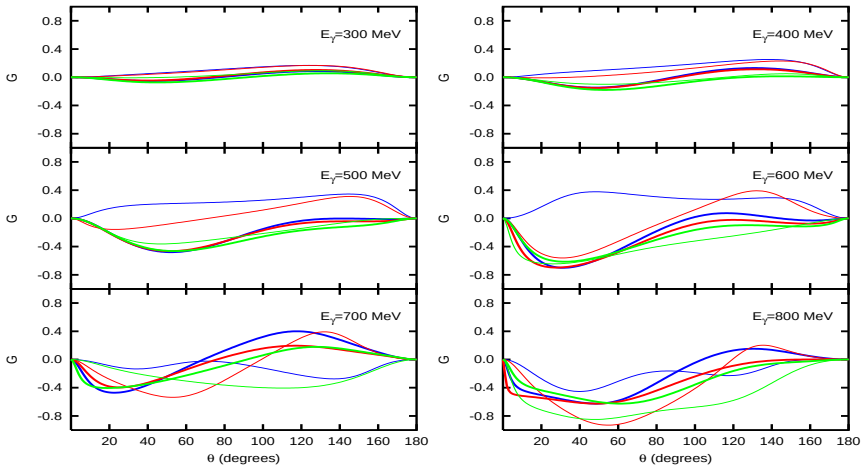

Fig. 11.7. G asymmetry of the $\gamma p \to \pi^0 p$ reaction. Same conventions as in Fig. 11.4.

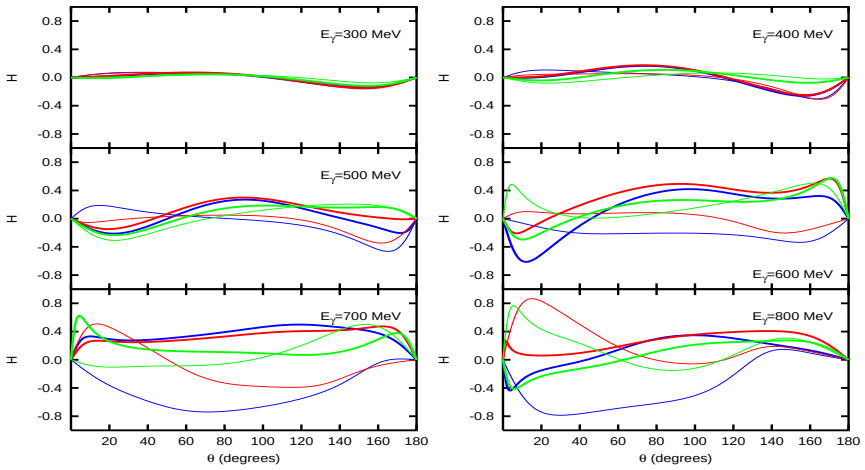

Fig. 11.8. H asymmetry of the $\gamma p \to \pi^0 p$ reaction. Same conventions as in Fig. 11.4.

data are available and differential cross section data are scant. In Fig. 11.9 I show differential cross sections and in Figs. 11.10, 11.11, 11.12, 11.13, and 11.14 the predicted asymmetries (P, T, Σ, G, and H respectively) obtained with the different sets of parameters. There is a reasonable agreement with data, and sets #1 and #4 (PDG values) provide the best overall results.

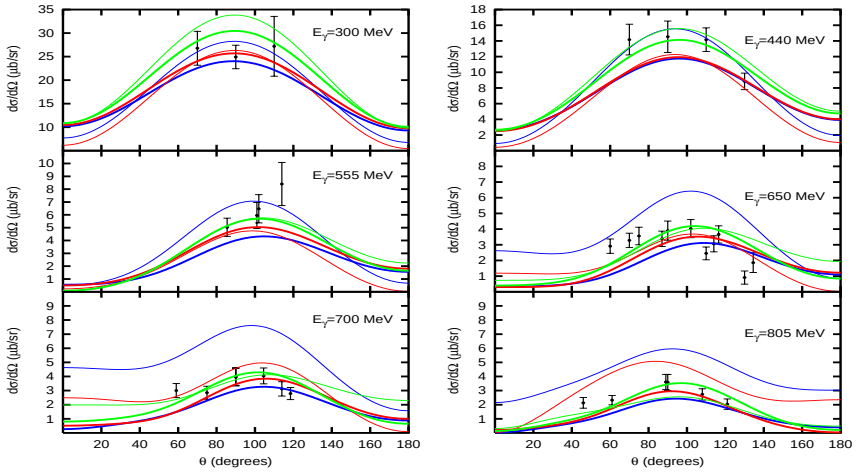

Fig. 11.9. Differential cross section of the $\gamma n \to \pi^0 n$ reaction. Experimental data are within the range $E_\gamma \pm 5$ MeV. Same conventions as in Fig. 11.2.

11.3 Charged Pion Production

In the next paragraphs I go in detail through the predicted differential cross sections and asymmetries for charged pion processes, and compare them to available data (Figs. 11.15–11.26).

$\gamma p \to \pi^+ n$ differential cross sections (Fig. 11.15) are well predicted by the model in the whole energy range by all parameter sets. In the high energy regime (two last figures of the panels) differential cross sections are not well predicted by any of the parameters sets in the forward scattering region, with the exception of set #1 (PDG with δ_{FSI}) which provides an impressively good agreement. For the P asymmetry (Fig. 11.16) all curves are alike and reproduce data correctly up to 400 MeV. As the energy is increased, sets #1 and #4 (PDG values) provide the best results. The T asymmetry is qualitatively well predicted, but quantitative agreement is only achieved up to 500 MeV (Fig. 11.17). Sets with and without FSI provide a good agreement with data for the Σ asymmetry (Fig. 11.18). Only in the last figure of the panel (700 MeV) I observe different qualitative behaviours from one set of constants to

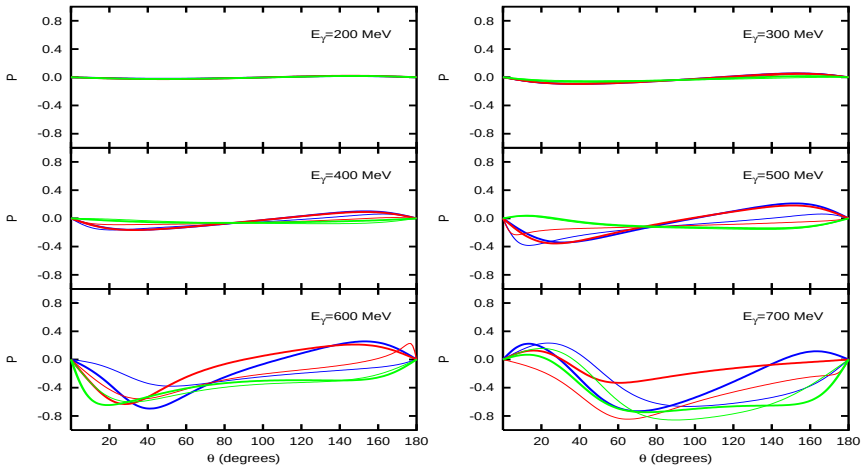

Fig. 11.10. Recoil nucleon polarisation of the $\gamma n \to \pi^0 n$. Same conventions as in Fig. 11.4.

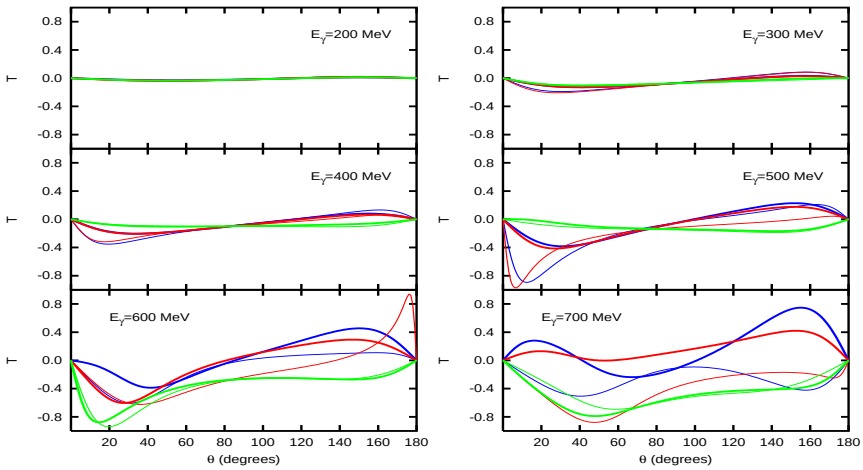

Fig. 11.11. Polarised target asymmetry of the $\gamma n \to \pi^0 n$ reaction. Same conventions as in Fig. 11.4.

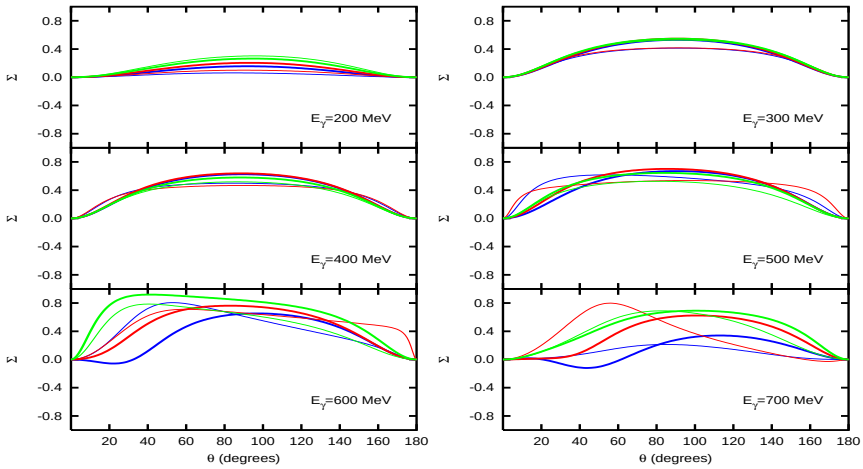

Fig. 11.12. Photon beam asymmetry of the $\gamma n \to \pi^0 n$ reaction. Same conventions as in Fig. 11.4.

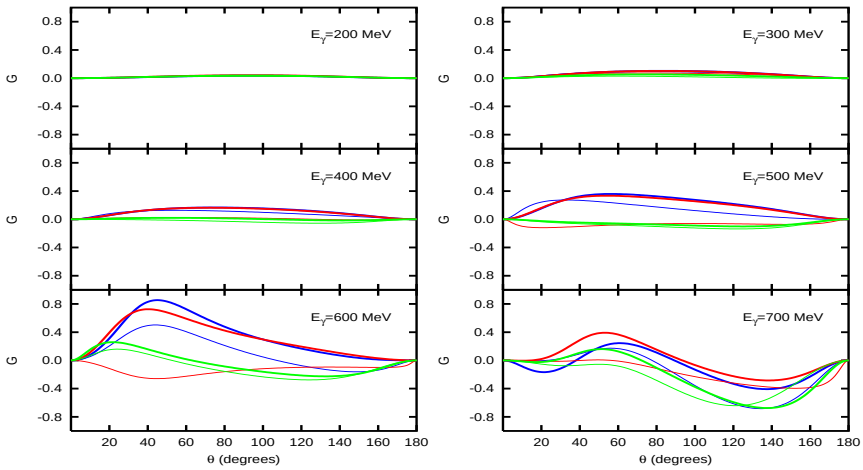

Fig. 11.13. G asymmetry of the $\gamma n \to \pi^0 n$ reaction. Same conventions as in Fig. 11.4.

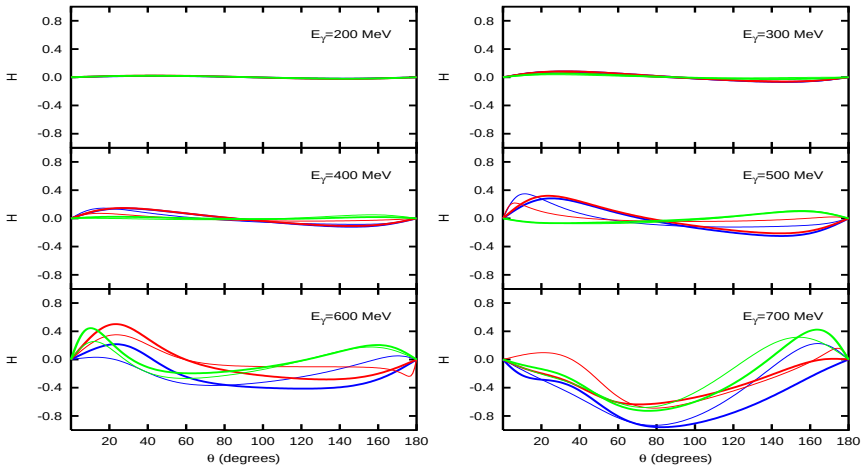

Fig. 11.14. H asymmetry of the $\gamma n \to \pi^0 n$ reaction. Same conventions as in Fig. 11.4.

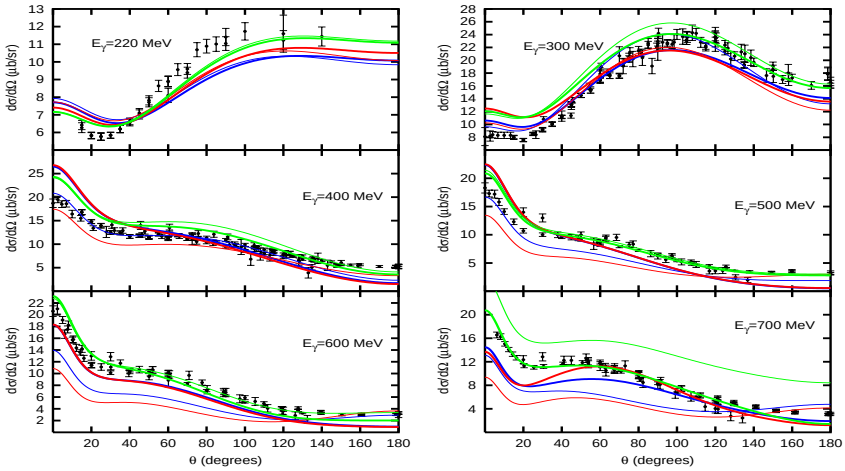

Fig. 11.15. Differential cross section of the $\gamma p \to \pi^+ n$ reaction. Experimental data are within the range $E_\gamma \pm 5$ MeV. Same conventions as in Fig. 11.2.

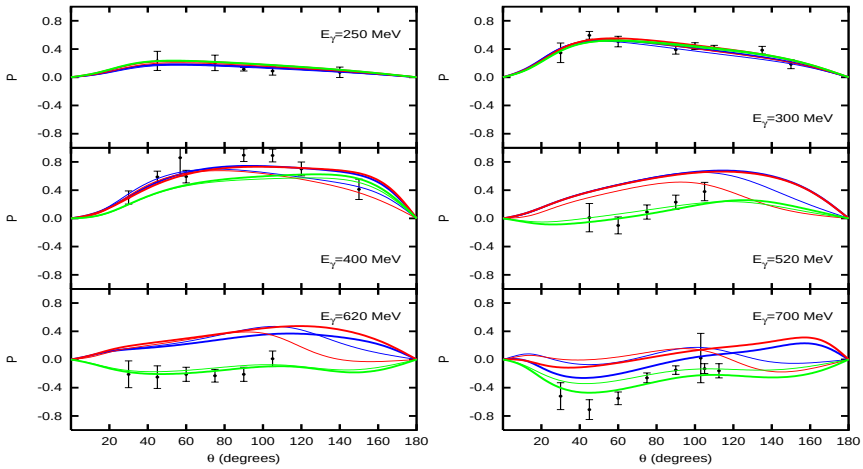

Fig. 11.16. Recoil nucleon polarisation of the $\gamma p \to \pi^+ n$ reaction. Experimental data are within the range $E_\gamma \pm 3$ MeV. Same conventions as in Fig. 11.4.

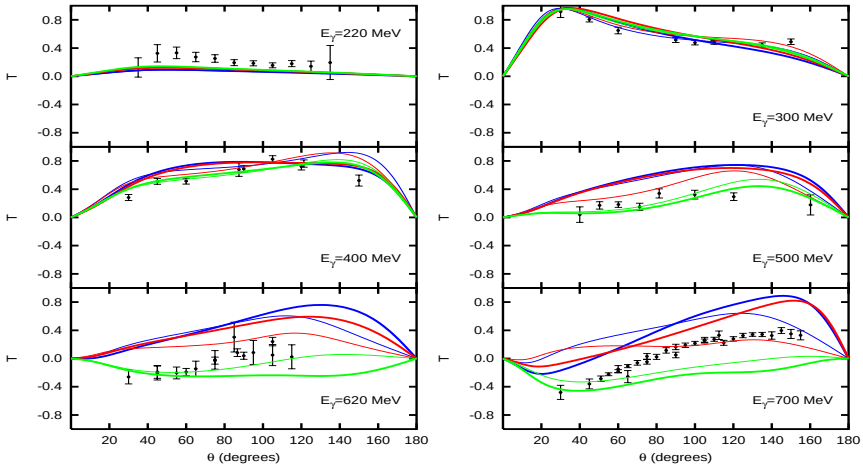

Fig. 11.17. Polarised target asymmetry of the $\gamma p \to \pi^+ n$ reaction. Experimental data are within the range $E_\gamma \pm 4$ MeV. Same conventions as in Fig. 11.4.

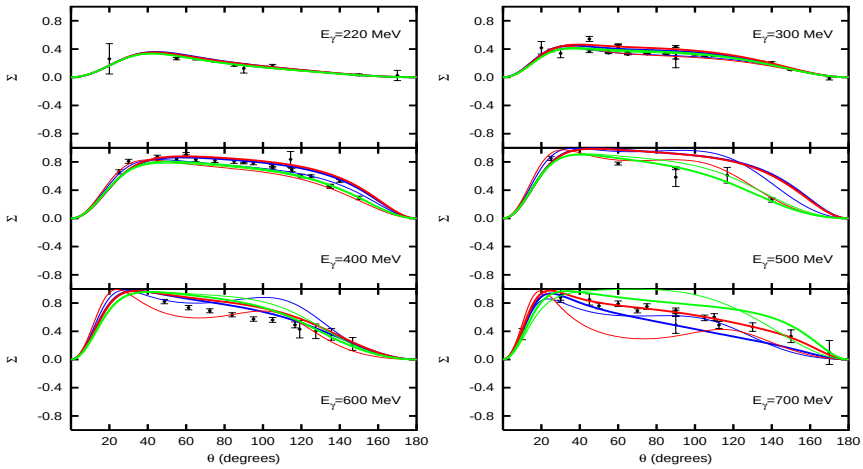

Fig. 11.18. Photon beam asymmetry of the $\gamma p \to \pi^+ n$ reaction. Experimental data are within the range $E_\gamma \pm 4$ MeV. Same conventions as in Fig. 11.4.

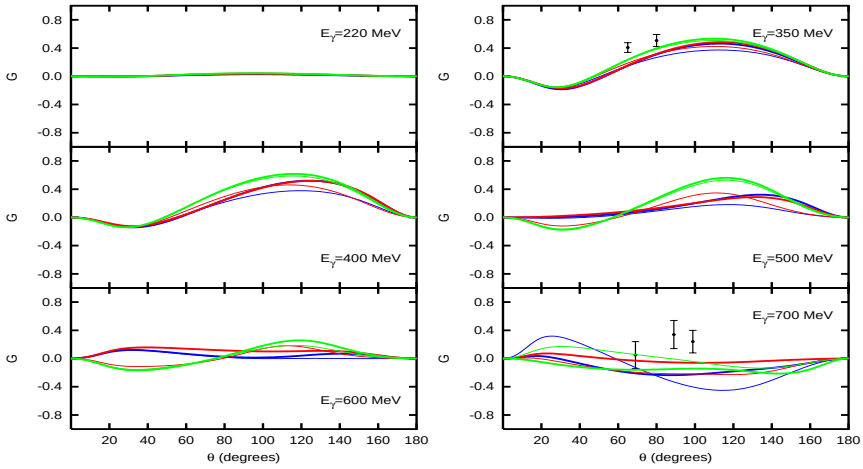

Fig. 11.19. G asymmetry of the $\gamma p \to \pi^+ n$ reaction. Experimental data are within the range $E_\gamma \pm 3$ MeV. Same conventions as in Fig. 11.4.

another. Data are scant and not reliable for G and H asymmetries. As for previous asymmetries, in the low energy regime all the curves are alike, but as energy is increased their predictions become different.

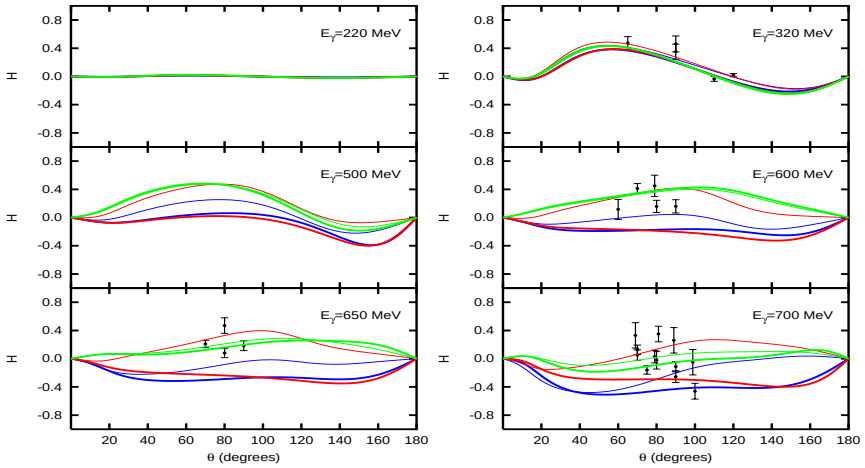

Fig. 11.20. H asymmetry of the $\gamma p \to \pi^+ n$ reaction. Experimental data are within the range $E_\gamma \pm 3$ MeV. Same conventions as in Fig. 11.4.

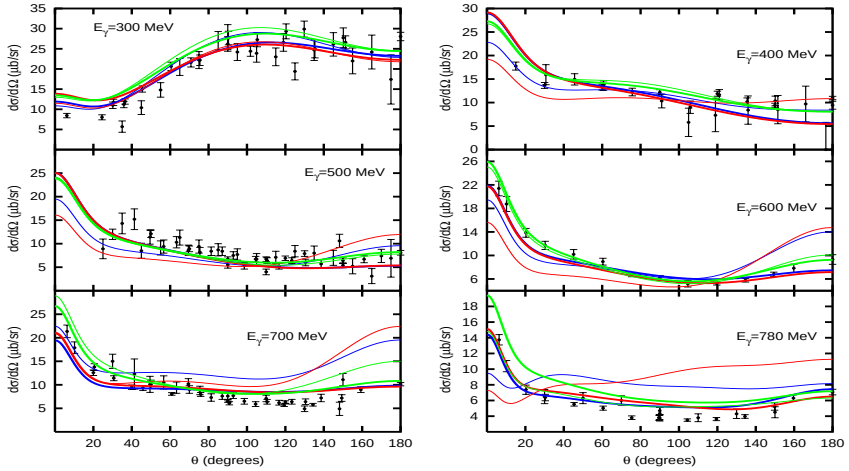

Fig. 11.21. Differential cross section of the $\gamma n \to \pi^- p$ reaction. Experimental data are within the range $E_\gamma \pm 4$ MeV. Same conventions as in Fig. 11.2.

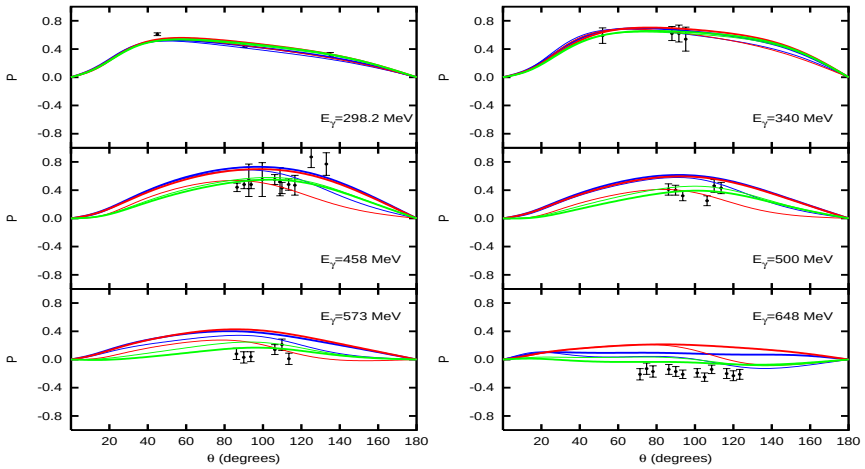

Fig. 11.22. Recoil nucleon polarisation of the $\gamma n \to \pi^- p$ reaction. Experimental data are within the range $E_\gamma \pm 1$ MeV. Same conventions as in Fig. 11.4.

Differential cross section data for the reaction $\gamma n \to \pi^- p$ are well predicted by the sets with FSI (#1, #2, and #3). All the curves are similar for the P asymmetry (Fig. 11.22) and are close to data. Overall agreement is good for the T asymmetry (Fig. 11.23). This agreement becomes excellent for the highest energy ($E_\gamma = 802$ MeV) if I consider only curves #2 and #3. Σ asymmetry (Fig. 11.24) is very well predicted by curves #2 and #3 in the whole energy range. All predictions are qualitatively quite similar for the G and H asymmetries (Figs. 11.25 and 11.26) except for $E_\gamma = 800$ MeV, where large differences are found.

The model works quite well for processes with charged pions. This is remarkable if I take into account that no δ_{FSI} have been included, and indicates that FSI are not as important in the studied energy region for charged pions as they are for neutral pion channels. Quantitatively, the model provides satisfactory results nearly in the whole energy range and in almost every observable. Even in the cases where good quantitative result is not achieved, at least the qualitative behavior of data is well reproduced (i.e. Figs. 11.15 and 11.17).

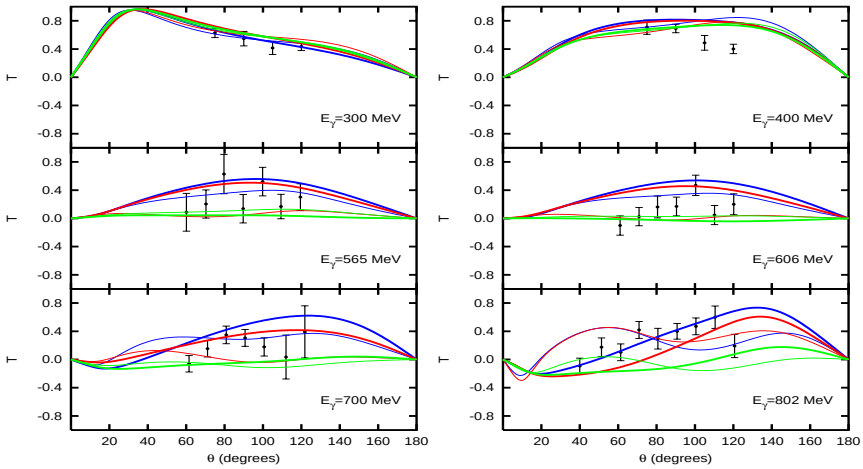

Fig. 11.23. Polarised target asymmetry of the $\gamma n \to \pi^- p$ reaction. Experimental data are within the range $E_\gamma \pm 5$ MeV. Same conventions as in Fig. 11.4.

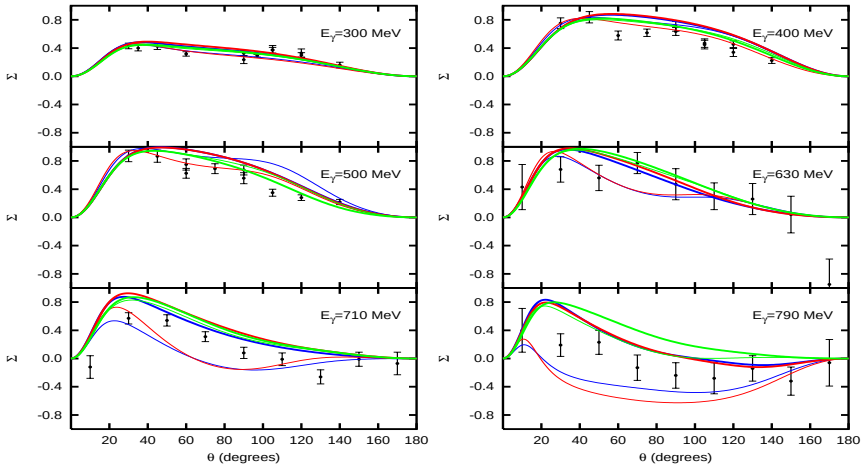

Fig. 11.24. Photon beam asymmetry of the $\gamma n \to \pi^- p$ reaction. Experimental data are within the range $E_\gamma \pm 1$ MeV. Same conventions as in Fig. 11.4.

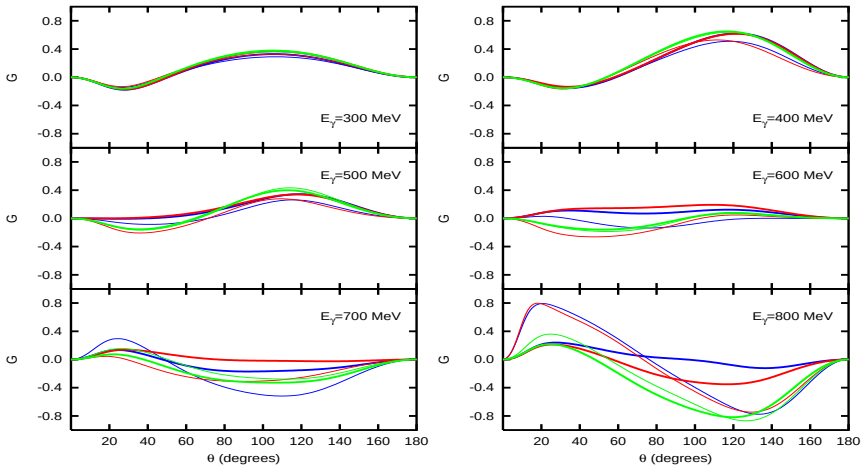

Fig. 11.25. G asymmetry of the $\gamma n \to \pi^- p$ reaction. Same conventions as in Fig. 11.4.

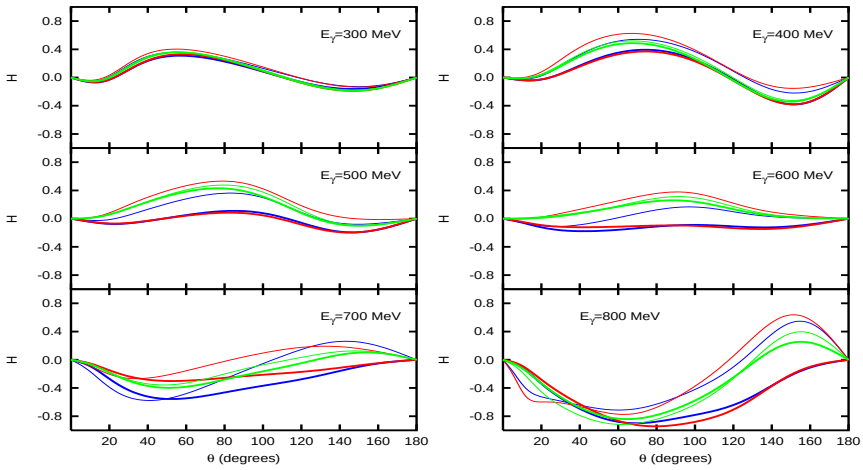

Fig. 11.26. H asymmetry of the $\gamma n \to \pi^- p$ reaction. Same conventions as in Fig. 11.4.

12 Cross Sections

FINALLY, in this chapter I present results for the total cross sections compared to available experimental data in Fig. 12.1. The two upper figures show the total cross section for charged pion channels and the two lower are for neutral pion photoproduction.

It is interesting to notice how some of the observed effects in the multipoles show up in the cross sections. For example, sets #1, #4, and #5 overestimate the first resonance region due to the overestimation of $M_{1+}^{3/2}$ peak. On the other hand, set #4 presents a cusp peak in multipole $\mathrm{Im}\left[E_{0+}^{p}\right]$, that also shows up in the cross section, specially so in the $\pi^+ n$ channel. The high energy behaviour is well regularized. Nevertheless, it has to be considered that I do not take into account resonances D_{15} and F_{15} which may change the shape of the cross section in the second resonance region.

The low enery behaviour of the charged processes is quite well reproduced by all the sets of parameters. Actually, curves obtained with coupling constants from sets #1 and #2 agree quite well with data in almost the whole energy range. Other sets do not provide good results: sets #5 and #6 overestimate greatly the second resonance region for $\pi^- p$ channel, and set #4 does the same in $\pi^+ n$ channel. Overestimation of the second resonance region by set #3 is due to the overestimation of multipoles related to resonance N(1520).

Concerning the $\gamma n \to \pi^0 n$ channel I found several differences among sets either in the region of the first or in the region of the second resonance. As no data are available for $\pi^0 n$ total cross sections, I rely on results on differential cross section to infer that up to 400 MeV, sets #2 and #3 may provide a good estimation of the total cross section and that beyond that energy, there may be probably an underestimation of the total cross section.

In summary, I conclude that set #2 is the most reliable one because it provides the best results when all data are considered as a whole. This is so regardless of the fact that other sets may provide better fits to individual cases. For instance, set #6 provides the best fit to $\pi^0 p$ total cross section and set #1 is very good for charged pion channels. As a matter of fact, set #2 has the lowest χ^2 for the electromagnetic multipoles. With this set, the only deviations from experimental data in the total cross section are the slight underestimation of $\pi^+ n$ and $\pi^0 p$ processes beyond 400 MeV.

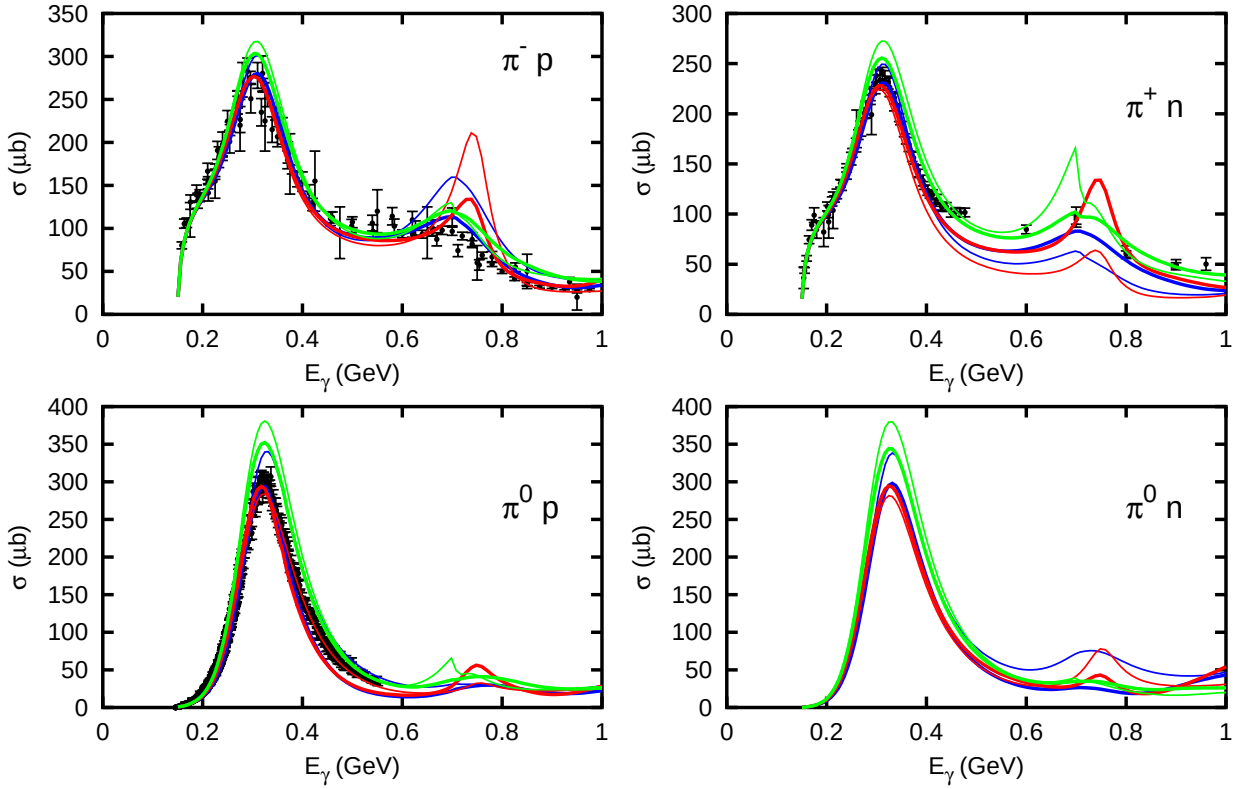

Fig. 12.1. Total cross section as a function of photon energy in laboratory frame. Same curve conventions as in Fig. 11.2.

13 Summary and Final Remarks

I have elaborated on a pion photoproduction model which is based on an Effective Lagrangian Approach (ELA) and is guided by Weinberg's theorem, fulfilling chiral symmetry, gauge invariance, and crossing symmetry. I have included Born terms, ρ and ω mesons exchange, and seven nucleon resonances: $\Delta(1232)$, N(1440), N(1520), N(1535), $\Delta(1620)$, N(1650), and $\Delta(1700)$. Under these premises, the model is independent of the underlying subnuclear physics (quarks, gluons), which is embedded in the parameters of the model, such as coupling constants, masses, and widths.

With respect to former models along similar lines, this is the first one that covers all the well established spin-1/2 and spin-3/2 resonances up to 1.7 GeV and, at the same time, fulfills gauge invariance as well as chiral and crossing symmetries. Crossing symmetry could not be achieved in previous models, such as the one of Ref. [GM 93] due, among other things, to pathologies of former spin-3/2 Lagrangians. This problem is fixed in the present work by:

(a) the use of a spin-3/2 Lagrangian due to Pascalutsa that contains no spurious spin-1/2 components in the direct channel,
(b) the use of consistent, energy dependent, strong couplings and widths, as well as form factors.

One of the goals of this thesis is to establish a reliable set of parameters for the model. In addition to the cutoff Λ – which is related to short-distance effects and can be considered as the only free parameter of the model – I adjust electromagnetic coupling constants of the nucleon resonances within the usually accepted ranges. The determination of the parameters has been performed by fit to the experimental $\gamma p \to \pi^0 p$ multipoles, through a minimization procedure. In the minimization I have considered three different sets of masses and widths:

(a) Masses and widths taken from PDG with electromagnetic coupling constants within the PDG error bars.
(b) Masses and widths taken from the multichannel analysis of Vrana et al. [VDL 00] with electromagnetic coupling constants considered as free parameters.
(c) Masses and widths obtained by means of a speed plot calculation with the electromagnetic coupling constants considered as free parameters.

On the other hand I have considered final state interactions (FSI) phenomenologically by adding an extra phase to the $\gamma p \to \pi^0 p$ multipoles, in order to match the current energy dependent solution of SAID phases [SAID]. In all, I have derived six sets of parameters, one with and one without FSI for each of the above mentioned sets of masses and widths:

(a) Sets #1 and #4.
(b) Sets #2 and #5.
(c) Sets #3 and #6.

Electromagnetic multipoles for $\gamma p \to \pi^0 p$ are globally well reproduced by sets #1, #2, and #3 that include FSI. The fits without FSI (#4, #5, and #6) are also good in the low energy regime. Other experimental observables are surveyed such as differential cross section, asymmetries, and total cross sections. At threshold I find good agreement with experimental data. In my model almost all the contribution at threshold comes from Born terms at variance with results in Ref. [GM 93].

For charged pion production, where I have no adjustable parameters, the agreement is remarkably good for almost all the observables. I note that FSI phases obtained for the $\gamma p \to \pi^0 p$ process are not applicable to charged pion production. Thus, no FSI phases have been included in these charged pion photoproduction calculations. The fact that I get good agreement with data indicates that FSI are small in $\gamma p \to \pi^+ n$ and $\gamma n \to \pi^- p$.

Although all the parameter sets are reasonable, I favour set #2 because of its lowest χ^2 to the multipole data and its better agreement with the total cross sections for all processes. Set #3, which also has a low χ^2, is very similar to set #2 and also yields similar helicity amplitudes for all the resonances except for $\Delta(1700)$. This resonance is poorly known and more precise information would be necessary. A better experimental knowledge of multipole $M_{2-}^{3/2}$ would improve the determination of the properties of $\Delta(1700)$ resonance. Similarly better knowledge of the M_{1-}^{p} multipole would help to establish more reliably properties of N(1440).

For the future, it would be interesting to analyze contributions from spin-5/2 nucleon resonances. Although they are not essential to the multipoles considered here, they may contribute to the background and their effect can be sizeable in the second resonance region of the total cross section and asymmetries. The incorporation of the spin-5/2 resonances will require to take into account higher order multipoles in the analysis. The inclusion of other resonances not considered here (three stars in PDG and *misssing* resonances) could also improve the fits in some energy regions, but it is difficult to perform a reliable determination of the parameters without the aid of other physical processes where their contribution would be more sizeable.

I have also studied the existence of a quadrupole deformation in the $\Delta(1232)$ resonance. The EMR of the $\Delta(1232)$ has been obtained (EMR$= (-1.30 \pm 0.52)\,\%$) which compares well with the latest lattice QCD calculations and allows to reconcile the lattice QCD results with the experiments.

The results obtained here are encouraging and estimulate the application of this model to other processes such as pion electroproduction, two pion production in nucleons [GO 94] and nuclei, as well as electro- and photoproduction of other mesons [JRDC 02b, JRDC 02a].

Publications Related to this Ph.D. Thesis Dissertation

Articles

1. C. Fernández-Ramírez, E. Moya de Guerra, J.M. Udías, "Effective Lagrangian Approach to pion photoproduction from the nucleon", *Annals of Physics* (New York) 321 (2006) 1408-1456, `arXiv:nucl-th/0509020`
2. C. Fernández-Ramírez, E. Moya de Guerra, J.M. Udías, "Hints on the quadrupole deformation of the $\Delta(1232)$", *Physical Review* C 73 (2006) 042201(R), `arXiv:nucl-th/0601037`

Proceedings

1. C. Fernández-Ramírez, E. Moya de Guerra, J.M. Udías, "Producción electromagnética de piones en núcleos". Talk. XXIX Bienal de la Real Sociedad Española de Física. July 2003. Madrid, Spain. Resúmenes de las comunicaciones, p. 747-748, ISBN: 84-688-2573-5. Editors: L. Vázquez Martínez, A. Dobado González, and J.P. Sánchez Fernández.
2. C. Fernández-Ramírez, E. Moya de Guerra, J.M. Udías, "Pion electro and photoproduction on nuclei in a lagrangian approach". Talk. Sixth Workshop on Electromagnetically Induced Two-Hadron Emission. September 2003. Pavia, Italy. Proceedings of the Sixth Workshop on Electromagnetically Induced Two-Hadron Emission, p. 234-239, ISBN: 88-85159-20-6. Editors: A. Braghieri, C. Giusti, and P. Grabmayr.

Posters

1. C. Fernández-Ramírez, E. Moya de Guerra, J.M. Udías, "Pion electro and photoproduction on nuclei in a Lagrangian approach". Nuclear Gordon Conference. July 2003. Colby College, Waterville (Maine), USA.

Other Scientific Documents

1. C. Fernández-Ramírez. "Producción de piones en núcleos". Diploma Thesis. Supervisors: Prof. Dr. E. Moya Valgañon and Dr. J.M. Udías. Devel-

oped in order to obtain "Diploma de Estudios Avanzados" (M.Sc.). Departamento de Física Atómica, Molecular y Nuclear, Universidad Complutense de Madrid, June 2003.

2. C. Fernández-Ramírez, J.M. Udías, E. Moya de Guerra, J.R. Vignote, F.J. Llanes-Estrada, J.López Herraiz, A.M. Lallena, J. Vijande, A. Valcarce, "Intermediate Energy Physics at γ-ALBA, the Proposed Photon Laser Backscattering Facility for Spain". Workshop of the Working Group for the Preparation of a Proposal for the Construction of a Gamma Ray Beam Line at ALBA. October 2004. Barcelona, España.
3. J.L. Taín (coordinator), A.M. Lallena (coordinator), M. Ebrahim, J.M. Alvarez, M. Hernanz, G. Martínez-Pinedo, F. Calviño, M.A. Duch, Yu. Kubyshin, A. Poch, J. Sempau, F. Verdera, M. Anguiano, J. Nieves, I. Martel, P. Vaz, D. Cano-Ott, E. González-Romero, C. Guerrero, T. Martínez, M.J.G. Borge, C. Fernández-Ramírez, E. Moya de Guerra, O. Tengblad, A. Jungclaus, L.M. Fraile, J. López-Herraiz, J.M. Udías, J.R. Vignote, F.J. Llanes-Estrada, G. Co', T.M.C. Maiolo, L. Roso, A. Valcarce, J. Vijande, J. Benlliure, D. Cortina, E. Casarejos, I. Durán, J. Gómez-Camacho, J.M. Espino, F.J. Santos-Arévalo, P. von Balmoos, A. Faus, S. Martí, E. Oset, B. Rubio, "Proposal for the Construction of a Gamma-Ray Beam Line at the Spanish Synchrotron ALBA". Presented to Consorcio para la construcción, equipamiento y explotación del laboratorio de luz sincrotrón CELLS-ALBA. December 2004.
`http://www.cells.es/Divisions/Experiments/BeamlineProposals/`

References

[ABCDM 02a] J.E. Amaro, M.B. Barbaro, J.A. Caballero, T.W. Donnelly, and A. Molinari, "Relativistic pionic effects in quasielastic electron scattering", *Nucl. Phys.* A 697 (2002) 388-428, `arXiv:nucl-th/0106035`.

[ABCDM 02b] J.E. Amaro, M.B. Barbaro, J.A. Caballero, T.W. Donnelly, and A. Molinari, "Gauge and Lorentz invariant one-pion exchange currents in electron scattering from a relativistic Fermi gas", *Phys. Rep.* 368 (2002) 317-407, `arXiv:nucl-th/0204001`

[ABSW 02] R.A. Arndt, W.J. Briscoe, I.I. Strakovsky, and R.L. Workman, "Analysis of pion photoproduction data", *Phys. Rev.* C 66 (2002) 055213, `arXiv:nucl-th/0205067`

[Ale 05] C. Alexandrou, Ph. de Forcrand, H. Neff, J.W. Negele, W. Schroers, and A. Tsapalis, "N-to-Δ electromagnetic-transition form factors from Lattice QCD", *Phys. Rev. Lett.* 94 (2005) 021601, `arXiv:hep-lat/0409122`

[ALR 90] R.A. Arndt, Z. Li, and L.D. Roper, "Determination of the πNN coupling constant from elastic pion-nucleon scattering data", *Phys. Rev. Lett.* 65 (1990) 157-158.

[ASW 96] R.A. Arndt, I.I. Strakovsky, and R.L. Workman, "Updated resonance photodecay amplitudes up to 2 GeV", *Phys. Rev.* C 53 (1996) 430-440.

[AW 03] G. Altarelli and K. Winter (eds.), "Neutrino mass", Springer-Verlag, Berlin-Heidelberg-New York, 2003.

[AWLR 90a] R.A. Arndt, R.L. Workman, Z. Li, and L.D. Roper, "Partial-wave analysis of pion photoproduction", *Phys. Rev.* C 42 (1990) 1853-1863.

[AWLR 90b] R.A. Arndt, R.L. Workman, Z. Li, and L.D. Roper, "Pion photoproduction resonance couplings in the second resonance region", *Phys. Rev.* C 42 (1990) 1864-1866.

[Azn 03] I.G. Aznauryan, "Multipole amplitudes of pion photoproduction on nucleons up to 2 GeV using dispersion relations and the unitary isobar model", *Phys. Rev.* C 67 (2003) 015209, `arXiv:nucl-th/0206033`

[BDM 89] M. Benmerrouche, R.M. Davidson, and N.C. Mukhopadhyay, "Problems of describing spin-3/2 baryon resonances in the effective Lagrangian theory", *Phys. Rev.* C 39 (1989) 2339-2348.

[BDS 75] I.S. Barker, A. Donnachie, and J.K. Storrow, "Complete experiments in pseudoscalar photoproduction", *Nucl. Phys.* B 95 (1975) 347-356.

[BDW 67] F.A. Berends, A. Donnachie, and D.L. Weaver, "Photoproduction and electroproduction of pions (I) dispersion relation theory", *Nucl. Phys.* B 4 (1967) 1-53.

[Bec 97] R. Beck *et al.*, "Measurement of the E2/M1 Ratio in the $N \to \Delta$ transition using the reaction $p(\vec{\gamma}, p)\pi^0$", *Phys. Rev. Lett.* 78 (1997) 606-609.

[Bel 99] V. Bellini *et al.*, "Coherent π^0 photo-production on ^{4}He at intermediate energies with polarized photons", *Nucl. Phys.* A 646 (1999) 55-66.

[Ber 90] J.R. Bergervoet, P.C. van Campen, R.A.M. Klomp, J.-L. de Kok, T.A. Rijken, V.G.J. Stocks, and J.J. de Swart, "Phase shift analysis of all proton-proton scattering data below $T_{lab} = 350$ MeV", *Phys. Rev.* C 41 (1990) 1435-1452.

[Ber 91] J.C. Bergstrom, "$p(\gamma, \pi^0)$ cross section and the low energy theorem", *Phys. Rev.* C 44 (1991) 1768-1783.

[Ber 03] A.M. Bernstein, "Deviation of the nucleon shape from spherical symmetry: Experimental status", *Eur. Phys. J.* A 17 (2003) 349-355, `arXiv:hep-ex/0212032`

[BH 91] A.M. Bernstein and B.R. Holstein, "Threshold pion photoproduction and chiral invariance", *Comments Nucl. Part. Phys.* 20 (1991) 197-220.

[BHF 97] A.J. Buchmann, E. Hernández, and A. Faessler, "Electromagnetic properties of the $\Delta(1232)$" *Phys. Rev.* C 55 (1997) 448-463, `arXiv:nucl-th/9610040`

[BKM 92] V. Bernard, N. Kaiser, and U.-G. Meißner, "Threshold pion photoproduction in chiral perturbation theory", *Nucl. Phys.* B 383 (1992) 442-496.

[BKM 95] V. Bernard, N. Kaiser, and U.-G. Meißner, "Chiral dynamics in nucleons and nuclei", *Int. J. Mod. Phys.* E 4 (1995) 193-344, `arXiv:hep-ph/9501384`

[Bla 97] G. Blanpied *et al.*, "$N \to \Delta$ transition from simultaneous measurement of $p(\vec{\gamma}, \pi)$ and $p(\vec{\gamma}, \gamma)$", *Phys. Rev. Lett.* 79 (1997) 4337-4340.

[Bla 01] G. Blanpied *et al.*, "$N \to \Delta$ transition and proton polarizabilities from measurements of$p(\vec{\gamma}, \gamma)$, $p(\vec{\gamma}, \pi^0)$ and $p(\vec{\gamma}, \pi^+)$", *Phys. Rev.* C 64 (2001) 025203.

[BM 65] C.M. Becchi and G. Morpurgo, "Vanishing of the E2 part of the $N^*_{33} \to N+\gamma$ amplitudes in the non-relativistic quark model of "elementary" particles", *Phys. Lett.* 17 (1965) 352-354.

[BM 98] A. Bohr and B. Mottelson, "Nuclear Structure, Volume II: Nuclear Deformations", World-Scientific, Singapore, 1998.

[Britannica] Britannica Encyclopædia, `http://www.britannica.com/`

[Bur 00] C.P. Burgess, "Goldstone and pseudo-Goldstone bosons in nuclear, particle and condensed-matter physics", *Phys. Rep.* 330 (2000) 193-261, `arXiv:hep-th/9808176`

[Bus 79] P.J. Bussey *et al.*, "Measurements of the double polarisation parameters G and H in neutral pion photoproduction", *Nucl. Phys.* B 159 (1979) 383-396.

[Bus 80] P.J. Bussey *et al.*, "Measurement of the polarisation parameters G and H in positive pion photoproduction", *Nucl. Phys.* B 169 (1980) 403-414.

[BW 91] J. Blatt and V.F. Weisskopf, "Theoretical Nuclear Physics". Dover Publishers, New York, 1991.

[CFHK 79] R.E. Cutkosky, C.P. Forsyth, R.E. Hendrick, and R.L. Kelly, "Pion-nucleon partial-wave amplitudes", *Phys. Rev.* D 20 (1979) 2839-2853.

[CGLN 57] G.F. Chew, M.L. Goldberger, F.E. Low, and Y. Nambu, "Relativistic dispersion relation approach to photomeson production", *Phys. Rev.* 106 (1957) 1345-1355.

[CR 00] S. Capstick and W. Roberts, "Quark models of baryon masses and decays", *Prog. Part. Nucl. Phys.* 45 (2000) S241-S331, `arXiv:nucl-th/0008028`

[Cur 79] T. Curtright, "Massless field supermultiplets with arbitrary spin", *Phys. Lett.* B 85 (1979) 219-224.

[DBT 94] M.J. Dekker, P.J. Brussaard, and J.A. Tjon, "Relativistic meson exchange and isobar currents in electron scattering: Noninteracting Fermi gas analysis", *Phys. Rev.* C 49 (1994) 2650-2670.

[DGL 02] D. Dutta, H. Gao, and T.-S.H. Lee, "Nucleon resonances with double polarization observables of pion photoproduction", *Phys. Rev.* C 65 (2002) 044619,arXiv:nucl-th/0111005

[DHKT 99] D. Drechsel, O. Hanstein, S.S. Kamalov, and L. Tiator, "A unitary isobar model for pion photo- and electroproduction on the proton up to 1 GeV", *Nucl. Phys.* A 645 (1999) 145-174, arXiv:nucl-th/9807001, http://www.kph.uni-mainz.de/MAID/

[DKD 76] J. Dubach, J.H. Koch, and T.W. Donnelly, "Exchange currents in electron scattering from light nuclei", *Nucl. Phys.* A 271 (1976) 279-316.

[DM 70] R.H. Dalitz and R.G. Moorhouse, "What is a resonance?", *Proc. Roy. Soc. Lond.* A 318 (1970) 279-298.

[DMW 86] R. Davidson, N.C. Mukhopadhyay, and R. Wittman, "Ratio of electric quadrupole to magnetic dipole amplitudes in the nucleon-delta transition", *Phys. Rev. Lett.* 56 (1986) 804-807.

[DMW 91] R.M. Davidson, N.C. Mukhopadhyay, and R.S. Wittman, "Effective Lagrangian approach to the theory of pion photoproduction in the $\Delta(1232)$ region", *Phys. Rev.* D 43 (1991) 71-94.

[DW 01a] R.M. Davidson and R. Workman, "Effects of form factors in fits to photoproduction data", *Phys. Rev.* C 63 (2001) 058201, arXiv:nucl-th/0102046

[DW 01b] R.M. Davidson and R. Workman, "Form factors and photoproduction amplitudes", *Phys. Rev.* C 63 (2001) 025210, arXiv:nucl-th/0101066

[Edm 74] A.R. Edmonds, "Angular Momentum in Quantum Mechanics", Princeton University Press, 1974.

[ESW 60] F. Ernst, R. Sachs, and K. Wali, "Electromagnetic form factors of the nucleon", *Phys. Rev.* 119 (1960) 1105-1114.

[EW 88] T. Ericson and W. Weise, "Pions and Nuclei", Clarendon Press, Oxford, 1988.

[FA 03] M.G. Fuda and H. Alharbi, "Photoproduction of mesons from the nucleon", *Phys. Rev.* C 68 (2003) 064002.

[Fae 00] A. Faessler, "Is the nucleon deformed?", *Prog. Part. Nucl. Phys.* 44 (2000) 197-210.

[Fer 03] C. Fernández-Ramírez, "Producción de piones en núcleos", Diploma Thesis. Universidad Complutense de Madrid (2003).

[Fer 04] C. Fernández-Ramírez, J.M. Udías, E. Moya de Guerra, J.R. Vignote, F.J. Llanes-Estrada, J.L. Herraiz, A.M. Lallena, J. Vijande, and A. Valcarce, "Intermediate Energy Physics at γ-ALBA, the Proposed Photon Laser Backscattering Facility for Spain", Workshop of the Working Group for the Preparation of a Proposal for the Construction of a Gamma Ray Beam Line at ALBA, Barcelona, Spain (2004).

[FF 78] J. Fang and C. Fronsdal, "Massless fields with half-integral spin", *Phys. Rev.* D 18 (1978) 3630-3633.

[FM 97] T. Feuster and U. Mosel, "Electromagnetic couplings of nucleon resonances", *Nucl. Phys.* A 612 (1997) 375-390, arXiv:nucl-th/9604026

[FM 98] T. Feuster and U. Mosel, "Unitary model for meson-nucleon scattering", *Phys. Rev.* C 58 (1998) 457-488, arXiv:nucl-th/9708051

[FMU 03] C. Fernández-Ramírez, E. Moya de Guerra, and J.M. Udías, "Pion electro- and photoproduction on nuclei in a Lagrangian approach", Proceedings of the 6th Workshop on Electromagnetically Induced Two-Hadron Emission, 234-239. Eds: A. Braghieri, C. Giusti, and P. Grabmayr. Pavia, Italy (2003).

[FMU 06a] C. Fernández-Ramírez, E. Moya de Guerra, and J.M. Udías, "Effective Lagrangian Approach to pion photoproduction from the nucleon", *Ann. Phys.* (N.Y.) 341 (2006) 1408-1456 arXiv:nucl-th/0509020

[FMU 06b] C. Fernández-Ramírez, E. Moya de Guerra, and J.M. Udías, "Hints on the quadrupole deformation of the $\Delta(1232)$", *Phys. Rev.* C 73 (2006) 042201(R), arXiv:nucl-th/0601037

[Fro 78] C. Fronsdal, "Massless fields with integer spin", *Phys. Rev.* D 18 (1978) 3624-3629.

[Gay 03] O. Gayou *et al.*, "Measurement of G_{E_p}/G_{M_p} in $e\vec{p} \to e\vec{p}$ to $Q^2 = 5.6$ GeV^2", *Phys. Rev. Lett.* 88 (2003) 092301, arXiv:nucl-ex/0111010

[Gla 79] S.L. Glashow, "The unmellisonant quark", *Physica* A 96 (1979) 27-30.

[GM 93] H. Garcilazo and E. Moya de Guerra, "A model for pion electro- and photo-production from threshold up to 1 GeV", *Nucl. Phys.* A 562 (1993) 521-568.

[GM 94] H. Garcilazo and E. Moya de Guerra, "Reaction $\gamma d \to \pi^0 d$ and the small components of the deuteron wave function", *Phys. Rev.* C 49 (1994) R601-R604.

[GM 95] H. Garcilazo and E. Moya de Guerra, "Pion photoproduction of the deuteron: The reaction $\gamma d \to \pi^0 d$", *Phys. Rev.* C 52 (1995) 49-60.

[GO 94] J.A. Gómez Tejedor and E. Oset, "A model for the $\gamma p \to \pi^+\pi^- p$ reaction", *Nucl. Phys.* A 571 (1994) 667-693.

[GO 96] J.A. Gómez Tejedor and E. Oset, "Double pion photoproduction on the nucleon: Study of the isospin channels", *Nucl. Phys.* A 600 (1996) 413-435, arXiv:hep-ph/9506209

[Gol 89] D.E. Goldberg, "Genetic Algorithms in Search, Optimization & Machine Learning", Addison Wesley, 1989.

[Gre 97] W. Greiner, "Relativistic Quantum Mechanics — Wave Equations", Springer-Verlag, Berlin-Heidelberg-New York, 1997.

[GS 63a] M. Gourdin and Ph. Salin, "Analysis of photoproduction with an isobaric model", *Nuovo Cimento* 27 (1963) 193-207.

[GS 63b] M. Gourdin and Ph. Salin, "Some remarks about gauge invariance in the isobaric model for photoproduction", *Nuovo Cimento* 27 (1963) 309-312.

[Gup 98] R. Gupta, "Introduction to Lattice QCD", Lecture given at the LXVIII Les Houches Summer School "Probing the Standard Model of Particle Interactions", arXiv:hep-lat/9807028

[Hag 71] C.R. Hagen, "New inconsistencies in the quantization of spin-3/2 fields", *Phys. Rev.* D 4 (1971) 2204-2208.

[HM 84] F. Halzen and A.D. Martin, "Quarks and Leptons: An Introductory Course in Modern Particle Physics", John Wiley & Sons, 1984.

[Höh 98] G. Höhler, "Against Breit-Wigner parameters – a pole-emic", p. 624-625 and references therein in: C. Caso *et al.*, "Review of Particle Physics", *Eur. Phys. J.* C 3 (1998) 1-794.

[IJR 04] D.G. Ireland, S. Janssen, and J. Ryckebusch, "A Genetic Algorithm Analysis of N* Resonances in $p(\gamma, K^+)\Lambda$ Reactions", *Nucl. Phys.* A 740 (2004) 147-167, arXiv:nucl-th/0312103

[JRDC 02a] S. Janssen, J. Ryckebusch, D. Debruyne, and T. Van Cauteren, "Kaon photoproduction: background contributions, form factors and missing resonances", *Phys.Rev.* C 65 (2002) 015201, arXiv:nucl-th/0107028

[JRDC 02b] S. Janssen, J. Ryckebusch, D. Debruyne, and T. Van Cauteren, "Sigma photoproduction in the resonance region", *Phys.Rev.* C 66 (2002) 035202, arXiv:nucl-th/020207

[JS 61] K. Johnson and E.C.G. Sudarshan, "Inconsistency of the local field theory of charged spin-3/2 particles", *Ann. Phys.* (N.Y.) 13 (1961) 126-145.

[JS 81] H.F. Jones and M.D. Scadron, "Multipole $\gamma N - \Delta$ form factors and resonant photo- and electroproduction", *Ann. Phys.* (N.Y.) 81 (1973) 1-14.

[KB 98] S. Karataglidis and C. Benhold, "Probing proton halos through pion photoproduction", *Phys. Rev. Lett.* 80 (1998) 1614-1617.

[KS 00] S. Kondratyuk and O. Scholten, "Dressing the nucleon in a dispersion approach", *Phys. Rev.* C 62 (2000) 025203, `arXiv:nucl-th/0001022`

[KS 01] S. Kondratyuk and O. Scholten, "Compton scattering on the nucleon at intermediate energies and polarizabilities in a microscopic model", *Phys. Rev.* C 64 (2001) 024005, `arXiv:nucl-th/0103006`

[KS 03] B. Krusche and S. Schadmand, "Study of non-strange baryon resonances with meson photoproduction", *Prog. Part. Nucl. Phys.* 51 (2003) 399-485, `arXiv:nucl-ex/0306023`

[Kru 04] B. Krusche *et al.*, "Photoproduction of π^0-mesons from nuclei", *Eur. Phys. J.* A 22 (2004) 277-291, `arXiv:nucl-ex/0406002`

[Lan 68] P.V. Landshoff, "Cayley transform of the S matrix", *J. Math. Phys.* 9 (1968) 2279-2282.

[Leu 94] H. Leutwyler, "On the foundations of chiral perturbation theory", *Ann. Phys.* (N.Y.) 235 (1994) 165-203, `hep-ph/9311274`

[LDW 93] D.B. Leinweber, T. Draper, and R.M. Woloshyn, "Baryon octect to decuplet electromagnetic transitions", *Phys. Rev.* D 48 (1993) 2230-2249, `arXiv:hep-lat/9212016`

[LYL 97] Z.-P. Li, H.-X. Ye, and M.-H. Lu, "Unified approach to pseudoscalar meson photoproduction off nucleons in the quark model", *Phys. Rev.* C 56 (1997) 1099-1113, `arXiv:nucl-th/9706010`

[Mic 99] Z. Michalewicz, "Genetic Algorithms+Data Structures=Evolution Programs", Springer-Verlag, Berlin-Heidelberg-New York, 1999.

[MMD 96] P. Mergell, Ulf-G. Meißner, and D. Drechsel, "Dispersion theoretical analysis of the nucleon electromagnetic form factors", *Nucl. Phys.* A 596 (1996) 367-396, `arXiv:hep-ph/9506375`

[Mol 96] C. Molinari *et al.*, "Scattering of photons by the proton through $\theta_{cms} = 90^o$ in the Δ-resonance region", *Phys. Lett.* B 371 (1996) 181-185.

[Moy 86] E. Moya de Guerra, "Rotational nuclear models and electron scattering", *Phys. Rep.* 138 (1986) 293-362.

[NAG] Numerical Algorithms Group Ltd., Wilkinson House, Jordan Hill Road, Oxford OX2-8DR, UK. `http://www.nag.co.uk/`

[NBL 90] S. Nozawa, B. Blankleider, and T.-S.H. Lee, "A dynamical model for pion photoproduction on the nucleon", *Nucl. Phys.* A 513 (1990) 459-510.

[NEK 71] L.M. Nath, B. Etemadi, and J.D. Kimel, "Uniqueness of the interaction involving spin-3/2 particles", *Phys. Rev.* D 3 (1971) 2153-2161.

[NKF 90] H.W.L. Naus, J.H. Koch, and J.L. Friar, "Off-shell form factors and low energy theorems for pion photoproduction", *Phys. Rev.* C 41 (1990) 2852-2864, and references therein.

[OD 81] J.W. Van Orden and T.W. Donnelly, "Mesonic processes in deep-inelastic electron scattering from nuclei", *Ann. Phys.* (N.Y.) 131 (1981) 451-493.

[Ols 74] M.G. Olsson, "Solutions of the multichannel unitarity equations describing the addition of a resonance and background: Application to a pole model of photoproduction", *Nucl. Phys.* B 78 (1974) 55-76.

[OO 78] M.G. Olsson and E.T. Osypowski, "Vector meson exchange and unitarity effects in low-energy photoproduction", *Phys. Rev.* D 17 (1978) 174-184.

[Pas 98] V. Pascalutsa, "Quantization of an interacting spin-3/2 field and the Δ isobar", *Phys. Rev.* D 58 (1998) 096002, `arXiv:hep-ph/9802288`

[Pas 01] V. Pascalutsa, "Correspondence of consistent and inconsistent spin-3/2 couplings via the equivalence theorem", *Phys. Lett.* B 503 (2001) 85-90, `arXiv:hep-ph/0008026`

[PDG 04] S. Eidelman *et al.*, "Review of Particle Physics", *Phys. Lett.* B 592 (2004) 1-1109, `http://pdg.lbl.gov`

[Pec 68] R.D. Peccei, "Chiral Lagrangian calculation of pion-nucleon scattering lengths", *Phys. Rev.* 176 (1968) 1812-1821.

[Pec 69] R.D. Peccei, "Chiral Lagrangian model of single pion photoproduction", *Phys. Rev.* 181 (1969) 1902-1905.

[Pei 96] J. Peise *et al.*, "Compton scattering by the proton through $\theta_{cms} = 75^o$ in the Δ-resonance region", *Phys. Lett.* B 384 (1996) 37-42.

[Pen 02] G. Penner, "Vector Meson Production and Nucleon Resonance Analysis in a Coupled-Channel approach", Ph.D. Thesis Dissertation, Universität Gießen, 2002.

[PM 02] G. Penner and U. Mosel, "Vector meson production and nucleon resonance analysis in a coupled-channel approach for energies $m_N < \sqrt{s} < 2$ GeV. II. Photon-induced results", *Phys. Rev.* C 66, 055212 (2002), `nucl-th/0207069`

[PP 03] V. Pascalutsa and D.R. Phillips, "Effective theory of the $\Delta(1232)$ resonance in Compton scattering off the nucleon", *Phys. Rev.* C 67 (2003) 055202, `arXiv:nucl-th/0212024`

[PS 95] V. Pascalutsa and O. Scholten, "On the structure of the $\gamma N\Delta$ vertex: Compton scattering in the $\Delta(1232)$ region and below", *Nucl. Phys.* A 591 (1995) 658-674.

[PT 99] V. Pascalutsa and R. Timmermans, "Field theory of nucleon to higher-spin baryon transitions", *Phys. Rev.* C 60 (1999) 042201(R), `arXiv:nucl-th/9905065`

[PT 04] V. Pascalutsa and J.A. Tjon, "Pion photoproduction on nucleons in a covariant hadron-exchange model", *Phys. Rev.* C 70 (2004) 035209, `arXiv:nucl-th/0407068`

[PV 05] V. Pascalutsa and M. Vanderhaeghen, "Electromagnetic nucleon-to-Delta transition in chiral effective-field theory" *Phys. Rev. Lett.* 95, 232001 (2005), `arXiv:hep-ph/0508060`

[RGG 75] A. De Rújula, H. Georgi, and S.L. Glashow, "Hadron masses in gauge theory", *Phys. Rev.* D 12 (1975) 147-162.

[Ros 54] M. Ross, "A connection between pion photoproduction and scattering phase shifts", *Phys. Rev.* 94 (1954) 454-460.

[RS 41] W. Rarita and J. Schwinger, "On theory of particles with half-integral spin", *Phys. Rev.* 60 (1941) 61.

[SAID] R.A. Arndt, W.J. Briscoe, R.L. Workman, and I.I. Strakovsky, SAID database, `http://gwdac.phys.gwu.edu`

[Sha 04] A. Shafi *et al.*, "Measurement of inverse pion photoproduction at energies spanning the N(1440) resonance", *Phys. Rev.* C 70 (2004) 035204, `arXiv:nucl-ex/0405026`

[Sin 73] L.P.S. Singh, "Noncausal propagation of classical Rarita-Schwinger waves", *Phys. Rev.* D 7 (1973) 1256-1258.

[SKPN 96] O. Scholten, A.Yu. Korchin, V. Pascalutsa, and D. Van Neck, "Pion and photon induced reactions on the nucleon in a unitary model", *Phys. Lett.* B 384 (1996) 13-19, arXiv:nucl-th/9604014

[SL 96] T. Sato and T.-S.H. Lee, "Meson exchange model πN scattering and $\gamma N \to \pi N$ reaction", *Phys. Rev.* C 54 (1996) 2660-2684, arXiv:nucl-th/9606009

[SL 01] T. Sato and T.-S.H. Lee, "Dynamical study of the Δ excitation in $N(e, e'\pi)$ reactions", *Phys. Rev.* C 63 (2001) 055201, arXiv:nucl-th/0010025

[TDHKY 01] L. Tiator, D. Drechsel, O. Hanstein, S.S. Kamalov, and S.N. Yang, "The E2/M1 and C2/M1 ratios and form factors in $N \to \Delta$ transitions", *Nucl. Phys.* A 689 (2001) 205c-214c, nucl-th/0012046

[TL 04] J.L. Taín, A.M. Lallena, *et al.*, "Proposal for the Construction of a Gamma-Ray Beam Line at the Spanish Synchrotron ALBA". Presented to *Consorcio para la construcción, equipamiento y explotación del laboratorio de luz sincrotrón CELLS-ALBA*. December 2004. http://www.cells.es/Divisions/Experiments/BeamlineProposals/

[TW 01] A.W. Thomas and W. Weise, "The Structure of the Nucleon", Wiley-VCH, Berlin, 2001.

[Udi 03a] A. Udías Moinelo, F.J. Elorza Terreiro, M.A. Bermúdez, A. López, J.M. Udías, J. Aguirre, and A. Garriga, "Heuristic and mixed-integer programming for solving the scheduling and network operational optimization of LPG supply" in "Evolutionary methods for design, optimization and controlapplications to industrial and societal problems : proceedings of the Fifth Conference on Evolutionary Methods for Design, Optimization and Control with Applications to Industrial and Societal Problems", EUROGEN 2003, Eds: G. Bugeda, J.A. Désidéri, J. Periaux, M. Schoenauer, and G. Winter. Barcelona, Spain (2003)

[Udi 03b] A. Udías Moinelo, F.J. Elorza Terreiro, A. Garriga, M.A. Bermúdez, J.M. Parga, J.M. Udías, and A. López. "Análisis de la aplicación de algoritmos genéticos y de búsqueda exhaustiva a la gestión diaria de una red de distribución GLP". Published in: Actas del II Congreso Español sobre Metaheurísticas, Algoritmos Evolutivos y Bioinspirados, MAEB 2003, p. 476-485. Gijón, Spain (2003).

[VDL 00] T.P. Vrana, S.A. Dytman, and T.-S.H. Lee, "Baryon resonance extraction from πN data using a unitary multichannel model", *Phys. Rep.* 328 (2000) 181-236,arXiv:nucl-th/9910012

[VHRW 95] M. Vanderhaeghen, K. Heyde, J. Ryckebusch, and M. Waroquier, "Pion photoproduction through the Δ resonance region: relativistic versus non-relativistic unitary models", *Nucl. Phys.* A 595 (1995) 219-258.

[VZ 69a] G. Velo and D. Zwanziger, "Propagation and quantization of Rarita-Schwinger waves in an external electromagnetic potential", *Phys. Rev.* 186 (1969) 1337-1341.

[VZ 69b] G. Velo and D. Zwanziger, "Noncausality and other defects of interaction Lagrangians for particles with spin one and higher", *Phys. Rev.* 188 (1969) 2218-2222.

[Wal 69] R.L. Walker, "Phenomenological analysis of single-pion photoproduction", *Phys. Rev.* 182 (1969) 1729-1748.

[Wat 54] K.M. Watson, "Some general relations between the photoproduction and scattering of π mesons", *Phys. Rev.* 95 (1954) 228-236.

[Wei 79] S. Weinberg, "Phenomenological Lagrangians", *Physica* A 96 (1979) 327-340.

[Wei 95] S. Weinberg, "The Quantum Theory Of Fields, Vol. I: Foundations", Cambridge University Press, Cambridge, 1995.

[WF 80] B. de Wit and D.Z. Freedman, "Systematics of higher-spin gauge fields", *Phys. Rev.* D 21 (1980) 358-367.

[Wis 99] F. Wissmann *et al.*, "Compton scattering from the free and bound proton at backward angles above π-threshold", *Nucl. Phys.* A 660 (1999) 232-245.

[Wu 03] W. Wu *et al.*, "Plane-wave impulse approximation extraction of the neutron magnetic form factor from quasielastic $^3\vec{\mathrm{He}}(e,e')$ at $Q^2 = 0.3$ to 0.6 $(\mathrm{GeV/c})^2$", *Phys. Rev.* C 67 (2003) 012201(R).

[WW 80] S. Weinberg and E. Witten, "Limits on massless particles", *Phys. Lett.* B 503 (1980) 59-62.

[WW 87] A. Wirzba and W. Weise, "The E2/M1 transition ratio for $\gamma N \to \Delta(1232)$ in a modified skyrme model", *Phys. Lett.* B 188 (1987) 6-10.

[WWA 96] P. Wilhelm, Th. Wilbois, and H. Arenhövel, "Unitary ambiguity in the extraction of the E2/M1 ratio for the $\gamma N \leftrightarrow \Delta$ transition", *Phys. Rev.* C 54 (1996) 1423-1426, `arXiv:nucl-th/9606015`

[ZALW 02] Q. Zhao, J.S. Al-Khalili, Z.-P. Li, and R.L. Workman, "Pion photoproduction on the nucleon in the quark model", *Phys. Rev.* C 65 (2002) 065204, `arXiv:nucl-th/0202067`

List of Figures

List of Tables

List of Acronyms

c.m.: Center of Mass

EMR: E2/M1 Ratio (referred to $\Delta(1232)$)

ChPT: Chiral Perturbation Theory

CMB: Carnegie-Mellon-Berkeley model

ELA: Effective Lagrangian Approach

DOF: Degrees Of Freedom

Fig.: Figure

FSI: Final State Interactions

GA: Genetic Algorithm

GI: Gauge Invariant (referred to high spin couplings)

GRAAL: GRenoble Anneau Accelerateur Laser (Laser Backscattering Facility at Grenoble, France)

HC: Hermitian Conjugate

JS: Johnson-Sudharsan (referred to the nonpositive definite conmutators problem)

LEGS: Laser Electron Gamma Source (Laser Backscattering Facility at Brookhaven, USA)

LEPS: Laser Electron Photons at SPring-8 (Laser Backscattering Facility at Harima, Japan)

LET: Low Energy Theorems

MAID: Mainz Unitary Isobar Model

MAMI: MAinz MIcrotron (Nuclear physics facility at Mainz, Germany)

NAG: Numerical Algorithms Group

P: Recoil Nucleon Polarisation

PCAC: Partially Conserved Axial-Vector Current

PDG: Particle Data Group

PV: Pseudovector [coupling to the pion]

PS: Pseudoscalar [coupling to the pion]

QCD: Quantum Chromo Dynamics

Ref.: Reference

Σ: Polarised Beam Asymmetry

SAID: Scattering Analysis Interactive Dial-in (George Washington University analysis of meson production)

SP: Speed Plot

T: Polarised Target Asymmetry

VDL: Vrana, Dytman, and Lee (referred to the Vrana, Dytman, and Lee set of masses and widths of the nucleon resonances)

VZ: Velo-Zwanziger (referred to the acausal propagation problem)

Index